MCAT Institute
Final Report
May 1989 - January 1995
NCC-604-95-05

DEVELOPMENT OF A QUIET SUPERSONIC WIND TUNNEL WITH A CRYOGENIC ADAPTIVE NOZZLE

Stephen W. D. Wolf

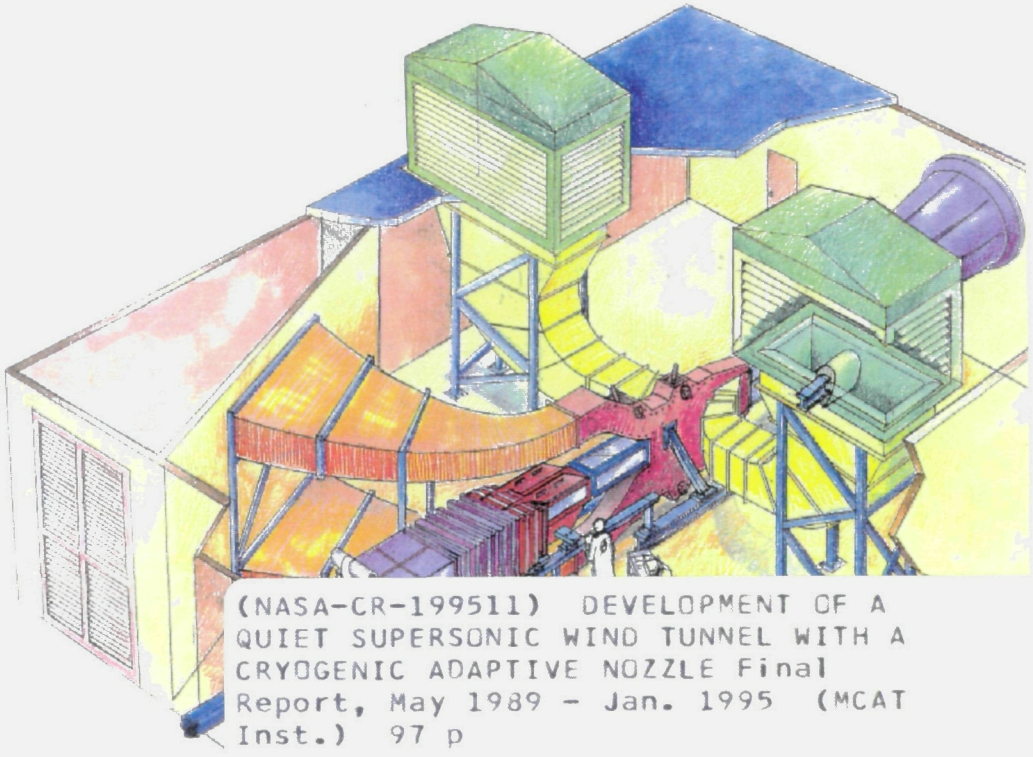

January 1995

MCAT Institute
3933 Blue Gum Drive
San Jose, CA 95127

CONTENTS

1. Introduction

Low-disturbance or "quiet" wind tunnels are now considered an essential part of meaningful boundary layer transition research. In particular, the normal high levels of wind tunnel disturbances can significantly affect the complex transition phenomena under investigation. Consequently, the wind tunnel environment can only simulate free flight conditions with a low-disturbance free stream. Actually, the receptivity of supersonic boundary layers to external disturbances was first documented by Laufer in 1954. Recent interest in this topic has resulted from a growing respect for the pioneering research of Laufer at the Jet Propulsion Laboratory (JPL) from the mid-1950s to the early-1960s, and the work of Pate and Schueler in the late-1960s. Also, there is growing skepticism that flight test transition experiments can provide the necessary data for Computational Fluid Dynamics (CFD) validation.

Advances in Supersonic Laminar Flow Control (SLFC) technology for swept wings depends on a better understanding of the receptivity of the transition phenomena to attachment-line contamination and cross-flows. This need has provided the impetus for building the Laminar Flow Supersonic Wind Tunnel (LFSWT) at NASA-Ames, as part of the NASA High Speed Research Program (HSRP). The LFSWT was designed to provide NASA with an unequaled capability for transition research at low supersonic Mach numbers (<2.5). Prior to our involvement, NASA quiet wind tunnel research had been concentrated at Langley Research Center on supersonic and hypersonic flow regimes above Mach 3.5. Numerous NASA quiet tunnels were developed over the last 10 years. The complexity of the Langley approach to achieving quiet flow at high Reynolds numbers and Mach numbers has deterred other research centers from becoming involved. Consequently, the only activity elsewhere has been at Montana State University (Mach 3.0) and ONERA Chalais-Meudon/Toulouse, France (Mach 3.5), until our work began here at NASA-Ames. Hence, the LFSWT is currently the only quiet tunnel, which can test close to the expected cruising speed of the High Speed Civil Transport (HSCT) and planned SLFC flight tests. Interestingly, the old JPL 20-inch Supersonic Wind Tunnel (JPL-SWT), upon which the LFSWT is based (since the JPL-SWT is the first documented quiet supersonic wind tunnel), will soon be re-commissioned at NASA-Langley, and may eventually operate quietly over part of its Mach 1.4 to 5.0 test envelope.

This Cooperative Agreement was the result of Dr. Sanford Davis realizing that a supersonic wind tunnel with low-disturbance flow was required to enhance the research capabilities of the Fluid Mechanic Laboratory (FML) at NASA-Ames. At the beginning of this effort, the FML had no supersonic wind tunnels or any experimental SLFC experience. The ensuing work by the Principal Investigator (PI), Dr. Stephen W.D. Wolf, is summarized herein, and had the following objectives in support of the new FML quiet supersonic wind tunnel:

1) Develop a unique injector drive system using the existing FML indraft compressor.

2) Develop an FML instrumentation capability for quiet supersonic wind tunnel evaluation and transition studies at NASA-Ames.

3) Determine the *State of the Art* in quiet supersonic wind tunnel design.

4) Build and commission the LFSWT (see Figure 1).

5) Make detailed flow quality measurements in the LFSWT.

6) Perform tests of swept wing models in the LFSWT in support of the NASA HSR program.

7) Provide documentation of research progress.

It should be noted that during the early stages of this work, a decision was made to defer the application of adaptive wall and cryogenic technologies to suppress transition along the walls of a supersonic nozzle. This decision was based on the knowledge of the expected LFSWT test

envelope, which was considered conducive to laminar flow control by passive means. The decision undoubtably reduced the complexity of the eventual tunnel, and contributed to the LFSWT actually being built. However, the PI has remained involved with adaptive wall technology and during this Cooperative Agreement, several review papers and articles were published[1-6] by the PI, highlighting the strides that have been made in transonic testing techniques with solid adaptive walls.

The quiet tunnel development at NASA-Ames was effectively split into two parts. The first part involved the designing and study of an eighth-scale pilot tunnel, called the Proof of Concept (PoC) tunnel. The PoC was used to reduce the risk involved in designing the drive system for the full-scale tunnel. Also, we used the PoC to develop expertise in instrumentation and transition research in the FML for eventual use with the full-scale tunnel.

The second part involved the design, fabrication and testing of the LFSWT (the full-scale tunnel). The instrumentation and transition research expertise built-up with the PoC was transferred to the new tunnel. However, the injector drive system required extensive tuning before the tunnel could be commissioned. The unique flow characteristics of the tunnel were studied through extensive flow quality measurements, designed to set new standards for quiet flow calibration. The quiet test core was defined to the extent possible, and swept-wing models were tested to help validate CFD and flight test data, initially using only mean pressure distributions (as discussed later).

This report is intended to be an overview of the extensive research carried out during the almost six years of the Cooperative Agreement NCC2-604, and is a summary of numerous published Annual Reports.[7-10] References are provided so that more detailed information can be found at the reader's discretion. This report illustrates the breadth of work tackled by a single Principal Investigator, Dr. Stephen W.D. Wolf, working in close cooperation with a small and effective team of NASA experts. The work is split into logical headings, which are related to the work objectives. A summary and conclusion section highlights the significance of this Anglo-British effort, made possible by the funding mechanism of this Cooperative Agreement between NASA-Ames and the MCAT Institute.

2. Quiet Wind Tunnel Development

2.1 Proof of Concept (PoC) Supersonic Wind Tunnel:

The desire to use the existing FML single-stage centrifical compressor system (which can only produce a minimum manifold pressure of about 8 psia - 0.55 bar) dictated the use of a unique drive system for the LFSWT. Originally, it was hoped that the excess mass flow capability of the FML compressor could be used to drive a single stage of relatively large injectors to pull the supersonic flow through the test section at the desired test conditions. Our initial design point was Mach 2.5, with a stagnation pressure (Po) of 5 psia (0.34 bar) to achieve flight Reynolds numbers. The compression ratio of the LFSWT necessary to run at this low stagnation pressure would be a very low 0.625:1. This ratio is defined as the ratio between the stagnation (inlet) pressure (Po) and the manifold (exit) pressure (Pe). For a typical Mach 2.5 wind tunnels, a compression ratio of 5:1 is necessary to achieve a start, and a ratio of 2:1 is required to run. Hence, the necessary LFSWT drive system would have to perform in a unique and superior way to achieve LFSWT operation. In recognition of the high risk involved with this unique drive system, a decision was made in April 1989 to build an eighth-scale model of the FML supersonic tunnel. We called this model the *Proof of Concept* (PoC) supersonic wind tunnel. The PoC test section was sized as 1 inch (2.54 cm) high and 2 inches (5.08 cm) wide (See Figure 2), based on mass flow limitations for the full-scale tunnel.

The initial design of the PoC was simple, except for providing adjustability of the injector geometries for drive system studies. It was intended that this work should include a detailed study of the relationship between mass flow and injector exit Mach number. Simplified PoC drive system analyses (based on the work of Riise) were performed on a PC

computer to gain a feel for the performance we could expect. It became clear that the theoretical assumptions of the original design by Riise were not realistic in compressible flow. This was particularly true, with regard to the assumption of perfect mixing of the injector and test section flows occurring within the limited and finite length of the tunnel. In the PoC design, injector mass flow and exit Mach number could be independently varied. The only design features for low-disturbance flow were the minimization of flow joints, and highly polished flow surfaces in the nozzle and test section. These features were considered the basics of maintaining supersonic laminar flow by passive means.

Rapid progress was achieved through the continual involvement of the small design team with the PoC fabrication process, and the PoC was commissioned in October 1989, a mere 4 months after construction was started. However, the initial performance of PoC was well below levels predicted by Riise. Our decision to use an eighth-scale model was well vindicated, in this instance.

We initially achieved Mach 2.5 in the test section with a minimum stagnation pressure (Po) of about 12 psia (0.83 bar). This value of Po was of course significantly above our goal of 5 psia (0.34 bar). The ambient injectors were nevertheless operating at the maximum exit Mach number of 2, set by the fixed compression ratio across them.

The initial poor performance of the PoC drive system demanded more detailed research in the test section and mixing region. Consequently, we designed new side plates for the PoC to provide optical access to the nozzle, test section, and supersonic diffuser (see Figure 3) for use with schlieren/shadowgraph techniques. The flow visualization gave many clues about the complex flow phenomena that existed in the PoC. We noticed a flow separation in the test section exit, leading to premature flow breakdown. We then found that a second throat in the test section exit could significantly delay this separation. By the end of August 1990, we could operate with the Po reduced to 9.9 psia (0.68 bar).

We explored the effect of different second throats downstream of the test section, using a variety of both fixed and variable geometries. Theoretically predictions of these throat effects were computed by King, using a Navier-Stokes code for comparison with PoC data. Unfortunately, the comparisons are only good when the flow in the PoC was well established with Po substantially above its minimum value, and no flow separations present.[11]

Use of long second throats, about 5 times the test section height, provided our best operating condition with a Po of about 8 psia (0.55 bar). The compression ratio across the test section in this condition was unity. This was a major breakthrough in drive system efficiency. The previous best compression ratio was reported as 1.4:1. In addition, no overpressure was required to achieve a start, which of course is in stark contrast to conventional drive systems for supersonic wind tunnels.

With PoC in this configuration, changing the mass flow ratio between injector and test section flow uncovered an optimum value for this configuration at about 7.2:1. This ratio is less than half of what was predicted by Riise. So, if we were to scale up this PoC drive system for the LFSWT, the full-scale tunnel would not utilized the entire mass flow capability of the FML compressor. Consequently, we decided to use this excess mass flow to drive a second stage of ambient injectors and examine any improvement. A second-stage of injectors (orientated at 90° to the primary injectors) with an exit Mach number of 2.0 was installed in the existing subsonic PoC diffuser, during January 1991 (see Figure 4a). The effect on performance was dramatic, and allowed the primary injector Mach number to be raised from 2 to 2.5. This change allowed the PoC to operate at a new low Po of 5.6 psia (0.39 bar) with near Mach 2.5 flow in the test section. Interestingly, still no overpressure was required to start the test section flow. The PoC had finally achieved our original LFSWT design point.[11]

In August 1991, we demonstrated that the PoC's two injector stages could be moved closer together, with no detriment to the drive system performance at Mach 2.5 (see Figure 4b). This finding allowed the proposed LFSWT drive system to be shortened by a significant 16.5 feet

(5.03 m). A schematic of the PoC is shown on Figure 4b to highlight the orientation of the test section to the two injector stages

Because of delays in the LFSWT funding, a new settling chamber was installed in the PoC in October 1991, to provide a low-disturbance free stream for quiet flow studies (described later). This modification was designed to be modular, so that the flow conditioning could be altered as the research progressed (see the settling chamber schematic on Figure 5a and photographs on Figure 5b).

In December 1991, we examined a reduction of the secondary injector mass flows. This work arose from concerns that the scaled-up PoC drive system mass flow may have grown too big for the FML compressor to maintain a Pe of 8 psia (0.55 bar). This drive system tuning showed that, the original PoC drive system was operating close to its minimum mass flow. Any reductions of mass flow incurred an undesirable rise in the minimum Po. We concluded that the LFSWT Mach 2.5 drive system would require a minimum air mass flow of 184 lbs/sec (83.3 kg/sec) with an exit pressure (Pe) of 8 psia (0.55 bar).

A series of compressor tests were carried out in February 1992 to find out if the compressor was indeed capable of driving the proposed LFSWT.[12] Misconceptions about the compressor were revealed, leading to a conclusion that the FML compressor alone could not drive the proposed LFSWT at Mach 2.5. The maximum mass flow capability of the FML compressor was only 163 lbs/sec (73.8 kg/sec), whilst maintaining a Pe of 8 psia (0.55 bar). Consequently, the decision was then made to drop the design Mach number from 2.5. A Mach number of 1.6 was chosen so that the LFSWT test conditions could match actual HSRP flight test conditions flown and to be flown.

To prove the LFSWT drive system at Mach 1.6, a new fixed block nozzle was installed in PoC, and the first runs occurred at the beginning of May 1992. Using the Mach 2.5 two-stage injector system, the PoC operated successfully over a stagnation pressure (Po) range from 5.18 psia (0.36 bar) to 11.99 psia (0.83 bar), as limited by test section mass flow.[13]

As part of our LFSWT cost saving effort, we examined the need for secondary injectors in the LFSWT Mach 1.6 drive system. Since the normal start compression ratio for Mach 1.6 flows is 1.12:1 compared to 2:1 for Mach 2.5 flows, running a tunnel at Mach 1.6 is easier than at Mach 2.5. However, use of the existing FML compressor requires that the LFSWT must still be capable of operating with compression ratios less than unity, to achieve the desired test envelope. A series of PoC tests were performed with different secondary injector mass flows and corresponding changes to the exit pressure (Pe). These tests were based on previous compressor studies[13], which showed that Pe will rise with increasing mass flow in the potential operating band of the LFSWT.

The results of the PoC Mach 1.6 drive system tests are summarized on Figure 6, which shows experimental data plotted against minimum Po and Pe. This data summary clearly shows the need for secondary injectors, if we are to achieve the desired minimum Po. The influence of the secondary injector mass flow on minimum Po is significant compared to the influence of Pe. Consequently, the mass flow of the LFSWT secondary injectors has to be maintained at high levels, similar to the 110 lbs/sec (49.8 kg/sec) proposed for the Mach 2.5 drive system.

The design requirements for the LFSWT (discussed later) are based on our PoC studies, with some flexibility to allow for unforeseen difficulties (see Appendix A). The primary injectors were built with adjustability so that mass flow and Mach number could be changed independently. The range of mass flow available is 62 to 124 lbs/sec (28 to 56.2 kg/sec), and the Mach number range is 1.8 to 2.2. These ranges are intended to allow tunnel operation with a variety of drive system configurations, depending on test Mach number and compressor power available. The secondary injectors have fixed nozzle blocks designed for Mach 2.0 exit velocity with a combined mass flow of 110 lbs/sec (49.8 kg/sec).

During the period December 1992 to February 1993, the effect of model blockage on the

PoC drive system was investigated. Potential models were simulated by a 0.1 inch (2.54 mm) diameter cylinder/probe positioned in the test section, as shown on Figure 7.

Static pressures measured on the PoC sidewall without the probe installed are shown on Figure 8a. These pressure distributions illustrate how the test section flow shocks down in the supersonic diffuser (immediately downstream of the test section exit) at different Po. As expected, the shocks move upstream with decreasing Po. However, over the Po range down to about 5 psia (0.34 bar), the test section is free of shocks. A decrease of test section pressure coefficient (Cp) in the flow direction is attributed to inadequate wall divergence to allow for the boundary layer growth along the test section walls.

Static pressure distributions measured with the probe installed are shown on Figure 8b. These pressure distributions illustrate the dramatic effect of introducing the probe across the tunnel width, at the higher and lower ends of the Po range. The test section flow is started ahead of the model for all probe configurations. Furthermore, the effect of this model blockage was maximized by placing the probe near the entrance of the test section. The shock train generated by the probe was reflected at least four times within the long PoC test section/supersonic diffuser. We expect the number of shock train reflections to reduce to about two in the LFSWT test section. Consequently, we can expect the total pressure of the LFSWT test section flow exiting into the mixing region to be higher than that achieved in the PoC. This increase of total pressure will provide the LFSWT drive system with extra power to overcome unexpected pressure losses elsewhere in the tunnel.

2.2 Laminar Flow Supersonic Wind Tunnel (LFSWT):

The design philosophy of the LFSWT is based on the continuously operating JPL 20-inch Supersonic Wind Tunnel (JPL-SWT), which is now being re-commissioned at NASA-Langley for blowdown operation.[15] The JPL-SWT was the first supersonic wind tunnel with a quiet test envelope at low Re. Documentation of the JPL-SWT quiet flow is unfortunately very sparse at low supersonic speeds[15], so the LFSWT quiet test envelope is actually an extension of the JPL-SWT envelope. Currently, the LFSWT Mach 1.6 test envelope covers part of the Mach 1.6 test conditions flown by NASA F-16XL aircraft (Ship 1 and 2) in support of NASA SLFC studies, as shown on Figure 9. A flexible walled nozzle with SLFC features, a heater and an auxiliary compressor will be required to expand the LFSWT test envelope to cover most of the HSCT operating envelope shown on Figure 9. The LFSWT will then be capable of operating over a low Re range of 1 to 3 million per foot (3.28 to 9.84 million per meter) from Mach 1.6 to 2.5.

The design features of the current LFSWT drive system, settling chamber and supersonic nozzle have been the subject of a joint experimental/computational research effort since 1989 (the beginning of this Cooperative Agreement). The LFSWT represents the first purpose-built quiet wind tunnel for low supersonic testing. The distinctive aerodynamic features of the LFSWT are a low-disturbance settling chamber, laminar boundary layers on the nozzle and test section walls, steady supersonic diffuser flow, and low structural vibration of the nozzle and test section walls.[16,17] Furthermore, the tunnel is designed to run continuously at unusually low stagnation pressures, with uniquely low compression ratios (less than unity). The tunnel achieves this capability by utilizing a unique two-stage injector drive system, described previously.[13]

The LFSWT has an 8 inch (20.32 cm) high, 16 inch (40.64 cm) wide and 32 inch (81.28 cm) long test section, designed with optical access from all four sides. The test section was sized for continuous operation with mass flows up to 27 lbs/sec (12.2 kg/sec). The injector drive system gives the LFSWT a very unusual layout, as shown in the tunnel schematic on Figure 10. Existing support equipment (i. e. the FML indraft compressor and the NASA-Ames 3000 psi - 207 bar dry air supply) were used to substantially reduce the project costs and management complexity. Both these factors significantly contributed to the LFSWT being run for the first time in June 1993, after only 18 months of design and fabrication. A picture of the LFSWT is shown on Figure 1, in situ and operational.

The main features of the LFSWT are research flexibility (ease of removing components and gaining access to the nozzle and test section), a modular and low-disturbance settling chamber, polished flow surfaces, settling chamber/nozzle/test section vibration isolation and 2 stages of ambient injectors as a drive system. Section 5 is devoted to a detailed description of the tunnel.

As project engineer for the LFSWT, the PI defined the aerodynamic lines of the LFSWT, as shown in Appendix A, which were used to write a Requirements Document. Detailed design of the LFSWT was started by NASA engineers in January 1992, and was finally completed in February 1993. During this period, constant supervision of the design became necessary as the PI realized there was inadequate design management. The only changes to the design during this period were the installation and size of the secondary injectors based on parallel PoC research described previously. Regular weekly meetings with Code-E designers and staff were essential to ensuring that the design progressed in an orderly fashion.

During May 1991, the PI assisted with the formulation of a detailed project plan for the interim LFSWT (LFSWT-I). This project plan reflects the support of the High Speed Research Program (HSRP), and was intended to bring the LFSWT-I on-line earlier to impact HSRP. The PI participated in several meetings with HSRP managers, in which we were able to emphasis the significance of ground testing in Supersonic Laminar Flow Control (SLFC) research. Clearly, flight test alone cannot provide the controlled environment, or data quality and density, necessary to validate CFD analyses. We now feel that supersonic ground testing at Ames and Langley has been accepted as an integral part of the HSRP SLFC Phase I and II effort.

Furthermore, the PI participated in five progress meetings with the NASA Ames Director of Aerophysics, Dr. Ron Bailey, through the fabrication process. In these meetings, I was responsible for presenting an update of PoC/LFSWT technical issues. The financial support of Aerophysics Directorate to build the LFSWT relied heavily on the success of these meetings.

Fabrication of the LFSWT started in September 1992 at March Metal Fab, Inc in Hayward, California. The NASA-Ames machine shop then carried out all the precision machining except for the LFSWT nozzle, which was constructed by Microcraft, Inc. in Tennessee. The tunnel installation was completed on schedule by March Metal Fab, Inc in June 1993, a mere 18 months after the LFSWT go-ahead was given. The effort by the PI and a dedicated print-checker to ensure the LFSWT drawings were accurate and coordinated, saved an enormous amount of otherwise wasted time during the fabrication process. Furthermore, the NASA-Ames machine shop has now adopted an improved scheme for tracking the progress of a project based on our requirements for meeting schedules and budgets.

The tunnel was first run in June 1993. Problems with the integration of the FML compressor with the LFSWT injector drive system were solved by extensive injector tuning (see sub-section 7.1). The first model was tested in June 1994 (see section 8), to gain a preliminary understanding of the steady pressures on a swept wing, as a prelude to transition studies later. Currently, an extensive series of flow quality measurements are underway to allow a standard of flow quality for low supersonic quiet wind tunnels to emerge.

3. PoC Laminar Flow Studies

The laminar flow studies with the PoC involved the use of different types of instrumentation to confirm the state of the test section boundary layers. The detection of boundary layer transition tends to be qualitative and our goal was to find at least two measurement techniques which agreed about the location of transition.

We found during January 1992, that the Mach 2.5 hot-wire measurements made above the PoC test section floor, in the outer portions of the boundary layer, indicated a sharp rise in signal rms when Po was about 9 psia (0.62 bar).[13] The signal spectrums were broadband with

no discrete frequencies. Furthermore, the associated rise in signal rms was independent of the signal bandwidth. The behaviour of the signal rms had been seen before in supersonic transition research, where the transition bursting reaches a maximum frequency during the transition process. Unfortunately, the uncalibrated hot-wire data could only be used qualitatively, and these data alone could not prove the existence of laminar flow in the PoC.

To check the reliability of the hot-wire data from the PoC test section, the honeycomb and Rigimesh sheet were removed from the settling chamber. The increase of free stream turbulence had the effect of initiating the rise in signal rms at a lower Po of about 6 psia (0.36 bar) and hence a lower Re. This result shows the strong influence of free stream turbulence on supersonic boundary layers at low supersonic speeds, as first reported by Laufer in 1956.[15]

In another series of tests in March 1992, the test section hot-wire was replaced by a Preston tube. This tube was sized to fit in the lower half of the floor boundary layer. The Preston tube data show that there is a significant rise in the probe Cp at a stagnation pressure of about 8.5 psia (0.59 bar).[13] This rise is associated with the known aerodynamic effects of transition onset, where the boundary layer profile starts changing from a laminar type to a turbulent type. This observation combined with the hot-wire data confirms that laminar flow existed in the PoC over 84% of the test section length, at Reynolds numbers up to about 2 million per foot, at Mach 2.5.

Furthermore, the sidewall boundary layers were studied with a flush-surface-mounted hot-film gage. This gage had previously been calibrated for transition detection in a Mach 3 quiet tunnel. The hot-film data show that the boundary layer on the sidewall remained laminar over the entire Reynolds number range. The hot-film signal rms was seen to jump to expected levels for turbulent flow, only when tunnel leaks caused the nozzle flow to unstart.[13] This flow break down caused transition bypass to occur on the sidewall. In addition, the same leaks caused transition bypass to occur on the test section floor and ceiling, as measured by the hot-wire probe in the test section.

During these studies, there was some concern about the drift in temperature of the inlet air and the PoC nozzle/test section structure. The air supply to the PoC was not heated and the inlet air temperature was always lower than ambient, due to the expansion across a single air regulator. We monitor the inlet air temperature on a regular basis to check for repeatability of test conditions. The thermal mass of the PoC is large compared to the heat transfer associated with the nozzle/test section flow. We have observed the PoC structure reaching near temperature equilibrium within about the first 5 minutes of running. This temperature equilibrium is affected only slightly by changes of inlet air mass flow, despite noticeable changes in the inlet air temperature. To assess the long term effects of temperature drift, we operated the PoC for 2 1/2 hours continuously and monitored our hot-wire and hot-film instrumentation. No significant changes in the test section flow were observed during this test.

When the new Mach 1.6 nozzle block was fitted to the PoC in May 1992, hot-wire measurements were repeated on the floor centerline of the test section. These measurements in the test section were made at the same convenient streamwise location used previously at Mach 2.5 (X=6.83). The hot-wire was 5 micron (200 micro-inches) in diameter and made of Tungsten. The height of the hot-wire above the floor was fixed at 0.069 inch (1.75 mm). The hot-wire signal rms over the frequency range 30 Hz to 50k Hz is shown on Figure 11, plotted against Po. At a Po of about 7.3 psia (0.5 bar), there is a decisive change in the slope of the data from numerous tests. This repeatable change in slope is a clear indication where transition has occurred. The comparison with the Mach 2.5 data shows that transition occurs at a lower Po at Mach 1.6, which may indicate a sidewall influence on the floor boundary layer. The transition Reynolds numbers (related to distance from the nozzle throat) is approximately 1.3 million at Mach 1.6, which is less than the 1.4 million Reynolds number at Mach 2.5.

Other boundary layer measurements were made with a 0.015 inch (0.38 mm) OD Preston tube in the same streamwise location as the hot-wire (X=6.83) at repeat test conditions, as shown on Figure 12. Again, there is a slope change in the data which is indicative of transition

at a Po of about 7 psia (0.48 bar). Notice that the probe Cp for laminar flow is less at Mach 2.5 than at Mach 1.6 as expected. The size of the Preston Tube was reduced to take account of the thinner boundary layer at Mach 1.6. Measurements from a larger 0.029 inch (0.74 mm) OD Preston tube were taken at different streamwise (X) locations, to confirm this situation. Only when the 0.029 inch (0.74 mm) OD probe is positioned at the downstream end of the test section (at X=8.38), where the boundary layer is thickest, does the probe detect transition.

Flow visualization of the supersonic boundary layer on the floor of the PoC was achieved by using a novel focusing schlieren technique with our original polycarbonate windows. Unfortunately, the reduction in light intensity due to these windows made boundary layer density gradients indistinct. Consequently circular glass inserts were fitted to improve the visualization, as shown on Figure 13. The new windows allowed our focusing schlieren system to capture images of the boundary layer at different Po. The depth of focus of the system was of the order 0.25 inch (6.35 mm). In Figure 14, we compare pictures of the boundary layer on the tunnel centerline, at two values of Po, after image processing (subtraction of a reference wind-off image and contrast enhancement). Clearly, the boundary layer at Po = 11 psia (0.76 bar) is thicker than at Po = 6.8 psia (0.47 bar), contrary to Reynolds number effects. Furthermore, some turbulent bursting is present in the boundary layer at Po = 6.8 psia - 0.47 bar (indicative of a transition process) which appears to stop when Po is approximately 7.2 psia (0.5 bar). This observation of a transition process, of course, compares very well with our other instrumentation. Furthermore, over the Po range from 7.2 to 11 psia (0.5 to 0.76 bar) no change in the boundary layer was observed, so the bursting phenomena is distinct from any other aerodynamic effects.

Real-time visualization of the floor boundary layer was also obtained using conventional Toepler schlieren. We made a high speed cine-film (400 fps) of the boundary layer over the complete Po range, which clearly showed the same turbulent bursting occurring around Po = 7 psia (0.48 bar). This further collaborated our previous findings, despite the fact that this schlieren technique integrates the boundary layer density gradients across the entire width of the tunnel. Interestingly, this flow visualization represents a first in quiet wind tunnel research, and clearly shows the transition process in the tunnel wall boundary layers.

Due to size constraints, it was impractical to traverse any probes streamwise through the PoC test section/nozzle. However, a hot-film array was bonded to the tunnel ceiling so that the movement of transition with Po could be observed. Care was taken to mount the array so that the flow over the array would not encounter any surface irregularities, such as the leading edge of the substrate. The array consisted of 20 hot-films attached to a Kapton substrate (see Figure 15a). A special PoC window was made which allowed one edge of the substrate to protrude through the window carrying the hot-film signal leads. The window sealed around the substrate to prevent flow into the tunnel. The substrate was 0.002 inch (0.051 mm) thick and the hot-film and leads were less than 0.001 inch (0.0254 mm) thick. The hot-film array was bonded to the ceiling of the PoC nozzle and test section, as shown in Figure 15b, and extended upstream to the entrance of the contraction. The hot-film sensors were positioned in the plane of the tunnel centerline at 0.5 inch (12.7 mm) intervals.

The hot-film signals were monitored one at a time, because only a single specialist constant-current circuit was available. The hot-films were operated at a current of 125 milliamps, which corresponds to a 1.3 overheat condition. The hot-films could not be operated in a wind off condition without risk of sensor burnout. The hot-film results are summarized on Figure 16 for different Po. There is a peak in signal rms for each Po which is due to transition on the PoC ceiling. These peaks move upstream with increasing Po, in the same manner as the transition front was observed to move using schlieren visualization. At the location of other test section flow measurements (X=6.83) transition is shown to occur at a Po of about 6 psia (0.41 bar), which is significantly lower value than found in the floor measurements. Unfortunately, bubbling of the hot-film array was observed during these hot-film tests, which curtailed further useful measurements, and may indeed have contaminated all or part of the hot-film data. However, these tests did confirm that there is a transition front moving the length of the test section walls. No transition was detected in the nozzle during these tests.

Horizontal-plane vibration measurements were made close to the PoC Mach 1.6 nozzle using a capacitive-type accelerometer. At Po = 5 psia (0.34 bar), the acceleration was 0.045g over the frequency range 14-1000 Hz. At Po = 9 psia (0.62 bar), the acceleration was 0.041g. In the PoC, there was no means of isolating the nozzle test section from the injector drive system. The effect of nozzle/test section vibration on laminar flow is currently unknown and will be studied in the LFSWT, which incorporates vibration isolation for the settling chamber, nozzle and test section.

Temperature of the PoC flow is controlled passively. The thermal mass of the PoC nozzle and test section is large relative to the flow surfaces. Hence, wall temperature stability is achieved within a few minutes of starting a run and is relatively insensitive to changes in Po (mass flow). The wall temperature is generally 20° F (11° C)below ambient, and is similar to the inlet stagnation temperature. Repeatability of laminar flow measurements is monitored at the end of each run to check for temperature drift. No effects of temperature drift have been observed in the measurements discussed here.

In conclusion, four transition locating techniques have been used in the PoC. Three of these techniques are in rough agreement. Clearly, laminar flow was being maintained through the nozzle and part of the test section on the centerline, satisfying one of the requirements of quiet flow. The actual cause of transition in PoC is not clear. In fact, transition was not predicted in any part of the PoC test section by CFD analysis. We are sure that more knowledge will be gained from studying the larger LFSWT. It may then be possible to delay the onset of transition until higher Reynolds numbers, above 2 million per foot, as achieved on flat plates.

4. PoC Flow Quality Measurements

Test section flow disturbance measurements were made in the plane of the PoC nozzle exit (X=3.47) on the tunnel centerline (see Figure 7). A 0.093 inch (2.36 mm) diameter Kulite pressure transducer was fitted to a pitot probe for these tests. The ratio of the total pressure rms (Prms) to stagnation pressure (Po) was below 0.09% over the entire Po range (for the frequency bandwidth from 30 Hz to 50k Hz), as shown on Figure 17. The dynamic pressure data had a broadband frequency response. These data indicate that the test section flow is low disturbance at the entrance over the Po operating range. As found in the settling chamber measurements, the pressure ratio (turbulence) increases linearly with Po. The two data sets are from different tunnel runs separated only by time. As expected, repeatability at low Po is difficult to achieve because the signal to noise ratio is very large.

A limited off-centerline survey of the flow at the test section entrance (X=3.47) is shown on Figure 18. These data indicate that the turbulence at this streamwise location has a three-dimensional distribution, which is not symmetrical about the tunnel centerline. For the data taken +0.9 inches (+2.3 cm) from the tunnel centerline, the pitot probe is within 0.05 inch (1.27 mm) of the sidewall, and is partially immersed in the sidewall boundary layer. Unfortunately, there is no corresponding turbulence survey of the settling chamber flow to determine if the settling chamber is the cause of this three dimensionality observed in the test section flow disturbances. Since disturbances from the tunnel walls will propergate downstream along Mach lines, the maximum streamwise displacement of wall/corner disturbance and centerline measurement is 1.396 inches (3.54 cm) at Mach 1.6. (Lower Mach numbers in the nozzle will reduce this displacement). So, if wall/corner disturbances were the cause, the origin of the disturbance must be downstream of the nozzle throat. Therefore, the disturbances cannot be directly linked to the upstream edges of the nozzle windows, which are located in the contraction, as shown on Figure 3.

Off-centerline surveys of the floor and ceiling boundary layers were made in the PoC test section using a 0.015 inch (0.38 mm) OD Preston tube. Measurements were performed at three streamwise locations on the floor (X=4.52, 6.83, and 8.38) and one streamwise location on the ceiling (X=6.83). The floor Preston tube data are shown on Figures 19a, 19b and 19c over the

Po range. At X=4.52, the boundary layer appears two-dimensional out to between +0.5 inch (+1.27 cm) and +0.75 inch (+1.9 cm) from the centerline. At X=6.83, the boundary layer has some symmetry about the plane of the tunnel centerline, but two-dimensionality is within ±0.25 inch (±6.35 mm) of the centerline. At X=8.38, the two-dimensionality of the boundary layer extends out to between +0.25 inch (+6.35 mm) and +0.5 inch (+12.7 mm) from the centerline. Interestingly, the flow should be shocking down at this downstream location, when Po is less than 6 psia - 0.41 bar (see Figure 8a), but this is not shown in the pressures. Data near the sidewall/floor corner shows that the probe Cp asymptotes to about 0.5 for Po greater than 6 psia (0.41 bar). The sidewall induced boundary layer flows described by King[14] may be responsible for this behaviour, and further studies will be carried out in the larger LFSWT.

There are several conclusions to be drawn from these measurements. Firstly, two-dimensional quiet flow is restricted in the PoC. Secondly, no propagation of disturbances can be inferred from the data. Finally, more research is required to realize the clearly defined quiet test core envisaged in quiet wind tunnels, as shown on Figure 20.

5. LFSWT Description

5.1 Inlet Air Supply:

The LFSWT test section is fed with regulated, unheated, dried air from the NASA-Ames 3000 psi (207 bar) supply. This supply provides a source of air with a low dew point of about -50° F (227 K) and does not drive the tunnel. Dried air is, of course, critical to the successful operation of a supersonic tunnel, and moisture in the inlet air is monitored periodically.

For current Mach 1.6 operations, the stagnation pressure (Po) in the settling chamber is variable up to 10.3 psia (0.71 bar), which corresponds to a maximum mass flow of 26.17 lbs/sec (11.85 kg/sec) with To = 0° F (255 K). This maximum mass flow does not compromise continuous operation, which is measured in hours. For higher Mach number operations, the mass flow will decrease as the size of the associated nozzle throat reduces. The low stagnation pressures are necessary to achieve low Re operation, and minimize the loading on settling chamber components.

The inlet air cools due to expansion, such that the stagnation temperature in the settling chamber drops about 60° F (33.3° C) below ambient. This large temperature drop stabilizes in the settling chamber after about 20 minutes of tunnel operation.

5.2 Settling Chamber:

We designed the settling chamber to take full advantage of the interactions between components for turbulence manipulation and minimization. Our goal was to provide low-disturbance flow (acoustic fluctuations < 0.2% and vortical fluctuations < 1%) upstream of the nozzle contraction. A modular settling chamber design was chosen to provide research flexibility, as shown schematically on Figure 21. The design is similar to that proven in our PoC tunnel.[13]

The settling chamber is equipped with pressure reduction elements, which restrict the inlet flow and help isolate the settling chamber from upstream inlet disturbances; a series of flow straighteners and flow conditioners; and vibration isolation from the inlet piping, and support and injector structures. The modular design allows for component holder interchangeability should improvements be necessary to overcome larger than expected inlet disturbances. The flow velocity through the settling chamber is governed only by the stagnation temperature (To), since the size of the nozzle throat is fixed. For example, a To of 9° F (260 K) produces a flow velocity of 44.04 fps (13.42 m/sec). The settling chamber is 39.24 inches (0.99 m) square, and is 76.75 inches (1.95 m) long between the most upstream and downstream screens.

The pressure reduction elements consist of concentrically mounted cans, as found in a

typical muffler (silencer). Each element (can) is lined with sheets of porous sintered filter material (call Rigimesh), which is supported by perforated sheets welded to the can frame. The Rigimesh used is Type-J, which is 0.006 (0.15 mm) thick and has a pore size of approximately 234 micro-inches (6 micron). Up to three pressure reduction elements can be used together. The most upstream element (and hence the smallest element) has a solid end cap, while the other elements have a perforated end cap to maintain some streamwise flow into the settling chamber. The flow out of the last (downstream) element is predominantly orthogonal to the tunnel centerline, since the ratio of the flow area around the cylinder to the flow area on the end-cap is 4.9:1. This flow condition ensures that the incoming air is forced to spread over the entire cross-section of the settling chamber. The inlet piping has an internal diameter of 7.19 inches (18 cm), so the air flowing into the settling chamber must experience a 38:1 change in cross-sectional area. However, the area of the flow exiting the last pressure reducing element is over 12.5 times the inlet pipe flow area. So, a 300% increase in flow area has to occurs in the short length of the housing for the pressure reduction elements.

The pressure drop across the three elements is useful for two reasons. First, the pressure drop is a good isolator to prevent propagation of upstream flow disturbances into the settling chamber. Second, the elevated pressure in the inlet piping prevents choking and allows smaller diameter pipes and valves to be used for the inlet air. The actual pressure drop across the elements varies up to an estimated maximum of 19 psia (1.3 bar). Actual measurements have been hampered by instrumentation drift. To achieve higher stagnation pressures (above 10 psia - 0.69 bar) in the settling chamber, it became necessary to remove the first pressure reduction element to lower the inlet piping pressure at high Po. No detriment to the settling chamber flow quality was observed by using only two pressure reducing elements.

The pressure reduction housing is 35.25 inches (89.5 cm) long and includes a rapid change in cross section shape from circular to square. The housing also includes a 0.5 inch (1.25 cm) thick rubber isolator (60 durometer) to prevent conduction of valve and inlet piping vibration into the settling chamber/test section walls.

Downstream of the pressure reduction housing is situated a 2-mesh "churning" screen, which is 57.8% open (to avoid jet coalescence and boundary layer disturbances[17]). This coarse screen is intended to manipulate the non-uniform flow exiting the Rigimesh[18] into a uniform turbulent flow across the cross-section of the settling chamber. This coarse screen is 13.62 inches (34.6 cm) downstream of the last pressure reducing element. A 44.5 inch (1.13 m) long plenum section follows this first screen to allow natural vortical decay to occur. The plenum length is equivalent to 89 mesh lengths, so is more than the 50 mesh lengths required for the screen turbulence to decay, according to Groth and Johansson.[19]

The second and third screens are respectively 20-mesh (57.8% open) and 42-mesh (59.1% open), situated 80 mesh lengths apart, for the reasons stated above. All the screens are held only by the edges, so no support structure disturbances are generated. The second and third screens are intended to break down any large eddy structures in the flow into smaller scale structures, which will pass harmlessly through the honeycomb without stalling cells. Situated 210 mesh lengths downstream of the 42-mesh screen is the honeycomb for flow straightening. The honeycomb cells are 0.25 inch (6.35 mm) across with an aspect ratio of 8:1. The 2 inch (5.08 cm) thickness of the honeycomb was a compromise between achieving a high enough cell aspect ratio, while preventing flow non-uniformity due to large low-Re boundary layer growth in the cells, at sub-atmospheric stagnation pressures. The option remains to increase the honeycomb thickness up to 6 inches (15.24 cm) with an aspect ratio of 24:1, if flow straightness becomes a problem in the settling chamber.

Eight inches (20.32 cm) or 32 cell lengths downstream of the honeycomb, we have positioned a series of four 42-mesh screens (59.1% open). This separation distance is sufficient to ensure honeycomb wake decay. The ratio of the honeycomb mesh to the screen mesh is 10.5:1, which is small enough to prevent a spectral gap between the two characteristic scales of turbulence. The four screens are placed 168 mesh lengths apart to allow sufficient decay of screen generated turbulence between screens. These multiple fine screens provide the

mechanism to breakdown the flow turbulence into miniature structures in a relatively short streamwise distance, before the squeezing and stretching of the contraction and nozzle. Incidentally, the last screen is used above its critical Reynolds number at between 50 and 100. However, the eddies shed from this screen are considered minute compared to the disturbances that already exist in the flow.

The contraction boundary layers are assumed to start from the most downstream screen of this series. Only a 4.5 inch (11.43 cm) thick instrument holder separates the most downstream screen from the contraction (See Figure 21). We consider it undesirable to separate the contraction and downstream screen by a significant streamwise distance. Minimizing boundary layer development ahead of the contraction will reduce the boundary layer thicknesses along the contraction and sidewalls. These thinner boundary layers are then less receptive to transition instabilities due to Görtler vortices in the concave sections of the contraction.

The instrument holder is permanently attached to the contraction, and its flow surfaces and joint to the contraction are hand finished to a very smooth 10L finish (described in the next sub-section). The holder has static pressure taps for Po measurement, and provides a mount for our settling chamber probes, described later.

5.3 Nozzle and Contraction:

The nozzle and contraction are fabricated as one component out of 6061-T6 aluminum, as shown on Figure 22. This material is capable of taking a fine polish and is relatively non-corrosive. The design removes the joint between the nozzle and contraction that might otherwise cause premature boundary layer transition on the walls. The complete assembly is 75.38 inches (1.91 m) long, consisting of 48 inches (1.22 m) of the three-dimensional contraction and 27.38 inches (69.54 cm) of nozzle length, from throat to exit.

The shape of the three-dimensional contraction was calculated separately for the horizontal and vertical walls, using fifth-order polynomials. These calculations were made with numerical boundary conditions of zero surface slope and curvature at the upstream and downstream ends. A fifth-order polynomial was chosen for the contraction shapes to minimize the potential for flow separations. The LFSWT contraction is significantly smoother than that of the JPL-SWT. The difference between the LFSWT contraction shapes for the floor/ceiling and the sidewalls is due to two factors. First, the sidewalls are flat and parallel 28 inches (71 cm) upstream of the nozzle throat, to allow nozzle windows to be fitted. Secondly, the nozzle throat is rectangular (wider than it is tall) as discussed later. Since the settling chamber is square, the contraction ratio based on the throat dimensions is 6.2:1 vertically and 2.45:1 horizontally, which combine to give an overall high contraction ratio of 15.25:1. (The overall contraction ratio based on the test section dimensions is 12:1, which is above average). The ratio of contraction length to unit area change is 0.86:1 horizontally, and 1.46:1 vertically. Ratios of one or greater would be preferred, but fabrication compromises led to a shorter than optimum sidewall contraction.

The corners between the contraction walls are near sharp, since the floor and ceiling were made separately and fit between the sidewalls. No radius was introduced in the corners to delay or modify corner flows, but this is an option for the future.

The nozzle is two-dimensional, fixed-block type designed according to the methodology of Riise[20] (as used on the JPL-SWT nozzle) with allowance for laminar boundary layer growth on all four walls. Consequently, the nozzle has an 1.267:1 area ratio which is larger than the theoretical value (1.25:1) for Mach 1.6 flow. The nozzle has a relatively long expansion section (compared to other design methodologies[21]) with surface curvature minimized. The maximum G?rtler number along the nozzle walls is about 7 (safely below the accepted transition threshold of 10.4), at a location some 19 inches (47.5 cm) from the throat. The nozzle exit was constrained to the test section dimensions during the design process.

A two-dimensional nozzle was chosen to eliminate nozzle shape imperfections being

focused on the tunnel centerline, and to provide optical access to the nozzle. A rectangular cross-section was chosen to move the sidewalls away from the tunnel centerline. The ratio of nozzle width to height is a maximum of 2.5:1 at the throat, reducing to 2:1 at the nozzle exit. Consequently, any disturbances in the corners of the nozzle and test section will radiate to the tunnel centerline further downstream than in a square test section. Also, we can speculate that the propagation of these corner disturbances may be delayed by making the corner vortices as close together as possible near the sidewalls, using a rectangular cross-section.

Both the nozzle and contraction flow surfaces were hand finished to an achievable 10L standard (roughness height 10 micro-inches - 0.25 micron), which is a mirror-like finish (See Figure 22). This roughness corresponds to a maximum roughness Reynolds number of 3.3 at the nozzle throat, which is below the generally accepted limit of 12 for laminar flow.[17] The 10L standard is an rms roughness, which could hide 100 micro-inch (2.5 micron) peaks, which are ten times the rms value according to Beckwith from NASA-Langley. A 2L finish is possible with the nozzle material. So, we could improve the LFSWT surface finish should we find that roughness is causing premature transition in the nozzle boundary layers. Incidentally, all hand finishing was performed only in the streamwise direction to minimize the potential for spanwise scratches, which are a well known source of transition.

The 75.38 inches (1.91 m) long nozzle/ contraction was constructed very precisely. For example, in the spanwise direction, the throat varies only 0.016 inch (0.04 mm) in height, with the contraction entrance and nozzle exit set within 0.001 inch (0.025 mm) using assembly fixtures. Deviations in the nozzle contour are very small (i.e. <0.006 inch - 1.52 mm), so wall waviness was minimized.

The nozzle sidewall windows extend from 8.89 inches (22.22 cm) upstream of the nozzle throat to 23.736 inches (60.29 cm) downstream. Vertically, the windows extend beyond the floor and ceiling, to give optical access to the wall surfaces. However, window blanks are currently fitted, which are made of the same material as the nozzle and contraction, to prevent steps and gaps being formed. The sidewall boundary layer could be tripped by the potential steps and gaps between the dissimilar materials of the windows and sidewalls. These disturbances could be the result of the temperature excursions during tunnel operation and/or temperature variation through the nozzle throat. To remove these steps and gaps when using the actual windows, a difficult shrink fit appears necessary at room temperature. Since, our attention is currently focused on the test section, we have decided that our experience with steps and gaps in the test section will determine how to best approach the fit of the windows in the nozzle sidewall.

The nozzle and contraction are supported by Korfund vibration isolators, which are mounted to a linear-bearing rail and support structure. Since the settling chamber is isolated from vibration coming from the inlet piping, and the test section is isolated from the injector disturbances, the nozzle and contraction structures are completely isolated. A capacitive-type accelerometer mounted on the nozzle sidewall has recorded accelerations of only 0.02 g (0.64 ft/sec/sec - 0.2 m/sec/sec) over a frequency range from 14-1000 Hz, with the tunnel running. This vibration level is half of that recorded on the non-isolated PoC wind tunnel. Of course, the large mass of the nozzle and contraction (2,354 lbs - 1,068 kg) also helps eliminate vibration due to radiated noise.

Modification of existing components or changes to the component configuration is relatively straight-forward. First, a pipe spacer and/or spool in the inlet piping must be removed. This action allows the tunnel to be parted at the desired joint, e.g. between contraction and settling chamber. Upstream tunnel components are simply pushed out of the way on a linear bearing system, which provides excellent re-alignment.

5.4 Test Section:

The test section is 8 inches (20.32 cm) high, 16 inches (40.64 cm) wide at its entrance, and 32 inches (81.28 cm) long. The design consists of four windows and a frame, as shown on

Figure 23. Like the nozzle, a rectangular cross-section was chosen for the test section to move the flow corners away from the tunnel centerline. The windows are made of 2.0 inches (5.08 cm) thick optical quality Plexiglas (UVT grade), and account for 61% of the test section surface area. The frame is fabricated from 6061-T6 aluminum. The windows are manufactured with an interference fit on the window frames at room temperature, to minimize steps and gaps. The environment for the test section windows is much more uniform than found in the nozzle. A 5° taper is provided on the window and frames to simplify window removal and replacement.

The stagnation temperature in the test section has been measured at 86° F (47.8° C) below ambient. This low temperature (typically -16° F - 246 K) is stabilized after about 20 minutes of tunnel operation. This temperature drop does have an effect on the magnitude of the steps and gaps between windows and frame. Before temperature equilibrium is reached, test section steps and gaps reach a maximum. Fortunately, only the upstream window joints are critical to boundary layer stability in the test section. Consequently, it may be possible to remove any gaps that do appear on the upstream joint with appropriate loading of the windows in the streamwise direction.

The test section floor and ceiling diverge at a total angle of 0.5° downstream as an allowance for boundary layer growth on all four walls. The sidewalls are parallel. The test section is cantilevered from the nozzle contraction, and the critical joints with the nozzle are hand finished to the same 10L standard applied to the nozzle and test section flow surfaces. The downstream end of the test section is attached to the supersonic diffuser/injectors by a rubber isolator, to prevent conduction of injector vibration into the test section/nozzle structure. A capacitive-type accelerometer mounted on the test section sidewall frame has recorded accelerations of 0.038 g (1.22 ft/sec/sec - 0.37 m/sec/sec) over the frequency range 14-1000 Hz, with the tunnel running.

Models and instrumentation can be mounted in the test section from window blanks fitted in any of the four possible locations. A pair of windows are fitted with thermocouple wells, so that the window temperature can be monitored at three streamwise locations.

5.5 Supersonic Diffuser:

Attached to the downstream end of the test section by a rubber isolator is the supersonic diffuser, which decelerates the test section flow to match the pressure in the injector mixing region. The total length of the diffuser is 16.75 inches (42.5 cm) including the rubber isolator and trailing edge cap. The ratio of length to height is 2:1. The diffuser is a parallel-walled type.

5.6 Injector Drive System:

The LFSWT injector drive system has two-stages of ambient injector and is a scaled-up copy of the system developed using the PoC wind tunnel.[22] Modifications to the drive system arose due to the interaction of the drive system with the FML indraft compressor (see sub-section 7.1). Nevertheless, the LFSWT has demonstrated that the drive system concept can be scaled up successfully, and the LFSWT does operate with compression ratios (ratio of stagnation pressure to exit pressure) less than unity.

We are now able to operate the LFSWT at Mach 1.6 over a useful range of Reynolds number from 2.6 to 3.8 million per foot (8.53 to 12.46 million per meter). The minimum Re is higher than planned due to both the lower than expected drive system performance, and the low stagnation temperature.

5.7 Tunnel Control System:

The LFSWT is operated using an industrial-type control system with a PC Windows man/machine interface, running on an ordinary 486/33M Hz computer. A real-time display shows inlet air parameters and the status of valves, which is continuously logged for post-test

analysis. The complexities of the LFSWT start and shutdown are handled automatically to prevent compressor surge. Control system tuning was achieved by mainly software changes, and this level of flexibility greatly reduced the tuning task begun in July 1993. At present, only Po is available for setting tunnel operating conditions. Control of To will be possible when an inlet air heater is installed.

Stagnation pressure is controlled by a PID loop with variable parameters. Operator input to Po set point and PID factors is via the real-time display using keyboard input or graphical 'drag and click' sliders. The PID controller can in general hold Po within 0.1 psia (0.007 bar).

6. Instrumentation Overview

Testing the PoC supersonic wind tunnel allowed the development of instrumentation for transition detection to proceed before the LFSWT was available. Furthermore, the PI assisted the FML in formulating instrumentation requirements for future supersonic testing, with particular reference to hot-wire probes, hot-film gages and arrays, temperature and pressure probes and transducers, and schlieren optics.

In October 1991, the PI brought together a dynamic data acquisition system built around a Tektronix 2642A Fourier Analyzer, coupled to a 486/33 MHz PC computer. This system has the capability of simultaneously sampling up to four channels of input, at rates up to 512k Hz with 16-bit resolution. Furthermore, Fast Fourier Transforms (FFTs) can be averaged and displayed in a few seconds with a user-friendly graphics interface. All calculations are carried out by parallel processors in the Fourier Analyzer.

For thermocouple data, the PI purchased a Dianachart Therm-ACQ system which can handle up to 48 channels of Type-T thermocouple input. The data from the Therm-ACQ system is transferred to a PC computer for display and storage. This system is used to monitor tunnel wall and model temperatures.

We now have a mark III version of our *Focusing Schlieren* system (shown on Figure 24) which is based on a design by Weinstein of NASA Langley.[23] The focusing schlieren system is set-up to focus on a slice of the illuminated flow field about 0.25 inch (6.35 mm) thick. Glass window inserts were fitted in the PoC to reduce out-of-focus images and increase illumination intensity. This change and increased separation between optical components made the schlieren system sensitive enough to visualize supersonic boundary layers with small density gradients at low stagnation pressures. Nevertheless, the boundary layer image captured on a single frame is difficult to see and requires image processing to improve image contrast. High speed video (200 fps) has proved to be successful and gives a clear view of transition bursting. In the LFSWT, glass windows are not yet available, so only shadowgraph is available to visualize shock patterns.

For static pressure measurements in the LFSWT, an array of pressure taps, 0.12 inch (3 mm) in diameter, were placed in the settling chamber and several 0.026 inch (0.66 mm) diameter taps in the test section. Up to 96 averaged pressures can be measured using a scanivalve system connected to a PC A-to-D card sampling at 1k Hz. The scanivalve contained 4 transducers, each of which can be connected to 24 pressures. A real-time display of up to 4 pressures was used by the researcher to judge when test conditions were set for data collection.

A custom-built single 5-micron (200 micro-inch) Tungsten wire was used in the test section probe, and a commercial single 4-micron (160 micro-inch) Tungsten (platinum coated) wire in the settling chamber. Both hot-wires were powered by the FML's own constant-temperature bridge circuits. Tuning of the circuits was completely manual using a square wave signal excitation. Optimum tuning was achieved with the tunnel running, such that a hot-wire response of 80k Hz was possible in the settling chamber and 25k in the test section. The output signals from the hot-wires were fed to a Tektronix 2642A Fourier Analyzer system, which handles up to 4 simultaneous inputs. The Fourier Analyzer can sample each input signal at up to 512k Hz with 16-bit resolution using a Hanning window and anti-alias filtering. The

Analyzer also provides averaged 4096-point real-time Fast Fourier Transforms (FFTs), data capture and display. Twenty FFTs were averaged for each power spectra measurement by inspection. In addition, we generally acquired several averaged power spectra at each test condition to determine the 'best' average. All data were then collected on a PC computer for data archiving, post processing and data presentation.

The settling chamber hot-wire was calibrated in-situ by varying Po during tunnel operation, which corresponded to changing only the flow density since the nozzle throat is fixed. A simple King's law relationship defines the wire's response very well. However, the calibration does rely on the assumption that the hot-wire's response to density changes is the same as the hot-wire's response to velocity changes. This is a reasonable assumption for the range of settling chamber conditions encountered. Fluctuating flow quantities were obtained from the sensitivity of the mean hot-wire voltage to mass flow changes (the product of density times velocity) after subtracting a wind-off rms voltage. The sensitivity was computed from mean data recorded at the same time as the fluctuating data. No calibration was possible of the hot-wire mounted in the test section, due to the uncontrollable coupling between LFSWT test conditions.

The miniature pressure transducers used were Kulite XCS-093 type with 15 psi (1 bar) pressure differential range. These transducers are 0.093 inch (2.36 mm) in diameter, and considerably more robust than hot-wires. The Kulites are sensitive to changes in To, so real-time calibrations are made for each run. Frequency response is up to 150k Hz. The Kulites are powered by high frequency response signal conditioners (Dynamic 8000s with a 3dB dropoff at 500k Hz). The output signals are then fed to the Fourier Analyzer for capture, analysis and display, as for the hot-wire signals. Fluctuating pressures were obtained from the sensitivity of the average DC transducer voltage to mean pitot pressure. This sensitivity was calculated from data recorded at the same time as the fluctuating data.

Dynamic flow measurements were made in the settling chamber and the test section. In the settling chamber, probes could be mounted from one or both of the sidewalls, 1 inch (5.1 cm) downstream of the last screen (X=-51.5) at the contraction entrance. The probes could be traversed across the entire span of the settling chamber. Three different instruments were used in the settling chamber: a pitot pressure probe; a hot-wire probe; and a pitot temperature probe containing a Type-T thermocouple.

In the test section, a sidewall window blank was used to mount two traversable probes at different streamwise and height locations. The probes were fitted with either a hot-wire or a Kulite pressure transducer. A manual traverse was used to accurately position the probes across the flow up to and beyond the tunnel centerline.

Dynamic pressure measurements were also made in the supersonic diffuser using a wall mounted Kulite XCS-190 pressure transducer with a 15 psi (1 bar) differential range.

7. LFSWT Commissioning

7.1 Drive System Tuning:

The initial LFSWT runs in June 1993 demonstrated a low level of performance, in terms of Mach number and Reynolds number range. This was a consequence of assuming that the FML indraft compressor would perform as it had for the small-scale PoC drive system.[21] However, the fact that the LFSWT was designed to have research flexibility, allowed us to tune the High Pressure Air (HPA), injector drive and compressor control systems. Initially, the most critical problems to be addressed were ensuring the compressor would survive a tunnel shutdown, and properly starting the injectors. The first problem was solved quickly by appropriately freezing the compressor controls before the tunnel shutdown. This procedure prevented the compressor safety parameters exceeding pre-determined surge limits, and required only control software changes. The problem with the injectors was much more complicated,

and centered around the inability of the compressor to pull the start-up shocks though the injector nozzles. The LFSWT drive system was a direct scale-up of the pilot PoC system described earlier. This problem did not occur in the PoC tests because the pilot tunnel's volume was much smaller than that of the compressor manifold.

The manifold pressure at the compressor inlet was as predicted, but what we could not predict was the size of the pressure surge in the manifold at tunnel startup. Here it is useful to explain that the tunnel starts by opening a 60-inch (1.52 m) diameter butterfly valve at the point where the LFSWT subsonic diffuser meets the compressor manifold. Hence, the manifold sitting at 8 psia (0.55 bar) ingests a relatively large slug of ambient air from the LFSWT at startup. This slug of air causes a pressure spike in the manifold with a peak typically greater than 10 psia (0.69 bar), as shown on Figure 25. This static pressure rise reduces the pressure ratio across the injectors (ratio of upstream stagnation pressure to downstream stagnation pressure) at a critical time when the maximum available pressure ratio is required. The tuning of compressor response to the 60-inch (1.52 m) valve opening, and making the valve open faster has reduced the duration of the pressure spike to a minimum of 3 seconds. We believe, the only way of further minimizing the effect of this pressure spike would be to suck down part or all of the injector drive system to the manifold pressure before startup. Unfortunately, major engineering changes would be necessary to provide this modified startup procedure. There is no doubt that the slug of ambient air entering the manifold at startup would be significantly reduced, and the injectors would experience a larger pressure ratio at startup. This modified startup procedure currently remains an engineering option for increasing the LFSWT Mach number at a future date.

Since the duration and amplitude of the manifold pressure spike could not be improved further, we attempted to overcome the injector starting problem by increasing the pressure ratio across the injectors. The inlet air to the injectors is ambient and uncontrollable. So, only the downstream stagnation pressure can be adjusted down to a minimum of 8 psia (0.55 bar). By reducing the overall tunnel mass flow, the manifold recovery pressure was lowered, based on our previous studies of the compressor performance.[12] The primary injectors were reduced in mass flow using the movable plates shown in the composite photograph on Figure 26. This adjustment lowered the tunnel mass flow from about 200 to 185 lbs/sec (90.6 to 83.8 kg/sec), which reduced the manifold pressure from 9.4 to 8.7 psia (0.6 bar). This change allowed us to achieve Mach 1.6 in the LFSWT test section, albeit with unstarted injectors. A further mass flow reduction of 24 lb/sec was achieved by installing pairs of 5 inch (12.7 cm) high wooden blocks in the fixed secondary injectors (as shown fitted to the right hand secondary injector exit on Figure 27). The tunnel mass flow was then reduced to about 160 lbs/sec (72.48 kg/sec), which dropped the manifold pressure to the minimum of about 8 psia - 0.55 bar (as shown on Figure 28). However, this change only slightly increased the secondary injector exit Mach number to 1.27, still significantly below the design Mach number of 2.0. Clearly, the injectors were still not started.

One of the two fixed secondary injectors was then instrumented with a streamwise row of pressure taps on the centerline, to identify the reason for the injectors not starting. As shown on Figure 29, the local static pressure reached a minimum before the nozzle exit independent of different test conditions, which confirmed that a startup shock system was trapped in the nozzle. This minimum injector pressure equates to a Mach number of about 1.8, which is significantly higher than the achieved exit Mach number of about 1.27. We can attribute the existence of this trapped shock system to a combination of a non-iscentropic nozzle shape, and an inadequate pressure ratio at startup. Since the pressure ratio could not be improved without significant tunnel modifications, the PI designed another nozzle shape. The new nozzle was half its original length (to match PoC nozzle experience) and more iscentropic to minimize shock disturbances and losses. In addition, the reduced secondary injector mass flow, previously achieved crudely with wooden blocks, was integrated in the new nozzle design. For simplicity, the new nozzle shape was achieved by modifying only the outside contour of the secondary injectors. The different nozzle geometries are compared on Figure 30. The required decrease in the injector exit area was accommodated in the subsonic diffuser by fitting sidewall ramps. These aluminum ramps were bolted to the subsonic diffuser walls (as shown fitted to the left

hand secondary injector exit on Figure 27). Experimentally, we found that the optimum diverging angle of the ramps was 4°. Any greater diverging angle reduced the exit Mach number of the nozzle, due to flow separations. The secondary injectors were modified one at a time to verify experimentally any performance gains (as shown on Figure 27).

Measurements in the new nozzle shape showed that the injectors were still not fully started, and the peak Mach number attained was still only 1.8. Consequently, we concluded that the startup pressure ratio across the injectors was insufficient to start Mach 2.0 flow, independent of nozzle shape. Based on this finding, the PI then designed another secondary injector nozzle with a lower design exit Mach number of 1.8 and the same mass flow. One secondary injector was then modified and a double section ramp was installed on the sidewall to accommodate the reduced injector exit area to achieve the lower exit Mach number. With an asymmetric configuration, we found that the Mach 1.8 nozzle ran with a much lower exit pressure than previously measured. Consequently, we decided to modify both secondary injectors to the new Mach 1.8 nozzle shape. This modification allowed the LFSWT to run over an increase Reynolds number range, although the measured secondary injector exit Mach number was still only 1.66, below the design value. At this stage, we decided that the secondary injectors were running well enough to allow us to turn our attention upstream to the primary injectors, which were still unstarted at this stage of tuning.

A bi-stable flow condition was observed in the mixing region (between the primary and secondary injector exits), such that either one or the other primary injector was operating properly, but never both at once. The mixing region is the volume in which the test section and primary injector flows are brought together. An obvious culprit was the large divergence angle (order 20° total angle) of the mixing region floor and ceiling. This large divergence angle came from the need to reduce the primary injector mass flow below original design specifications to 52 lbs/sec (23.56 kg/sec) mass flow (using the movable plates shown on Figure 26). Foam filled alloy blocks were fitted to both the top and bottom primary injectors. These blocks gave the mixing region a constant cross-section with large rearward facing steps in the plane of the secondary injector exits. In this configuration, no significant performance improvement was noticed in the primary injectors, accept the bi-stable flow condition was eliminated in the mixing region. The large separated flow region associated with the rearward facing steps on the floor and ceiling of the subsonic diffuser was thought to be adversely affecting the secondary injectors. Consequently, we filled in the rearward facing step with two long ramps attached to the floor and ceiling of the subsonic diffuser. These ramps were made using five sections of foam backed aluminum plates bolted to the floor and ceiling of the subsonic diffuser, as shown on Figure 31. The ramps were diverged with an 8° total angle relative to the subsonic diffuser non-horizontal centerline. Each ramp ends in a small step, a convenient 110 inches (2.79 m) from the subsonic diffuser entrance, where the flow is decelerated enough to make smooth geometry changes unnecessary. These ramps significantly reduced the turbulent losses in the subsonic diffuser, and all four injectors would start at once. The tunnel flows were all steadier than ever before, but the injector exit Mach numbers of 1.78 and 1.65 (in the primary and secondary injectors respectively) were still below design. The subsonic diffuser configuration is still not aerodynamically perfect, but allows the LFSWT to achieve a Mach 1.6 test envelope over the Reynolds number range from 2.6 to 3.8 million per foot. This test envelope is sufficient to overlap the HSRP flight test envelope at Mach 1.6 (as shown on Figure 9), so further drive system tuning was halted.

The injector drive system was observed to start with less flow oscillations in the subsonic diffuser, when the test section flow was started first before the injectors. So, to reduce loads on the subsonic diffuser ramps, our HPA control system was modified to allow priming of the HPA inlet piping before the injectors were started (i. e. the 60-inch (1.52 m) valve was opened). The HPA priming takes about 5 minutes before each run and is necessarily slow to prevent overpressure due to the excessive pressure step-down required of the system. The start-up and shutdown procedure is fully automated using a sophisticated man/computer interface in the PC Windows environment (see also sub-section 5.7).

7.2 Instrumentation Checkout:

During the lengthy LFSWT tuning phase, the PI made piggy-back tests in the settling chamber and test section to checkout instrumentation, and to monitor the temperature and accelerations experienced by the tunnel structure. Thermocouples (type-T) were positioned in the test section frame and windows. In addition, a pitot probe fitted with a type-T thermocouple was mounted either in the settling chamber or test section. The settling chamber reached temperature equilibrium at about 1° F (238 K) with an inlet air temperature of about 6° F (258.7 K) after about 20 minutes of running. At shutdown, the settling chamber air takes about 16 minutes to equalize with the wall temperature. The thermal inertia of the tunnel is such that after 350 minutes (nearly 6 hours) the tunnel is still below an outside ambient temperature of 60° F (288.7 K), as shown on Figure 32.

In another test, the cool-down was studied in the test section using a pitot mounted thermocouple. As shown on Figure 33, the test section total temperature reaches an equilibrium at about -24° F (242 K) after about 10 minutes of operation. In this case, the inlet air temperature was about 1.5° F (256 K) and the outside ambient temperature was 62.5° F (290.1 K). At shutdown, the test section air rapidly rises to that of the wall temperature, within about 10 minutes. Therefore, the test section and model experience significant thermal gradients during cool-down and warm-up. There are in fact indications from flow visualization in the test section that disturbances due to window joints exist during the roughly 20 minutes tunnel cool-down. The rapid model cool-down also places serious doubt on the ability of liquid crystals to show shear stress distributions before freezing.

Since the LFSWT operates at low stagnation temperatures, this raises the unit Reynolds number Re, cycles the tunnel structure and precludes some flow visualization techniques. Furthermore, the low To is a detriment to flow quality because of temperature non-uniformity in the test section due to hot non-adiabatic walls. Also, the growth of steps and gaps at tunnel joints due to thermal cycling may be the source of premature transition and/or variable test conditions. Heating of the LFSWT inlet air is still an option to minimize these problems in the future.

A capacitive-type accelerometer was fitted to the outside sidewall of either the nozzle or test section. Over a frequency range from 14-1000 Hz with the tunnel running, the lateral accelerations measured were 0.02g on the nozzle and 0.038g on the test section frame. These accelerations are very low and attest to the isolation quality of the special mounts and rubber isolator gaskets used in the LFSWT design. This low vibration environment provides an excellent basis for studying the effects of vibration on boundary layer transition on the tunnel walls and model.

7.3 Flow Quality Measurements:

7.3.1 Overview

The definition of quiet flow is based on achievable and measurable levels of low disturbances. Ultimately, this definition will be linked to the range of actual atmospheric disturbances at HSCT supersonic cruise altitudes (47,000 to 60,000 feet), and a better understanding of transition receptivity. Currently, the consensus is that flow is "quiet" if the free stream is spatially and temporally uniform with acoustic disturbances (the ratio of total pressure rms to total pressure - Prms/Pt) less than 0.1%. This requirement is met with laminar boundary layers on the supersonic nozzle and test section walls, and disturbance levels in the settling chamber of Prms/Po < 0.2% and velocity fluctuations u'/U < 1%.[24]

While, this definition is generally accepted in the aerospace community, there is growing concern that this definition is insufficient for modern testing requirements. In particular, the bandwidth of measurements is an important parameter. Also, which combination of instrumentation and data reduction techniques for dynamic measurements is used can significantly alter the interpretation of results. New standards of quiet flow will need to be

formulated, so that test conditions can be repeated in different wind tunnels. The LFSWT will be used to provide valuable information necessary for writing these new standards.

7.3.2 Settling Chamber Data

Normalized fluctuating pitot pressures were measured in the settling chamber near the contraction entrance (X=-51.5) over a range of Po (see Figure 34). Three sets of data measured on the tunnel centerline are plotted to show the level of repeatability obtained. The measurements were made using a traversable pitot probe spanning the settling chamber (see Figure 35). Pressure turbulence is calculated as Prms/Po over a frequency range from 250 to 50k Hz. This frequency range was chosen by experiment to cover the spectra of actual disturbances. The low frequency limit was set to eliminate the relatively large electronic signal noise below 250 Hz. Hence, very low levels of signal noise were obtained, as shown on Figure 34. Clearly, there are repeatability difficulties when measuring such small signal rms levels (order 4 or 5 milli-Volts after amplification) with low signal to noise ratios.

All the pressure fluctuations measured in the settling chamber meet the criteria of low disturbance (<0.2%). The data show a trend of increased pressure fluctuations with increasing Po. This trend can be related to increasing mass flow through the settling chamber, which generates increased inlet flow disturbances through the pressure reduction elements. Interestingly, at the low end of the Po range, the pressure fluctuations increase sharply below about Po = 7.4 psia (0.51 bar). This rise in pressure fluctuations coincides with the onset of flow unsteadiness in the supersonic diffuser, which grows from the downstream end of the diffuser all the way to the test section entrance as Po is decreased from 7.4 to 6.8 psia (0.51 to 0.47 bar). This flow unsteadiness must be fed upstream through the wall boundary layers, since the free stream is supersonic in the test section.

The actual pressure transducer signals measured on the centerline are shown on Figure 36 for two values of Po. These values of Po represent conditions of minimum disturbance (Prms/Po order 0.05%) and above. The spectral density of these signals is broadband except for a peak response at 1.625k Hz. In fact, we found that there was an increase of signal power at 1.625k Hz associated with raising Po. This effect may be related to the distance downstream from the last screen, where the measurements were taken.

The spanwise distribution of pressure fluctuations across the entire contraction entrance at the vertical tunnel centerline is shown on Figure 37, for the two values of Po previously examined with the centerline data. The fluctuations are erratic particularly at the higher Po, with a tendency to be higher on the left side of the settling chamber. Since the settling chamber and the probe are symmetrical, this non-symmetric distribution is not easily explained. Nevertheless, the flow is low-disturbance everywhere except close to the left sidewall (Z = -19.62 inches - 50 cm) on the horizontal measurement plane.

Preliminary hot-wire measurements were also made at the entrance to the contraction (X=-51.5) over a frequency range from 30 Hz to 50k Hz. A 10 inch (25.4 cm) long probe was mounted from the left sidewall of the instrument holder for these measurements. The reduced data are shown on Figure 38 over a range of Po. The velocity fluctuations (u'/U) measured in the settling chamber range between 0.66% and 0.82%. So, the settling chamber flow is low-disturbance at this measurement location (i.e. u'/U<1%). A gradual increase of velocity fluctuations is associated with raising Po and increasing tunnel mass flow, as for the pressure fluctuations. Velocity fluctuation levels in the settling chambers of the NASA-Langley Supersonic Low Disturbance Pilot Tunnel (SLDPT) operating at Mach 3.5, and the JPL-SWT are shown for comparison on Figure 38. The LFSWT velocity disturbances fall between those of the two other quiet tunnels, despite the measurements being taken on the worst side of the settling chamber for pressure disturbances.

The power spectra for a typical hot-wire signal is shown on Figure 39 for Po = 7.46 psia (0.51 bar). The signal rms is 8.61 milli-Volts with a signal to noise ratio of 6. There is a major peak centered at 26k Hz which is unaffected by changes to Po. The probe frequency is

2.125k Hz with six harmonics visible. The signal power is contained in frequencies below 10k Hz, and this is where the effects of Po variation are strongest.

7.3.3 Test Section Data

Flow characteristics in the test section were measured at three streamwise locations, X = 29.88, 43.38 and 54.38, which correspond to entrance, mid and exit regions of the test section. A traversable pitot probe was used to measure pressure fluctuations. The probe was mounted on the tunnel vertical centerline, at each of the streamwise locations in turn (see Figure 40). The traverse was fitted to either sidewall as required, allowing measurements over the 8 inch (20.32 cm) mid-span of the test section. Data measured from each sidewall overlapped by 2 inch (5.08 cm) to demonstrate repeatability.

Pressure fluctuations were calculated as the ratio of total pressure rms to the mean pitot pressure (Prms/Pt) over the frequency range 250 to 50k Hz. In the same manner reported by other quiet wind tunnel developers. The frequency range for the pressure fluctuations was the same as for the settling chamber pitot measurements, since the same transducer was used. Centerline measurements are shown on Figure 41 over a range of Po. The worst disturbances were found at the middle of the test section, and these disturbances were just above the quiet boundary (0.1%). The spread of data taken near the test section entrance (X=29.88) is an indication of poor repeatability due to the low signal to noise ratio. It is interesting to note that the pressure fluctuations do not increase linearly with streamwise distance. Tunnel unstart occurs at a minimum Po of 6.8 psia (0.47 bar) and is easily detected because the pressure fluctuations become enormous. No hysteresis was observed in the unstart, as found in our PoC tests.[22] The unstart (unstable shock patterns) could be positioned anywhere in the test section by simply varying Po between 6.8 and 7 psia (0.47 and 0.48 bar).

A typical power spectra for the pressure transducer mounted at X=29.88 with Po = 7.42 psia (0.51 bar) is shown on Figure 42. For comparison, the power spectra of the transducer wind-off signal is shown, which has an rms power equal to half that of the wind-on signal. Clearly, the wind-on signal is broadband with a 1.625k Hz spike as found in the settling chamber measurements.

Spanwise pressure fluctuations are shown on Figure 43 at X=29.88 for two different free stream conditions, at Po = 7.5 psia (0.52 bar). The settling chamber traverse was used as a disturbance generator to provide above normal free stream turbulence. In effect, a 0.25 inch (6.35 mm) diameter cylinder was stretched horizontally across the contraction entrance, with a pitot attachment placed on the tunnel centerline (See Figure 35). Interestingly, the wake of the pitot was observed in the test section 80.38 inches (2.04 m) downstream. The wake causes the pressure fluctuation non-dimensional quantity to reduce, possibly due to the total pressure drop. The fact that the settling chamber cylinder and the test section traverse are in the same plane complicates the situation and more studies are required. However, the change in free stream turbulence is seen to destroy quiet flow away from the tunnel centerline. The normal free stream disturbance produces pressure fluctuations that are worse on the right side of the tunnel. But the full mid-span of the test section is quiet at this upstream location. The importance of a low-disturbance free stream at low supersonic speeds is made very apparent by this experiment, first performed by Laufer in the 1950s.[26] The minimum pressure fluctuations are order 0.05% during normal operation.

A comparison of the spanwise distribution of pressure fluctuations at the three streamwise locations is shown on Figure 44 for Po = 7.5 psia (0.52 bar) and on Figure 45 for Po = 8.5 psia (0.58 bar). The data is not smooth and, as found on the centerline, there is no apparent propagation of disturbances downstream. For example, on Figure 44, the data from the middle of the test section (X=43.38) indicates a non-quiet region between $-3.5<Z<-0.5$ that is not found downstream. Data measured near the test section exit (X=54.38) contains some disturbance spikes at Z=-4 and Z=+1.5 which are repeatable. These spikes are caused by low frequency (below 10k Hz) disturbances observed from the signal spectra. The data at the higher Po does indicate a general increase of disturbances compared to the lower Po. An observation which can

be seen in the centerline data shown on Figure 41. The lowest flow disturbances were found near the test section exit for a given Po.

Since quiet flow is present in the test section, the nozzle and test section boundary layers must be laminar according to Laufer.[26] So a test was performed with the boundary layers tripped to turbulence This was achieved with trips (0.5 inch - 12.7 mm strips of 80 grit sandpaper) applied to each of the four walls at the test section entrance. The total height of the trips was estimated as 0.023 inch (0.584 mm). Centerline pressure fluctuations in the middle of the test section for the normal and tripped conditions are shown on Figure 46. The centerline pressure fluctuations are significantly higher for the tripped case (order 0.25%), and were observed not to vary spanwise. Typical signals from the pitot pressure transducer are shown on Figure 47 for Po $\approx$ 7.5 psia (0.52 bar). The signals are clear indicators of different flow conditions on the test section centerline. Furthermore, examination of the power spectra of these signals (shown on Figure 48) reveals a broad band increase of signal power, which is indicative of noise radiating from a turbulent boundary layer. Interestingly, this difference is not evident in the spectra variation observed spanwise and streamwise in the test section with no trips fitted. But, a broadband increase of signal power was observed in the data with above normal free stream disturbances (as shown on Figure 43).

In parallel with the pitot measurements on the tunnel centerline, a hot-wire probe was used to confirm the state of the floor and ceiling boundary layers. The hot-wire was mounted on the tunnel centerline away from the floor and ceiling a distance, roughly equal to a third of the minimum estimated boundary layer thickness at that streamwise location, as shown on Figure 40. At X=43.38, the stand-off distance was 0.025 inch (0.635 mm), and further downstream at X=54.38, the stand-off distance was 0.035 inch (0.889 mm). The pitot and hot-wire probes were used in pairs, at the same streamwise location to eliminate probe interferences.

Hot-wire measurements were made above the floor centerline at X=43.38 with and without the previously described boundary layer trips fitted. The hot-wire data is summarized on Figure 49 over a range of Po. Raw signal rms is presented because the hot-wire cannot be calibrated in the LFSWT supersonic flows. Nevertheless, the raw hot-wire data has been shown to be useful in determining qualitatively the state of the boundary layer at Mach 1.6.[13] In normal operation, the hot-wire rms was order 60 milli-Volts. With the trips fitted, the hot-wire rms rose to 150 milli-Volts. Examination of the hot-wire signals and power spectra (shown on Figures 50 and 51 respectively) revealed known boundary layer characteristics. With the boundary layer tripped, the hot-wire measured random pressure surges, which increased the power of the signal mostly at the low frequency end of the spectra. This situation is indicative of a turbulent boundary layer. With no trips, the signal spectra is relatively flat, which is indicative of a laminar boundary layer.

Hot-wire measurements were also made near the test section exit (X=-54.38) on the floor and ceiling. With no trips fitted, the hot-wire data does not indicate turbulent or transitional flow. However, boundary layer measurements in this location with trips fitted must be made before the state of the boundary layer can be known with any certainty.

7.4 Discussion of Findings:

The LFSWT floor boundary layer has been found to be laminar back to the mid-region of the test section and beyond, over the entire Po range.[24] To achieve this feat, the run of laminar flow from the contraction is of the order 84 inches (2.13 m) in length. So far, the prediction of our CFD analyses, that transition will not occur in LFSWT, has not been challenged on the tunnel centerline at least. We now need to turn our attention to the sidewalls, and determine the characteristics of the boundary layers there.

It is evident, that the limitations of our existing traverse prevent us from tracking disturbances upstream through the test section and nozzle. We can only speculate about the disturbance sources. The spikes in the pressure fluctuation distributions near the test section

exit are indicative of shock disturbances perhaps from the window joints. At Mach 1.6, the Mach angle is a relatively steep 38° and our distribution of measurements is too coarse. Detailed flow measurements are planned with a purpose-built traverse (described later) capable of 3-axis computer controlled movement. Only then will we be able to assess the flow quality over a range of streamwise locations during the same run. This knowledge will help us define the 3-D extent of the LFSWT quiet test envelope better than for other quiet wind tunnels.[25]

We can speculate that the spanwise disturbances, we have observed in the LFSWT, have grown from cross flows between the nozzle floor/ceiling and the sidewalls.[14] Also, secondary flows in the nozzle corners are a potential source of disturbances.[27] The influence of unsteady supersonic diffuser flow, joint steps and gaps, and wall vibration must also be studied. The LFSWT now gives us the opportunity to examine these potential sources of transition and study means of delaying transition due to the combined effect of all the flow disturbance generators in the tunnel. We will then be able to determine better tunnel design criteria to minimize these disturbances in low supersonic testing.

One LFSWT test parameter we have no control over at present is the stagnation temperature (To), which varies with ambient conditions. Consequently, when we compare data from different tunnel runs, there are slight differences in the Re for a given Po. The significance of this variation has yet to be determined, but this fact should be considered when discussing these flow measurements. Another possible effect of varying To is pressure transducer sensitivity to temperature. Real-time calibrations are performed for each test to try and eliminate this effect. However, the pressure fluctuations measured near the test section exit were made in warmer ambient conditions than the other data sets. It is interesting to see that the pressure fluctuations at the exit plane are lower than found at the mid-region of the test section. Repeat tests will continue to be carried out at different ambient conditions to study the long term effects of operating with a variable To.

A major part of the LFSWT design, the settling chamber, has worked successfully and is better than some other settling chambers fitted to other quiet tunnels.[25] However, we have seen that the pressure fluctuations do vary in the settling chamber in a non-linear way. Nevertheless, the fluctuations appear to be of sufficiently small enough amplitude so as not to affect the test section flow quality, where we have made measurements. It is interesting to see that the influence of the supersonic diffuser flow on the settling chamber flow (at the low end of the Po range) has not been observed in the test section. We can speculate that the much larger flow velocity in the test section (order 1,600 fps) masks disturbances due to the breakdown of the supersonic diffuser flow, until the test section flow itself begins to unstart.

The steady state flow quality of the LFSWT (flow angularity and uniformity) has been assessed using a known full-scale leading-edge segment of a swept wing (see sub-section 8). Pressure distributions were measured at two spanwise locations on the wing for various Re and angle of attack conditions. These experimental data compared very favourably with CFD generated data at matching test conditions, and consequently, flow anomalies in the LFSWT are unlikely.

The LFSWT operates at low stagnation temperatures, which raises Re, cycles the tunnel structure and precludes some flow visualization techniques. The minimum Re in the LFSWT is already significantly higher than originally planned (1 million per foot - 3.28 million per meter was our goal) due to difficulties with the drive system. So the Re increase due to a lower To compounds the situation but does not prevent an overlap of flight and LFSWT Re ranges (See Figure 9), nor the establishment of a quiet test core. The low To may be a detriment to flow quality because of temperature non-uniformity in the test section due to non-adiabatic walls. Furthermore, the growth of steps and gaps at tunnel joints due to thermal cycling may be the source of premature transition. Heating of the LFSWT inlet air is still an option to minimize these problems in the future.

8. LFSWT Wing Model Testing

A 70° swept wing was the first model tested in the LFSWT. The wing is an replica of a small section of the passive glove flown on the starboard wing of the NASA F-16XL ship 2. The model section shape is constant across its span, and matches an instrumented section on the actual wing glove (Station 105). The model planform is delta shaped for convenience of mounting (as shown on Figure 52). Model blockage was limited to 10% at an angle of attack of +8°, necessitating modification of the lower surface geometry.

Two models were actually constructed. One is solid for surface flow measurements and blockage testing, and the other is hollow and instrumented with two rows of pressure taps (a total of 63) and one row of 15 thermocouples between the pressure tap rows (as shown in the schematic on Figure 53). The inboard row of pressure taps is at one-third span (Row 1), and the outboard row is at two-thirds span (Row 0). The pressure taps on the model were positioned to exactly match the distribution on the flown wing glove. The tap sizes were also exactly matched to minimize extraneous effects on the data comparisons. The thermocouples were installed to monitor the model cool-down and eventually to assist in identifying transition due to non-adiabatic walls.

The solid model was tested in June 1994 to determine if the test section flow would start, as shown on Figure 54. No problems were encountered with the start over the model's angle of attack range ($-2° < \alpha < +8°$). Using shadowgraph and focusing schlieren (see section 6 for more details), we observed the rapid start-up characteristics of the injector drive system, and the steadiness of the model induced shock patterns over the angle of attack range. The length of the model in undisturbed flow is less than predicted by CFD, due to unexpected boundary layer interactions on the sidewalls. The maximum root chord length of undisturbed flow on the model is order 10.5 inches (26.7 cm) at the higher angles of attack. The composite picture on Figure 55 shows the relative position of the model pressure tap rows to the strong bow shock and reflection. The shadowgraph also shows the weak Mach lines originating from the joint between the nozzle and test section, and the floor/ceiling window joints. Theses Mach lines have a small but measurable effect on the wing pressure distribution (see data on Figure 56a at X-Xle $\approx$ 1.3). What actual impact these Mach lines have on the transition process remains to be determined.

The instrumented model was tested by the PI over an angle of attack range from $-1° < \alpha < +5°$ and a unit Reynolds number range from 2.5 to 3.4 million/foot. A total of 25 test points were taken. Repeatability of the wing pressures around the leading edge was excellent for both rows of taps, as shown on Figure 56a and 56b at zero angle of attack. The data repeats within the expected accuracy of the measurements (Cp accuracy is ± 0.009. Also shown for comparison are pressure distributions calculated for the wing in the test section by Garcia using a Navier-Stokes code.[28] The comparison is very encouraging for Row 1 back to the wall induced shocks, and demonstrates that the LFSWT does not have flow angularity in the test section. The comparison at Row 0 is complicated by a wall induced normal shock striking the model about 0.25 inch (6.35 mm) downstream from the leading edge. Nevertheless, there is good agreement around the leading edge itself.

The zero angle of attack test case represents a high blockage condition in the LFSWT. On Figure 57, the effect of different angles of attack on the pressure distribution on row 1 is shown. Clearly, as angle of attack is increased so the normal shock in the test section moves downstream from 5 inches (12.7 cm) downstream of the leading edge at zero angle of attack. The reflected bow shock striking the wing at about 6.25 inches (15.87 cm) downstream of the leading edge limits the run length of undisturbed flow at higher angles of attack.

The model temperatures showed that a 40° F (22.2° C) drop in temperature is normal during the first 10 minutes of tunnel operation. This rapid cooldown does not give liquid crystal coatings sufficient time to react to steady flow conditions before freezing. Hence, this method of transition detection is not appropriate in the LFSWT at the present time. When the model reaches thermal equilibrium after about 20 minutes of tunnel run time, the temperature

of parts of the model have dropped a maximum of 55° F (30.5° C) relative to ambient.

These tests are a very useful precursor to transition studies expected to begin in September 1995. By then, we hope to have a better calibration of the LFSWT quiet test core. Consequently, we will be able to present transition information on the model with data on the flow quality in which the model was tested. This extensive data presentation will assist in the evolution of new standards for transition research to promote better interpretation of experimental results.

9. State-of-the-Art Appraisal

The PI has carried out an ongoing library search for the duration of this Cooperative Agreement in the following topics: supersonic wind tunnel and nozzle design; surface temperature effects on transition; effects of surface shape and roughness on transition. This mamouth task was handled by creating a PC computer database. This database provides immediate access and sorting of all citations as these are found.

This library search revealed little research activity in the area of supersonic nozzle wall cooling/heating. Most wall cooling work has been directed towards pure boundary layer transition research on flat plates and cones. Currently the PI's *Supersonic Nozzle Bibliography* contains 1000+ citations dating back to 1926. An extract of the *Supersonic Nozzle Bibliography* has now been published as a NASA contractor's report.[21] This report is focused on nozzle design and contains 298 citations and abstracts.

An important aspect of appraising the *State-of-the-Art* is meeting other scientists at conferences. During the period of this report, I participated in the 4th Asian Congress of Fluid Mechanics (Hong Kong in August 1989), the 17th ICAS Congress (Stockholm, Sweden in September 1990), the High Speed Research Workshop (Williamsburg, Virginia in May 1991), the International Conference on Adaptive Walls and Wall Interference (Xian, China in June 1991), the International Conference on Experimental Fluid Mechanics (Chengdu, China in June 1991), the AIAA 9th Applied Aerodynamics Conference (Baltimore, Maryland in September 1991), the AIAA 7th Aerospace Ground Testing Conference (Nashville, Tennessee in July 1992), the International Conference on Methods of Aerophysical Research (Novosibirsk, Russia in August/September 1992), the European Forum on Wind Tunnels and Wind Tunnel Test Techniques (Southampton, England in September 1992), the Symposium on Aerodynamics and Aeroacoustics (Tucson, Arizona in February/March 1993), the Supersonic Tunnel Association Meeting (Cologne, Germany in October 1993), the AIAA 32nd Aerospace Sciences Meeting (Reno, Nevada in January 1994), the AIAA 18th Aerospace Ground Testing Conference (Colorado Springs, Colorado in June 1994), and the 2nd International Conference on Experimental Fluid Mechanics (Turin, Italy in July 1994). In addition, the PI visited NASA Langley on numerous occasions to discuss quiet wind tunnel testing and instrumentation development with our East coast counterparts. The PI was fortunate to meet with many scientists from China and the Commonwealth of States (formally the USSR). From discussions with these scientists, he was able to learn that there are no quiet supersonic tunnels in their respective countries. It would appear that the only operating quiet supersonic tunnels are in the USA and France at Mach numbers of 3 and above. It is clear that the LFSWT has given NASA a unique capability.

Quiet supersonic tunnels, as defined in the United States, are now operating in the USA (NASA-Ames, NASA-Langley, Montana State University, and Purdue University) and provisionally in Germany (DLR Goettingen) and Russia (Russian Space Institute, ITAM - Novosibirsk, and TsAGI - Moscow). There is also growing interest in swept wing transition at transonic and supersonic speeds amongst the scientific community, which can only encourage the spread of quiet wind tunnels worldwide.

10. Summary and Conclusions

1) We have carried out unique research on the use of large ambient injectors and supersonic mixing layers in a supersonic wind tunnel.

2) The LFSWT project is now firmly established as an integral part of the HSRP SLFC studies, and the main emphasis is on Mach 1.6 operation to support F-16XL SLFC flight tests.

3) The "State of the Art" in *Quiet* technology, supersonic transition, supersonic wind tunnel drive systems, and supersonic mixing layers has been established through an extensive literature search, part of which has already been published.

4) Natural laminar flow and transition along the walls of the PoC has been documented and visualized at Mach 2.5. and 1.6, using a variety of instruments and testing techniques including novel focusing schlieren.

5) An efficient tunnel drive system has been developed for Mach 2.5 operation, but the mass flow requirement is too large for the FML compressor alone.

6) The PoC test section flow is quiet (turbulence less than 0.1%) on the nozzle exit centerline.

7) Focusing schlieren has been used successful to provide the first observations of the transition phenomena along the walls of a supersonic wind tunnel.

8) The LFSWT was built rapidly in nine months due to good project management and the attention given to providing quality design prints.

9) Flow quality measurements indicate that the LFSWT does have a quiet test core at Mach 1.6 (pressure fluctuations < 0.1%). The full extent of the quiet core is not known. LFSWT measurements are ongoing and will help define a standard for quiet flow necessary to perform transition experiments at low-supersonic speeds.

10) Long lengths of laminar flow have been observed in the LFSWT. The tunnel wall boundary layers are laminar through the test section.

11) The LFSWT is now routinely operated over a useful Re range (2.6 to 3.8 million per foot - 8.53 to 12.46 million per meter) at Mach 1.6, which overlaps HSRP flight test conditions.

12) The LFSWT settling chamber design meets acceptable low-disturbance requirements for a quiet supersonic tunnel (velocity fluctuations < 1% and pressure fluctuations < 0.2%).

13) An unique two-stage injector drive system is now operational. This system routinely drives the tunnel at Mach 1.6 with compression ratios less than unity.

14) Two swept wing models have been designed and fabricated for flow quality and transition studies in the LFSWT. Model pressures compare very favourably with CFD predictions indicating no flow angularity in the test section.

15) The Fluid Mechanics Laboratory at NASA-Ames now has a supersonic testing capability with state-of-the-art flow quality for transition research.

16) Research under this Cooperative Agreement has been disseminated to the scientific community via eleven conference papers, five NASA contractor reports (including this final report), and one journal article.

References:

1. Wolf, S.W.D.: **Minimization of Boundary Interferences in Transonic Wind Tunnels - An Alternative Approach.** In: Proceedings of the 4th Asian Congress of Fluid Mechanics, Hong Kong, August 1989, vol. 1, pp. G61-G64.

2. Wolf, S.W.D.: **Status of Adaptive Wall Technology for Minimization of Wind Tunnel Boundary Interferences.** ICAS Paper No. 90-6.2.1. In: Proceedings of the 17th ICAS Congress, Stockholm, Sweden, September 10-14, 1990, vol. 1, pp. 352-362.

3. Wolf, S.W.D.: **Adaptive Wall Technology for Minimization of Wind Tunnel Boundary Interferences - A Review.** Paper 1. In: Proceedings of the International Conference on Adaptive Wall Wind Tunnel Research and Wall Interference Correction, Xian, China, 10-14 June, 1991, 15 pp. A91-52777.

4. Wolf, S.W.D.: **Adaptive Wall Technology for Improved Free Air Simulations in Wind Tunnels.** In: Proceedings of the International Conference on Experimental Fluid Mechanics, Chengdu, China, June 17-21, 1991, pp. 604-609, International Academic Publishers, 1992. ISBN 7-80003-186-1/O.42.

5. Wolf, S.W.D.: **Adaptive Wall Technology for Minimising Wind Tunnel Boundary Interferences - Where Are We Now?** In: Proceedings of the Symposium on Aerodynamics and Aeroacoustics, Tucson, Arizona, February 28 - March 2, 1993, Chapter 11, pp. 323-370, World Scientific Publishing Co., 1993. ISBN 981-02-1732-3.

6. Wolf, S.W.D.: **Adaptive Wall Technology for Improved Wind Tunnel Testing Techniques - A Review** In: Progress in Aerospace Sciences, vol. 31, no. 2, 1995. 85-136 pp.

7. Wolf S.W.D.: **Development of a Quiet Supersonic Wind Tunnel with a Cryogenic Adaptive Nozzle - Annual Progress Report, May 1990 - April 1991.** NASA CR-186769, February 1991, 106 pp. N91-23195.

8. Wolf S.W.D.: **Development of a Quiet Supersonic Wind Tunnel with a Cryogenic Adaptive Nozzle - Annual Progress Report, March 1991 - April 1992.** NASA CR-188055, May 1992, 68 pp. N92-27976.

9. Wolf S.W.D.: **Development of a Quiet Supersonic Wind Tunnel with a Cryogenic Adaptive Nozzle - Annual Progress Report, March 1992 - April 1993.** NASA CR-194548, October 1993, 138 pp. N94-15117#.

10. Wolf S.W.D.: **Development of a Quiet Supersonic Wind Tunnel with a Cryogenic Adaptive Nozzle - Annual Progress Report, May 1993 - July 1994.** NASA CR to be published. 55 pp.

11. Wolf, S.W.D.; Laub, J.A.; and King, L.S.: **An Efficient Supersonic Wind Tunnel Drive System for Mach 2.5 Flows.** AIAA Paper 91-3260. In: Proceedings of the AIAA 9th Applied Aerodynamics Conference, Baltimore, Maryland, September 23-25, 1991, vol.1, pp. 461-471. A91-53769.

12. Laub, J.A.; and Wolf, S.W.D.: **The FML Compressor as a Drive System for the LFSWT: A Narrative.** In: Development of a Quiet Supersonic Wind Tunnel with a Cryogenic Adaptive Nozzle - Annual Progress Report, March 1991 - April 1992, NASA CR-188055, May 1992, 10 pp. N92-27978.

13. Wolf, S.W.D.; Laub, J.A.; King, L.S.; and Reda, D.C.: **Development of the NASA-Ames Low-Disturbance Supersonic Wind Tunnel for Transition Research up to Mach 2.5.** AIAA Paper 92-3909. Presented at the AIAA 17th Aerospace Ground Testing Conference, July 1992, Nashville, Tennessee, 10 pp. A93-24488.

14. King, L.S.; and Demetriades, A.: **Comparison of Predictions with Measurements for a Quiet Supersonic Tunnel.** AIAA Paper 93-0344. Presented at the AIAA 31st Aerospace Sciences Meeting, January 1993, 11 pp.

15. Laufer, J.; and Vrebalovich, T.: **Stability and Transition of a Supersonic Laminar Boundary Layer on an Insulated Flat Plate.** *Journal of Fluid Mechanics*, vol. 9, October 1960, pp. 257-299.

16. Wolf, S.W.D.; Laub, J.A.; King, L.S.; and Reda, D.C.: **Design Features of a Low-Disturbance Supersonic Wind Tunnel for Transition Research at Low Supersonic Mach Numbers.** Presented at the International Conference on Methods of Aerophysical Research, August 31 - September 4, 1992, Novosibirsk, Russia, 4 pp.

17. Wolf, S.W.D.; Laub, J.A.; King, L.S.; and Reda, D.C.: **Design Features of a Low-Disturbance Supersonic Wind Tunnel for Transition Research at Low Supersonic Mach Numbers.** Presented at the European Forum on Wind Tunnels and Wind Tunnel Test Techniques, September 14-17, 1992, Southampton, England, 13 pp. A94-10424.

18. Piatt, M.J.: **An Experimental Investigation of a Large ΔP Settling Chamber for a Supersonic Pilot Quiet Tunnel.** NASA CR-3436, June 1981, 79 pp.

19. Groth, J.; and Johansson, A.V.: **Turbulence Reduction by Screens.** *Journal of Fluid Mechanics*, vol. 197, 1988, pp. 139-155.

20. Riise, H.N.: **Flexible-Plate Nozzle Design for Two-Dimensional Supersonic Wind Tunnels**, JPL Report 20-74, June 1954, 41 pp.

21. Wolf, S.W.D.: **Supersonic Wind Tunnel Nozzles - A Selected, Annotated Bibliography to Aid in the Development of Quiet Wind Tunnel Technology.** NASA CR-4294, July 1990, 84 pp.

22. Wolf, S.W.D.; and Laub, J.A.: **Development of the NASA-Ames Low-Disturbance Supersonic Wind Tunnel for Transition Studies at Mach 1.6.** AIAA Paper 94-0543. Presented at the AIAA 32nd Aerospace Sciences Meeting & Exhibit, January 10-13 1994, Reno, Nevada, 12 pp.

23. Weinstein, L.M.: **Large-Field High-Brightness Focusing Schlieren System.** *AIAA Journal*, vol. 31, no. 7, July 1993, pp. 1250-1255.

24. Wolf, S.W.D.; Laub, J.A.; and King, L.S.: **Flow Characteristics of the NASA-Ames Laminar Flow Supersonic Wind Tunnel for Mach 1.6 Operation.** AIAA Paper 94-2502. Presented at the 18th AIAA Aerospace Ground Testing Conference, June 1994, Colorado Springs, Colorado, 18 pp.

25. Beckwith, I.E.; and Moore, W.O.: **Mean Flow and Noise Measurements in a Mach 3.5 Pilot Quiet Tunnel.** AIAA Paper 82-0569. In: Collection of Technical Papers, the AIAA 12th Aerodynamic Testing Conference, March 1982, pp. 48-70.

26. Laufer, J.: **Factors Affecting Transition Reynolds Numbers on Models in Supersonic Wind Tunnels.** *Journal of Aeronautical Sciences*, vol. 21, no. 7, July 1954, pp. 497-498.

27. Kornilov, V.I.; and Kharitonov, A.M.: **Investigation of the Structure of Turbulent Flows in Streamwise Asymmetric Corner Configurations.** *Experiments in Fluids*, vol. 2, 1984, pp. 1-8.

28. Garcia, J; Tu, E.; and Cummings, R.: **A Parametric Study of Supersonic Laminar Flow for Swept Wings Using Linear Stability Analysis.** AIAA Paper 95-2277. To be presented at the 26th Fluid Dynamics Conference, San Diego, California, June 1995.

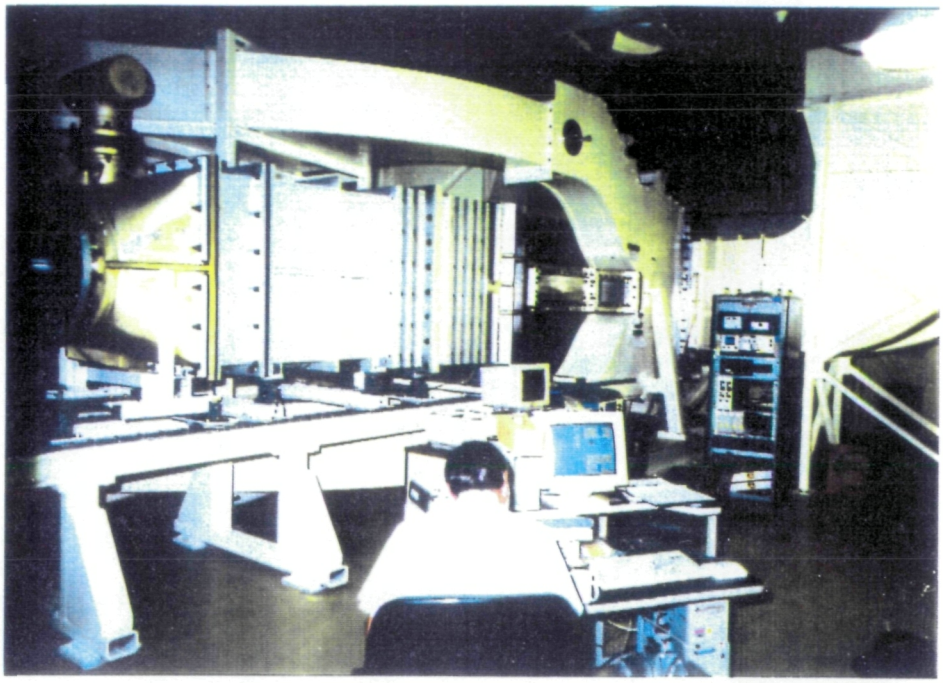

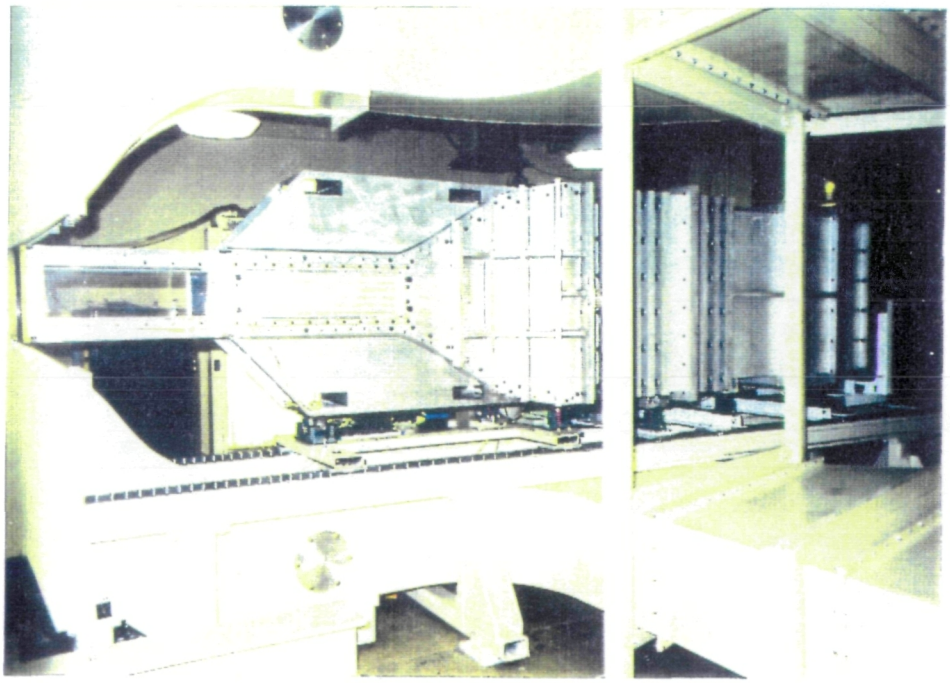

Fig. 1 - Different views of the LFSWT in situ and operational at NASA-Ames.

Fig. 2 - Original Proof-of-Concept Supersonic Tunnel with the cover plate removed.

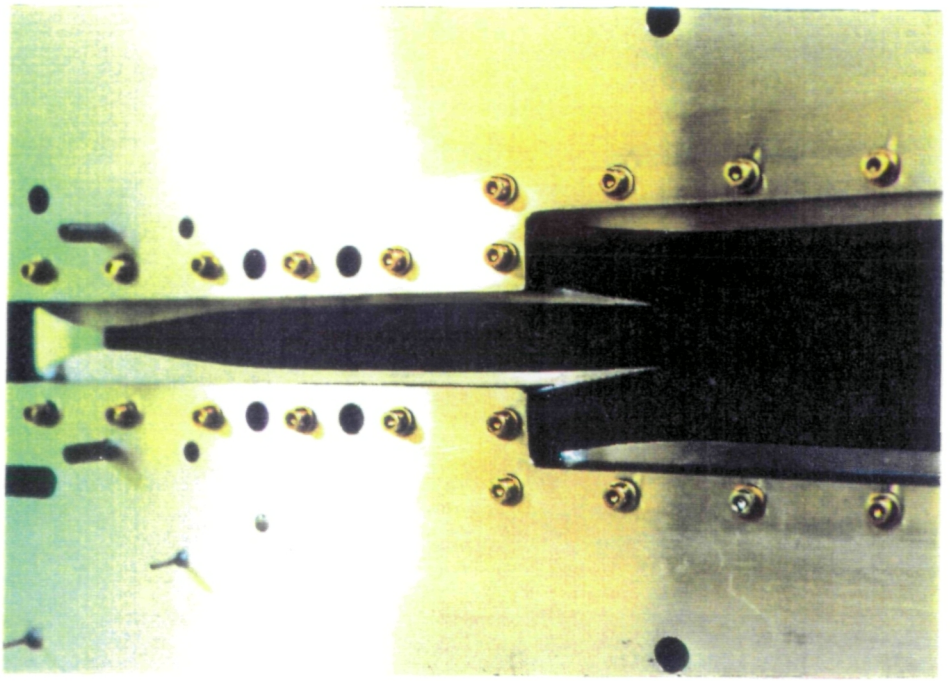

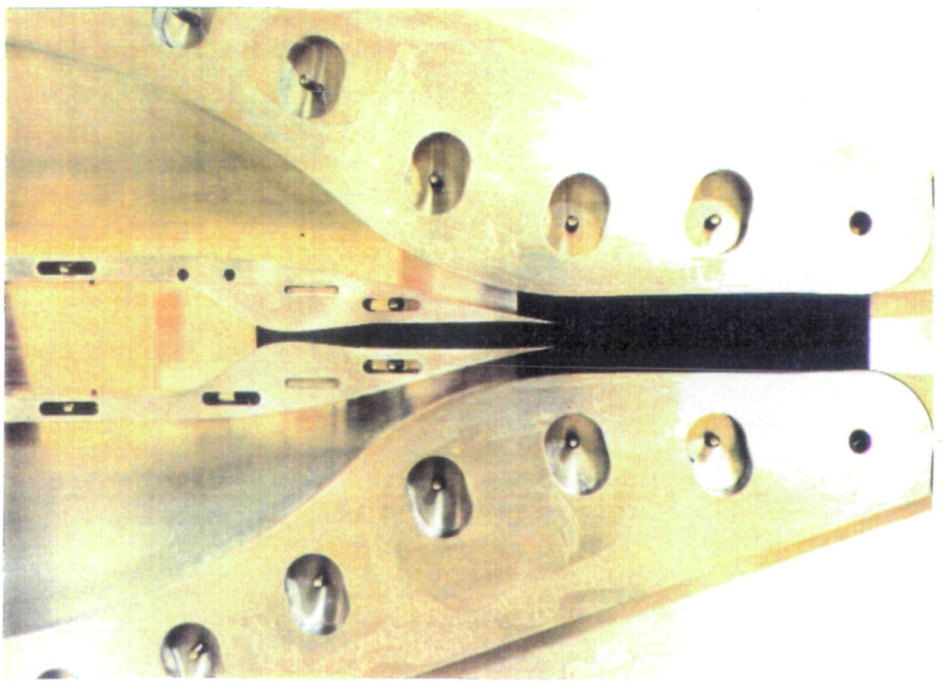

Fig. 3 - Two views of the major window modifications to the PoC sideplates.

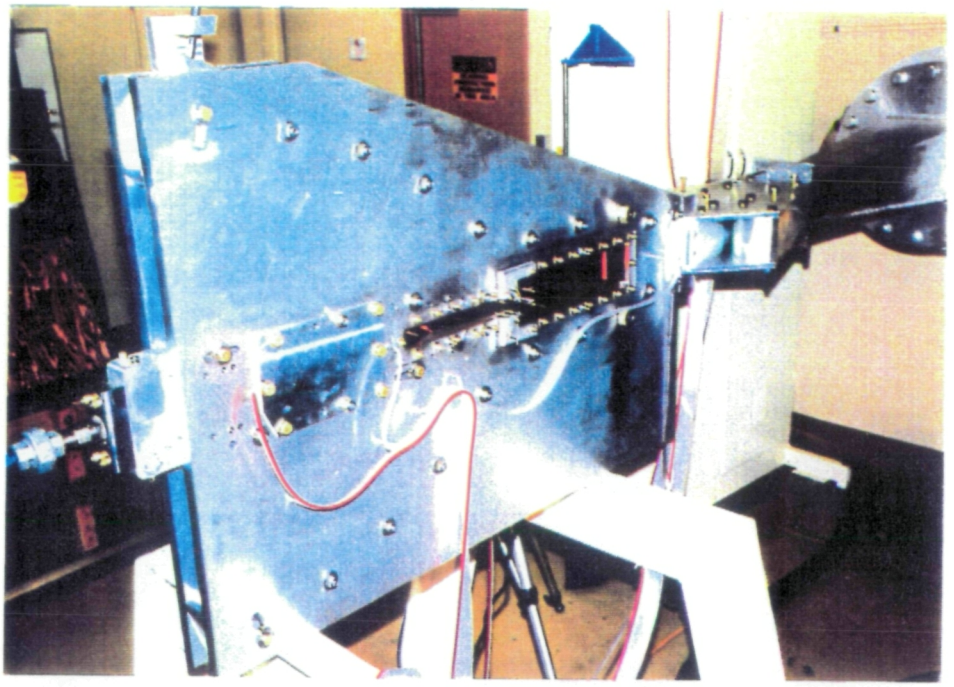

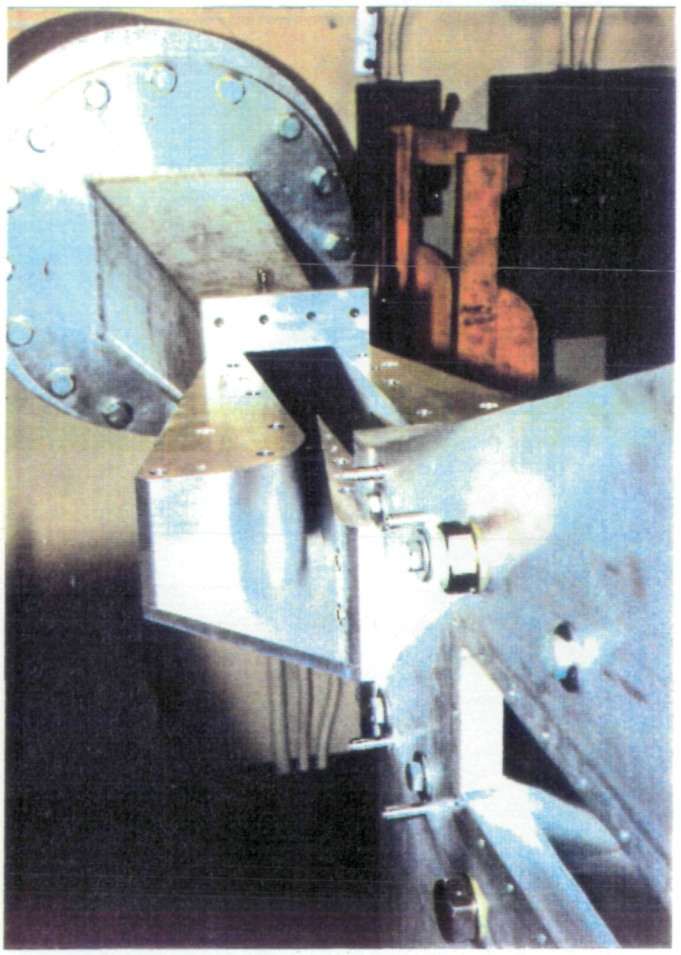

Fig. 4a - The initial PoC configuration with two stages of ambient injectors.

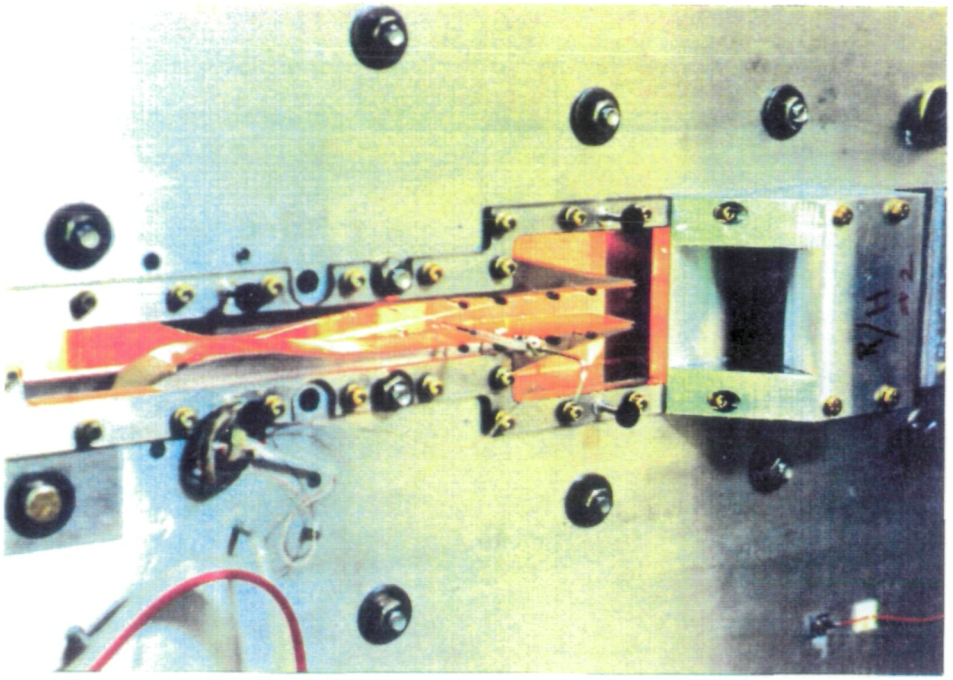

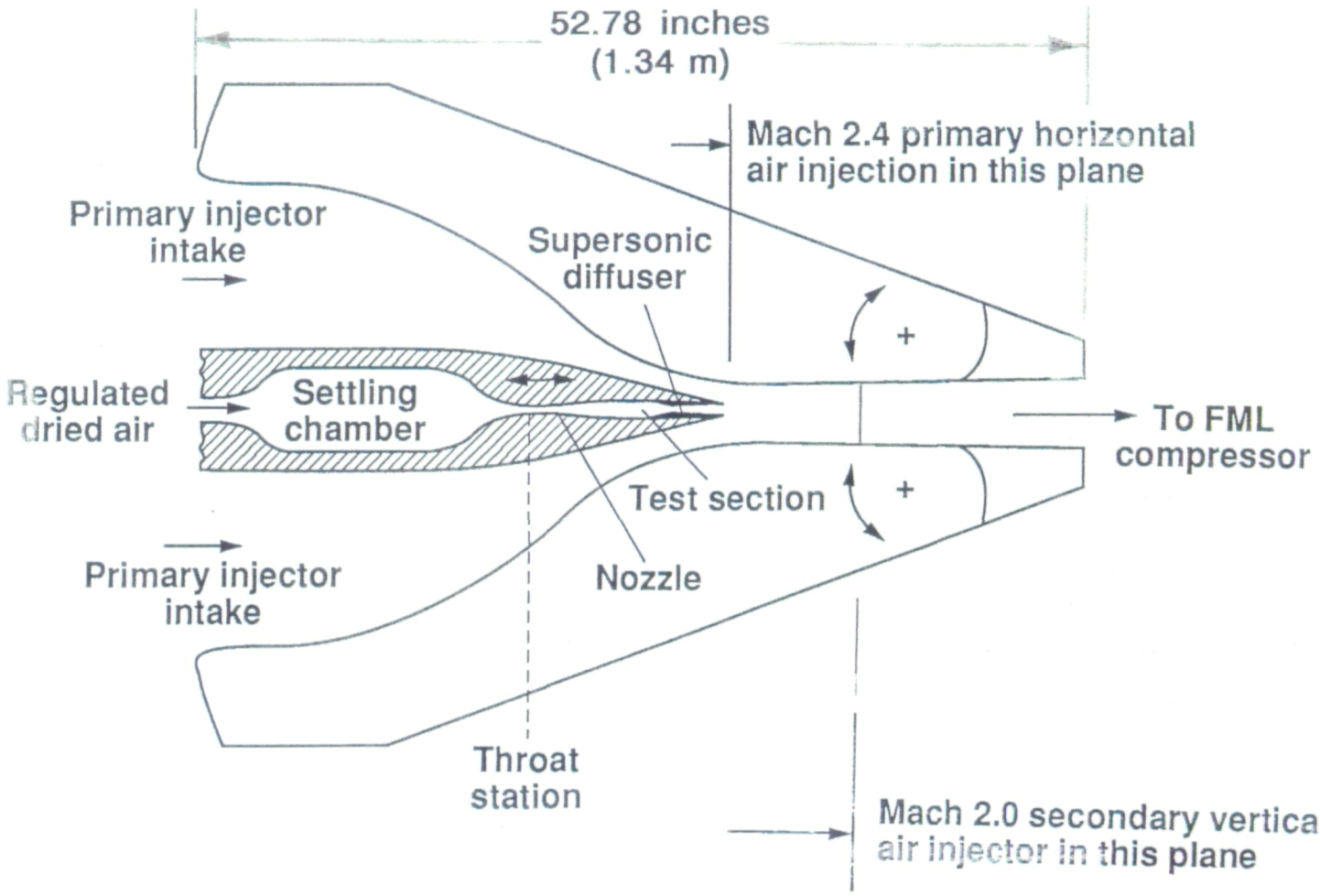

Fig. 4b - The second and final PoC configuration with two stages of ambient injectors.

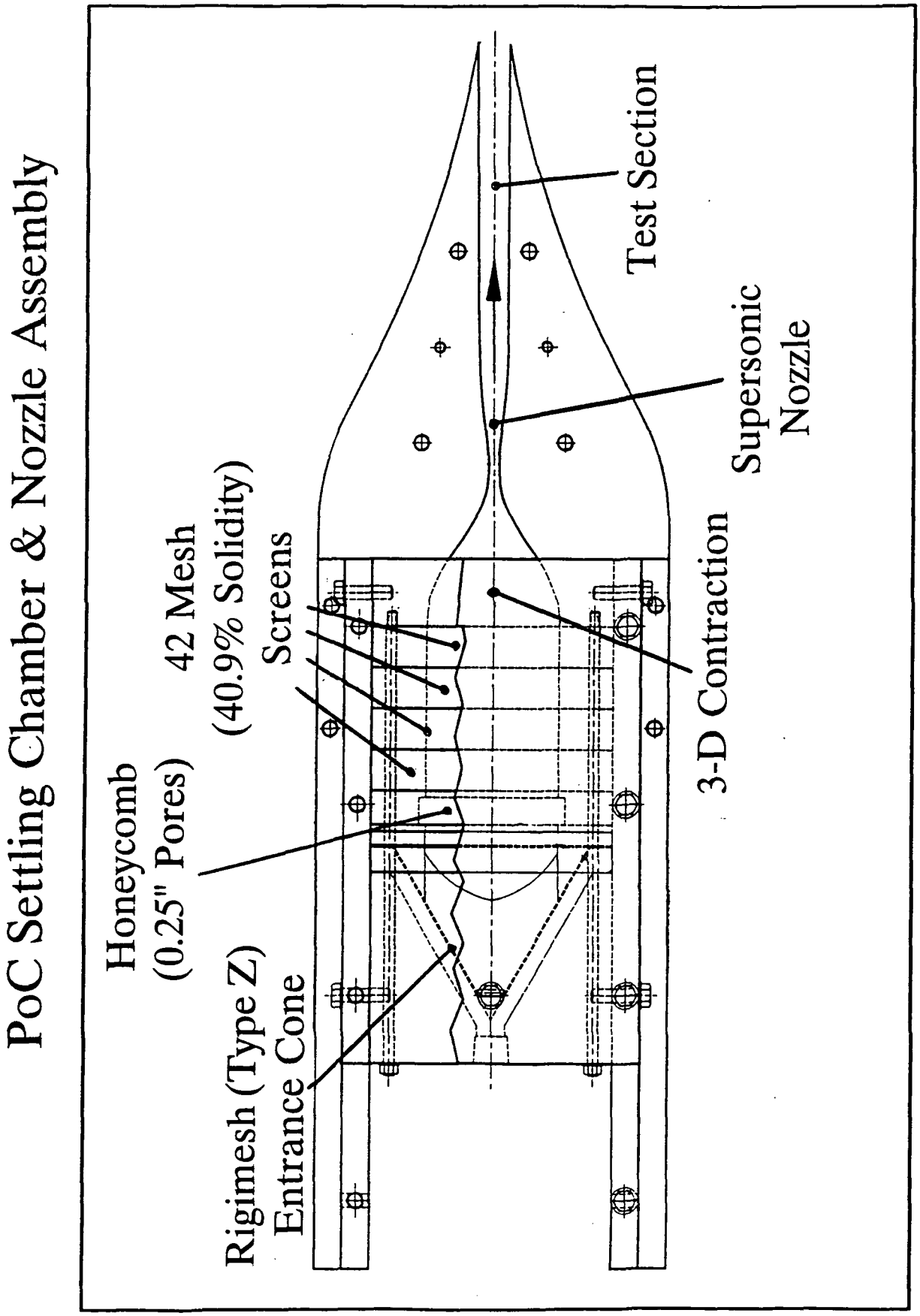

Fig. 5a - Schematic of the PoC low-disturbance settling chamber.

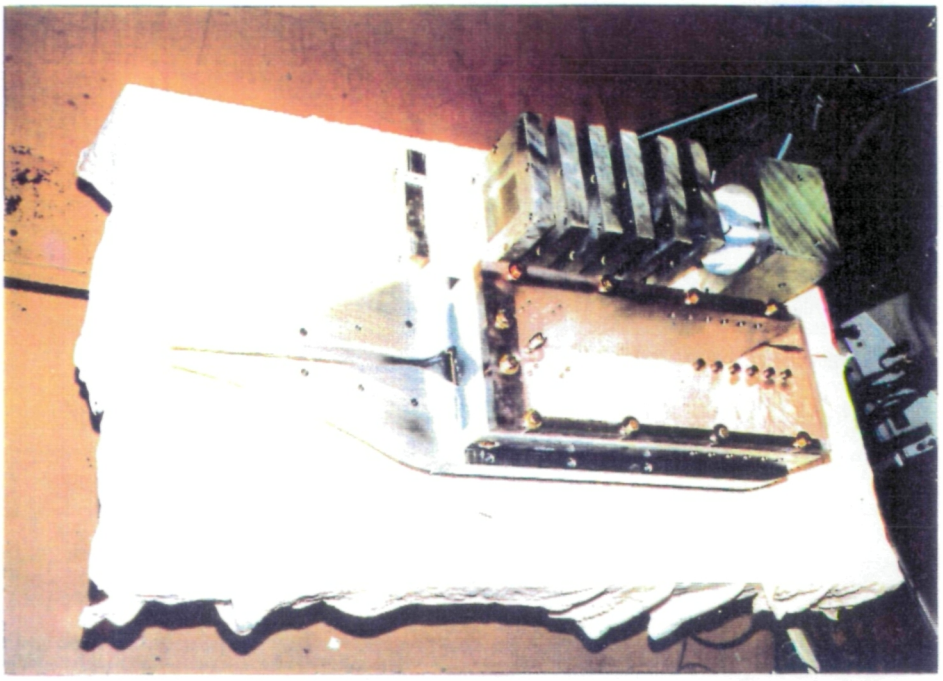

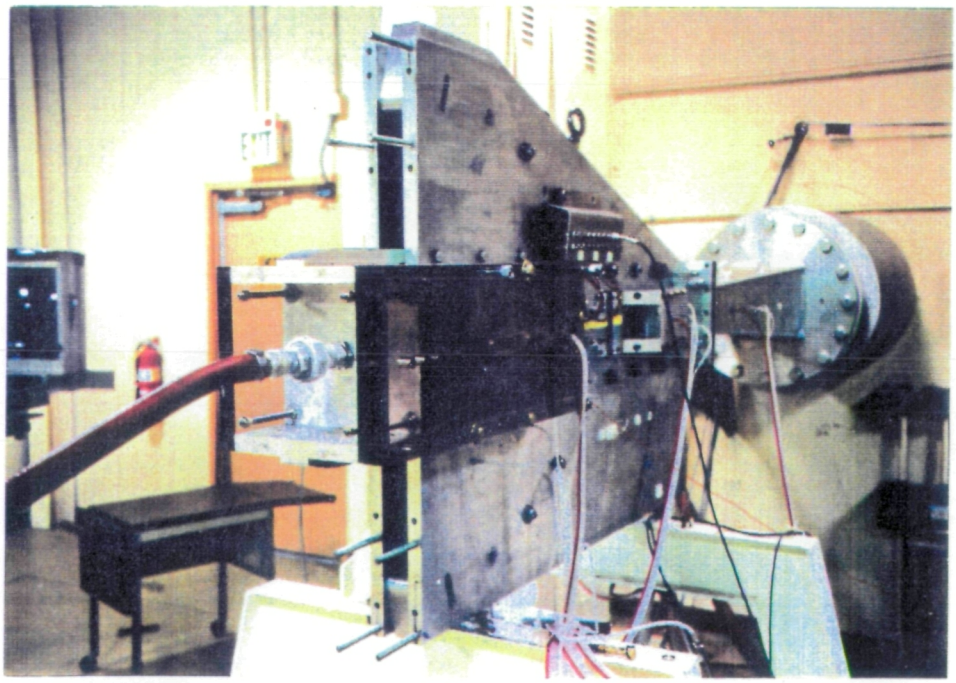

ORIGINAL PAGE
COLOR PHOTOGRAPH

Fig. 5b - Photographs of the modular PoC settling chamber before and after installation.

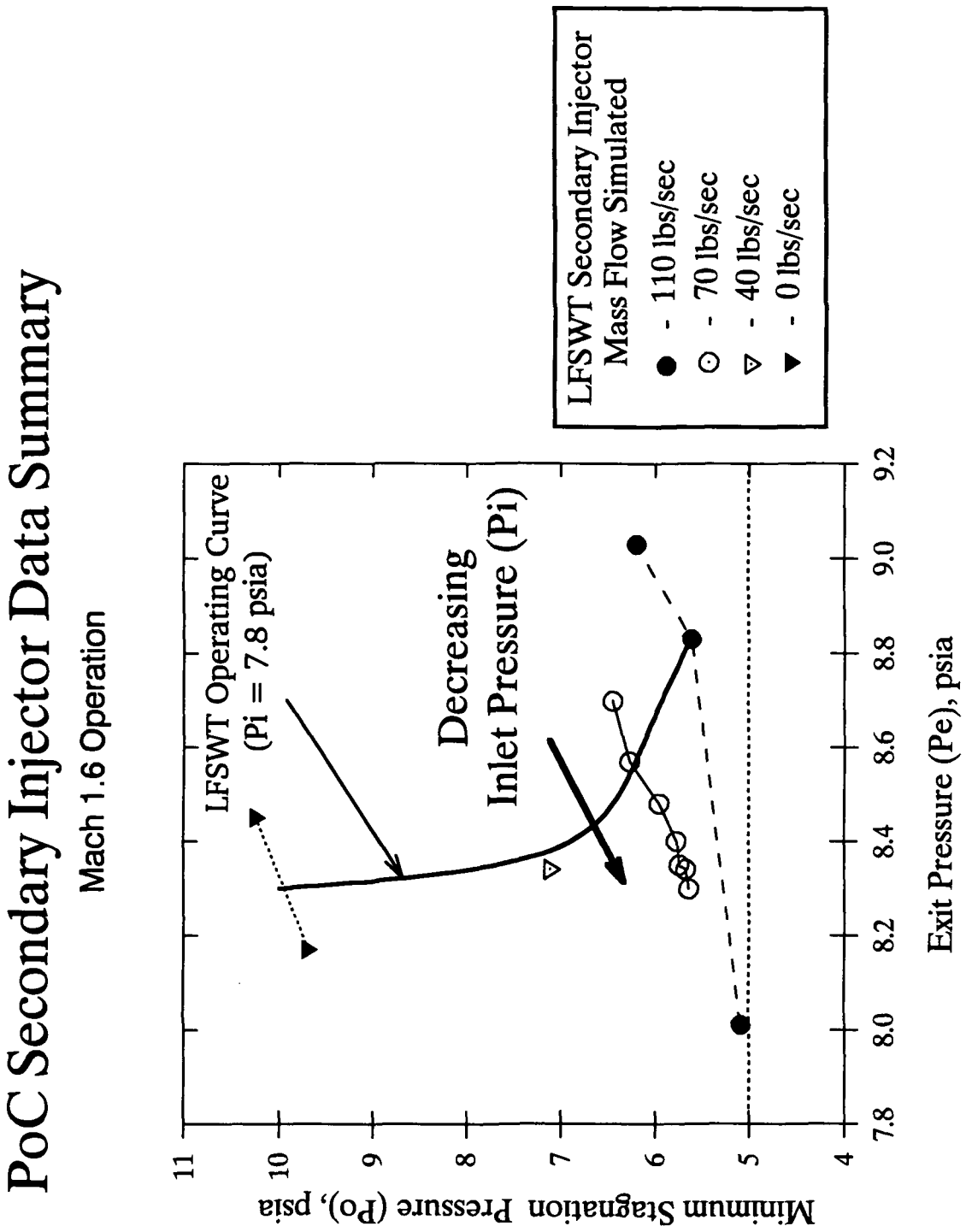

Fig. 6 - Influence of secondary injector mass flow on PoC performance.

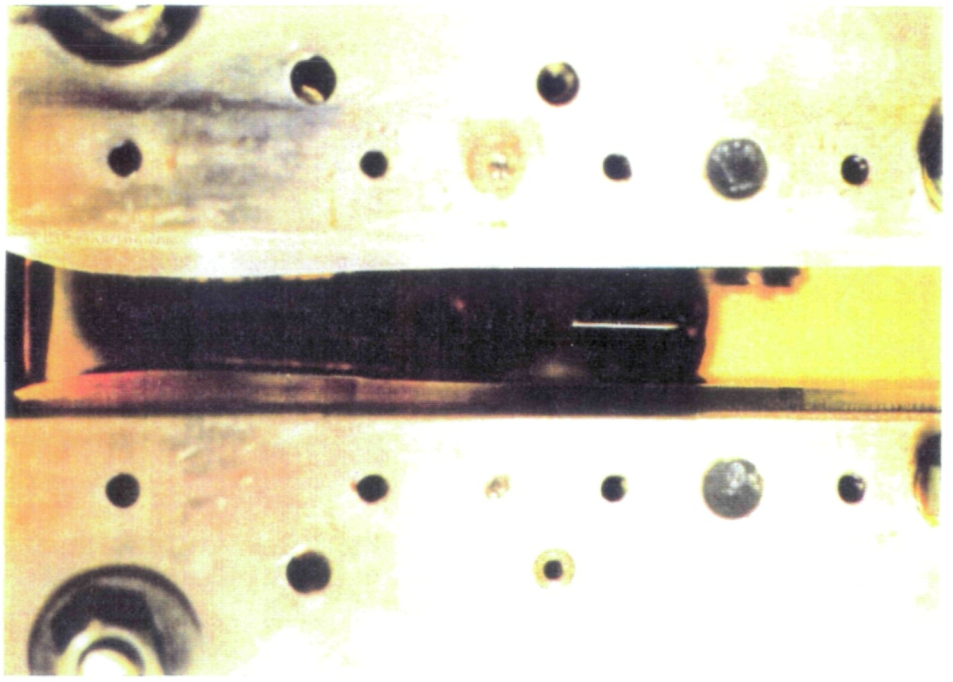

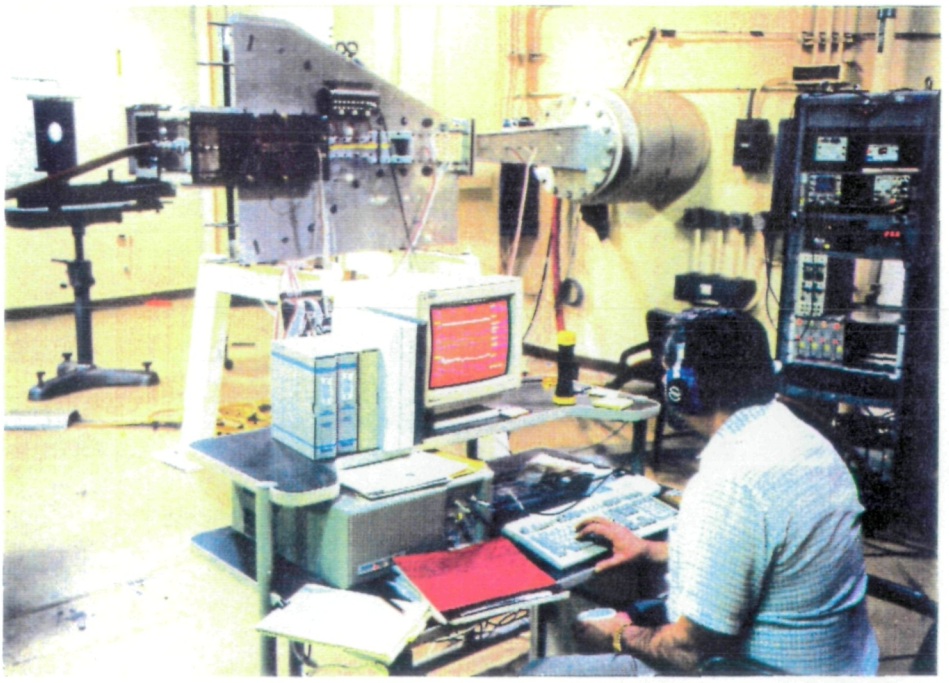

Fig. 7 - Blockage tests performed using a pitot probe mounted in the PoC test section.

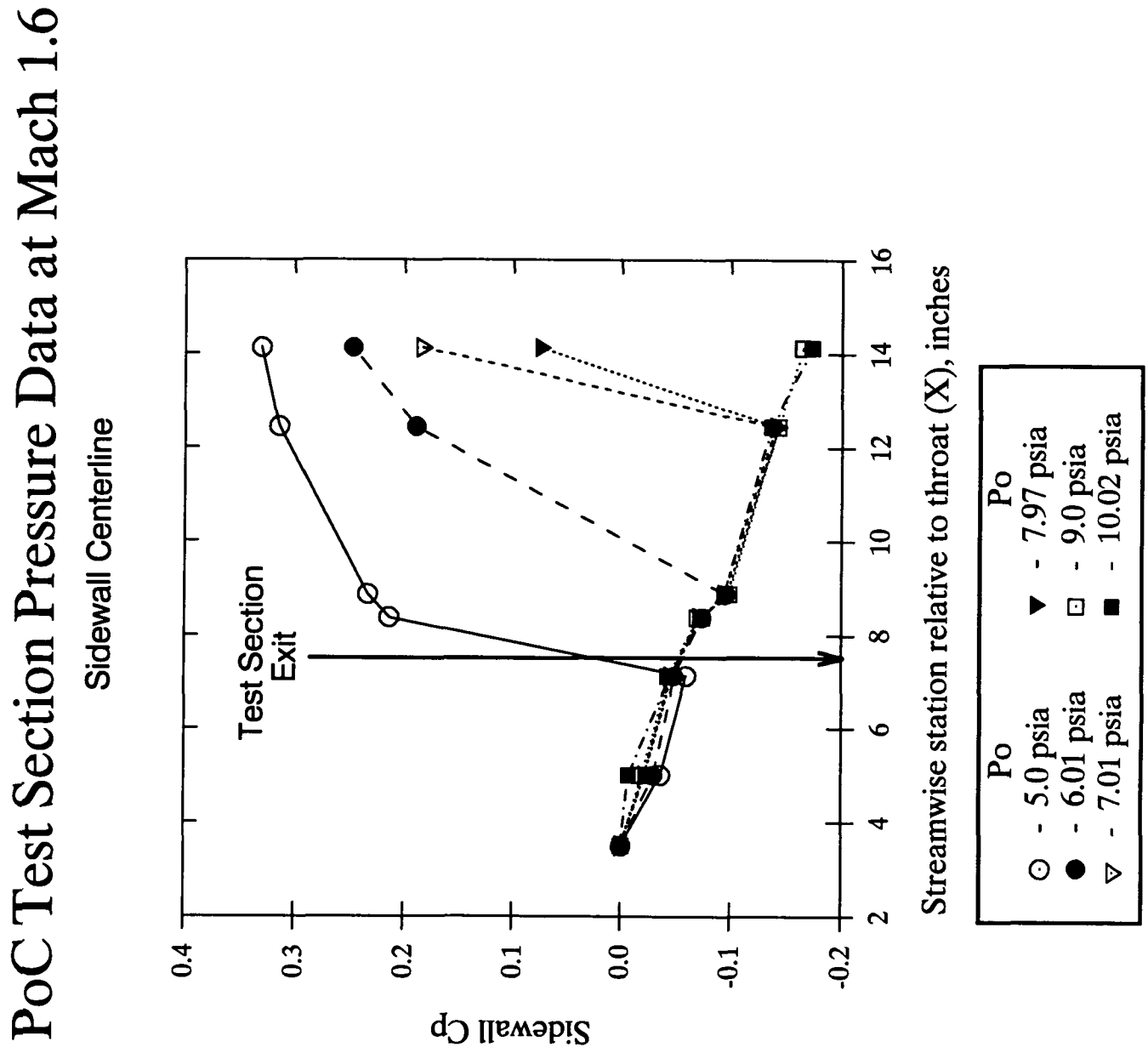

Fig. 8a - PoC test section pressure distributions with an empty test section.

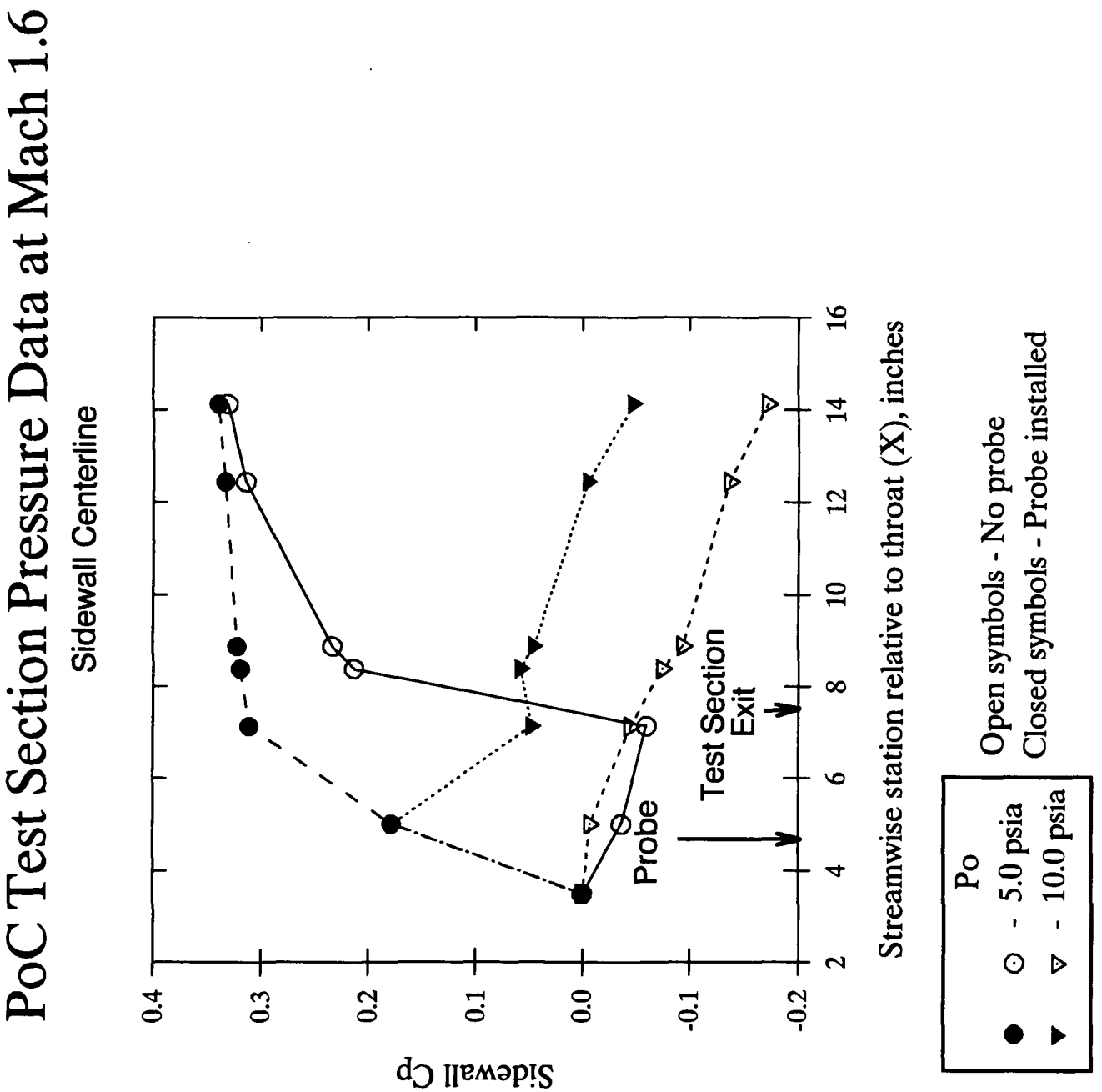

Fig. 8b - PoC test section pressure distributions with a pitot probe installed.

Comparison of Flight and WT Test Envelopes

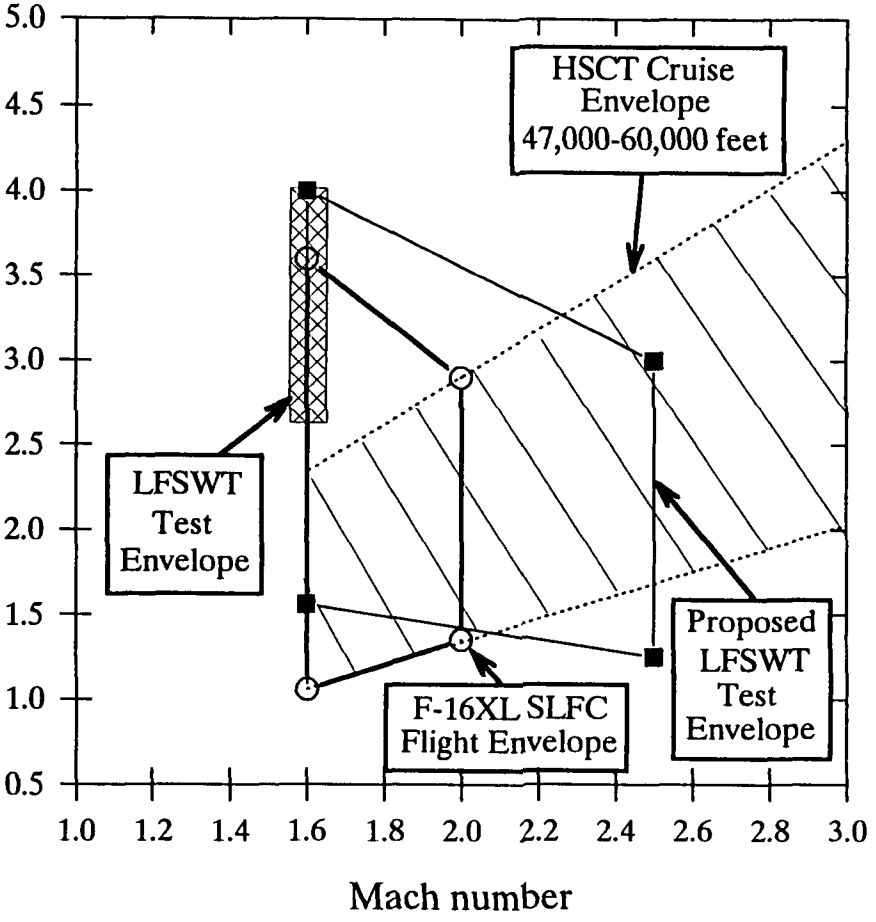

SW 5/20/94

Fig. 9 - Comparison of the current LFSWT test envelope with the F-16XL flight envelope.

Laminar Flow Supersonic Wind Tunnel

Fluid Mechanics Laboratory

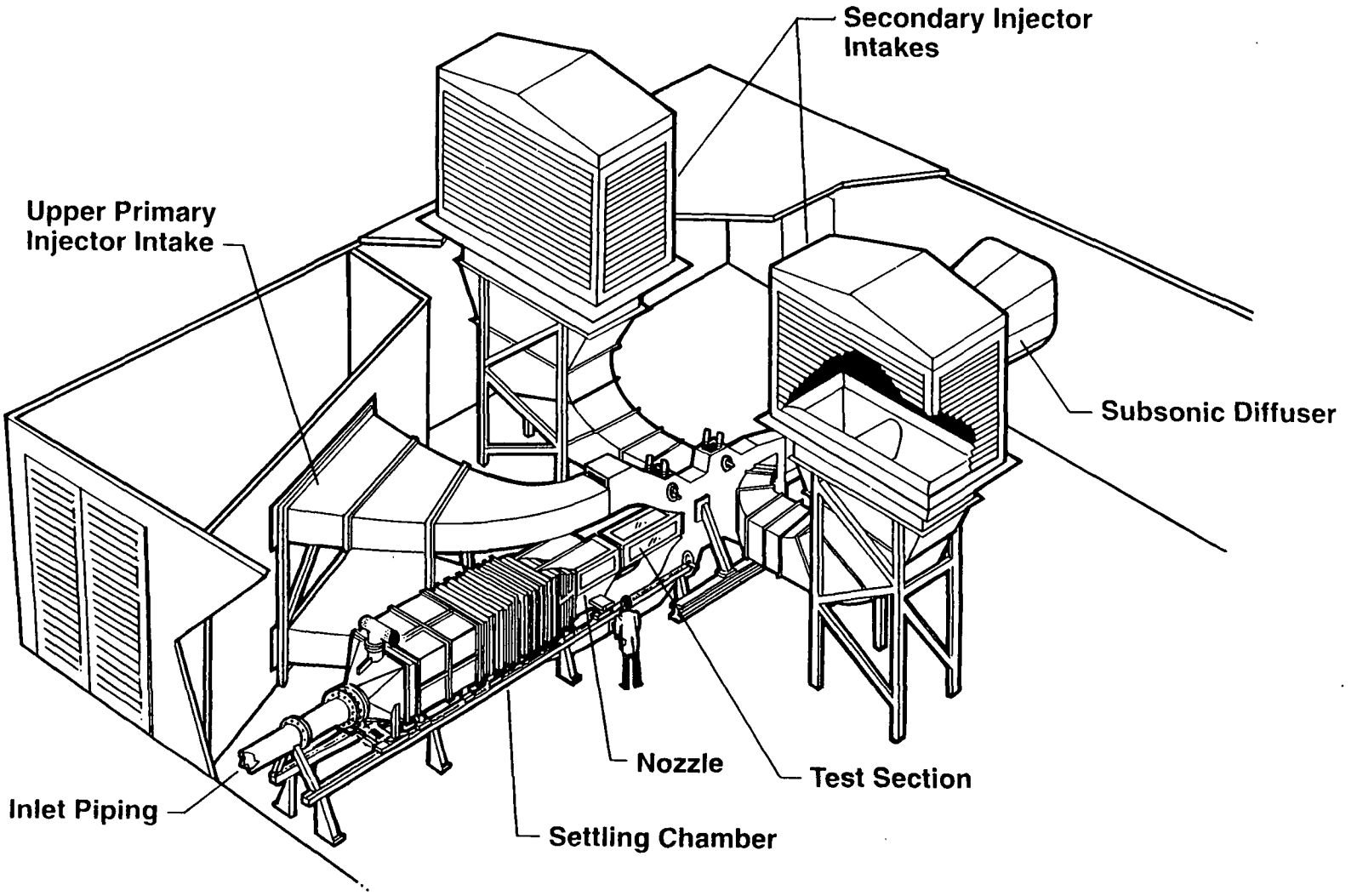

Fig. 10 - Schematic of the LFSWT layout with two stages of ambient injectors.

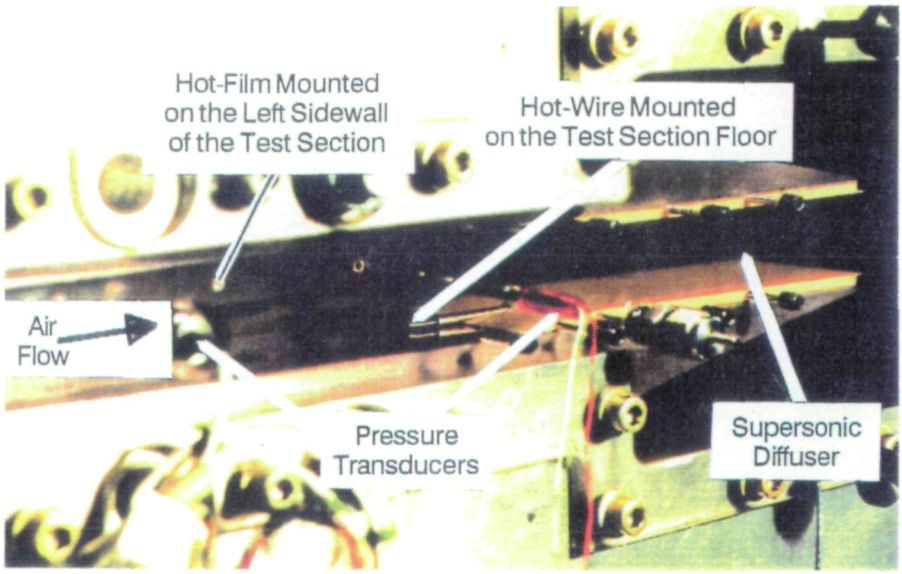

Fig. 11 - Instrumentation suite for laminar flow studies in the PoC test section.

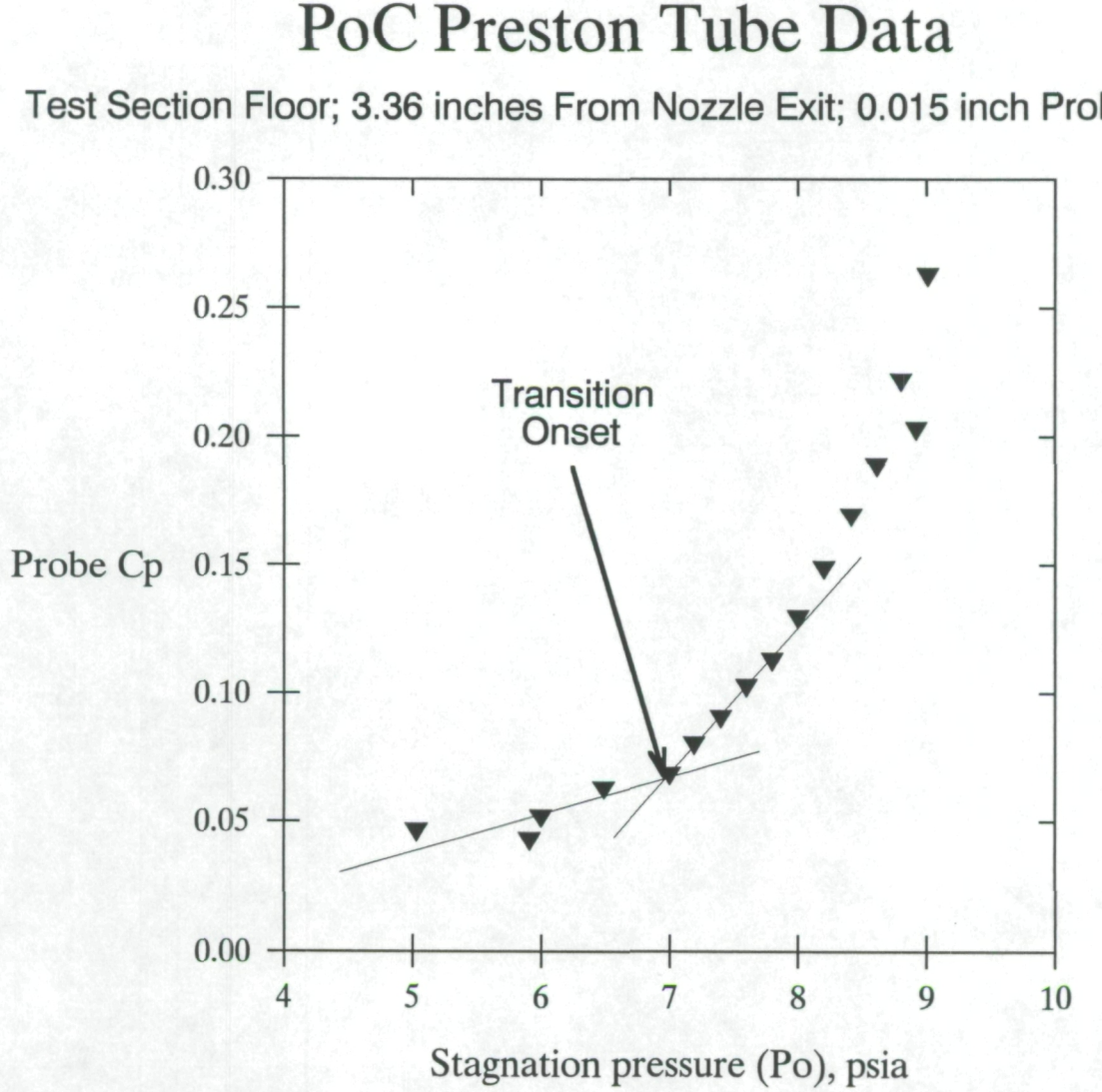

Fig. 12 - Preston tube Mach 1.6 boundary layer data in the PoC test section (X = 6.83).

Glass Inserts in the PoC Windows

October 1992

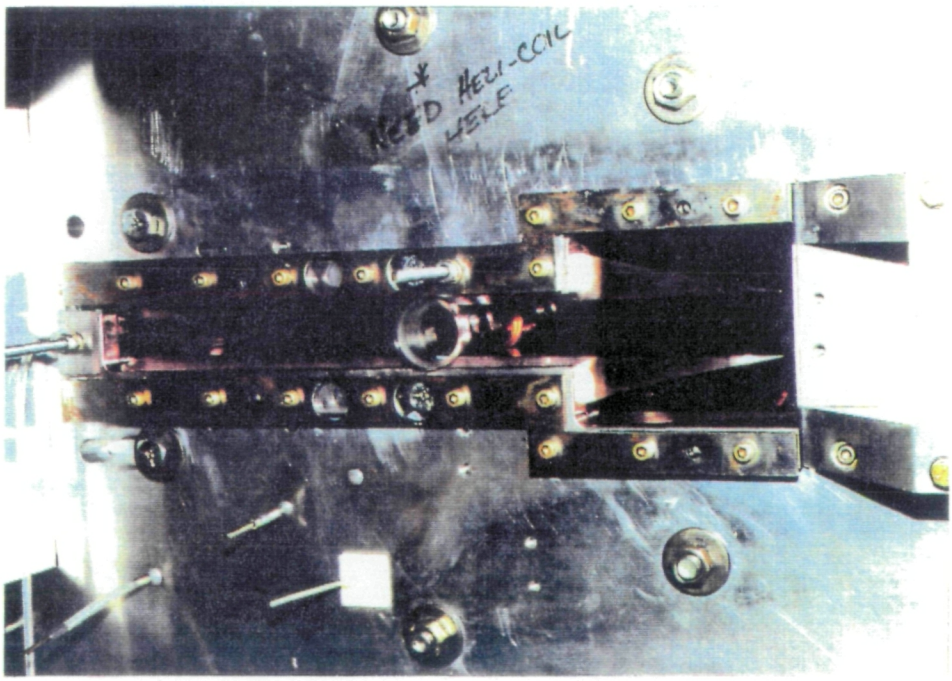

ORIGINAL PAGE
COLOR PHOTOGRAPH

Fig. 13 - Circular glass inserts in the PoC windows for boundary layer visualization.

PoC Focusing Schlieren Visualization

Test Section Floor (X=6.83); Focus Plane on Centerline; Mach 1.6 Operation

Po = 6.8 psia Transitional Boundary Layer

Po = 11 psia Turbulent Boundary Layer

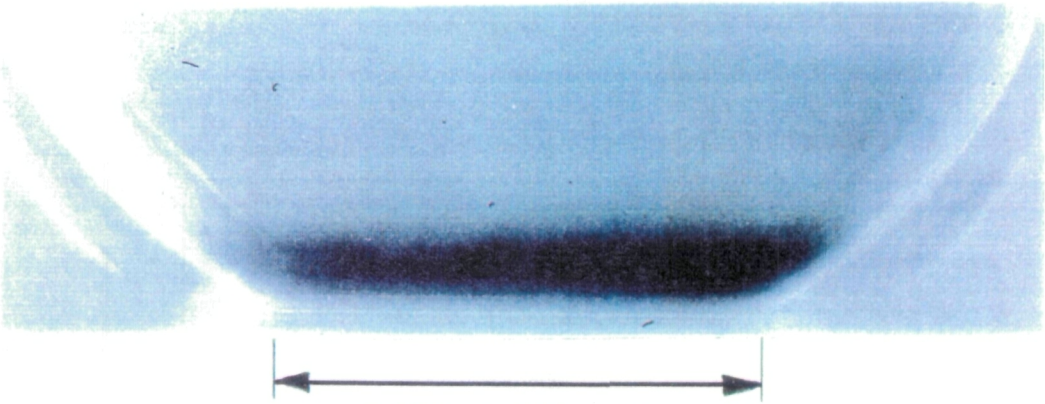

Fig. 14 - Focusing schlieren of the PoC floor boundary layer at two test conditions.

Fig. 15a - PoC hot film array prior to installation with the two-piece window blank.

PoC Hot-Film Array Setup
February 1993

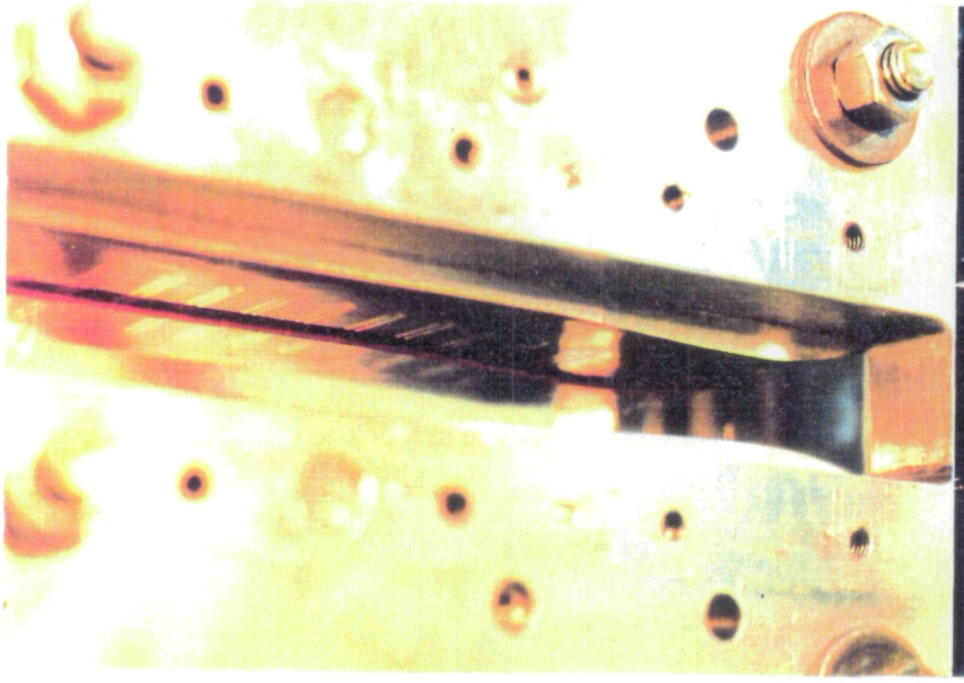

Hot-Film Array Bonded to the PoC
Nozzle/Test Section Top Wall

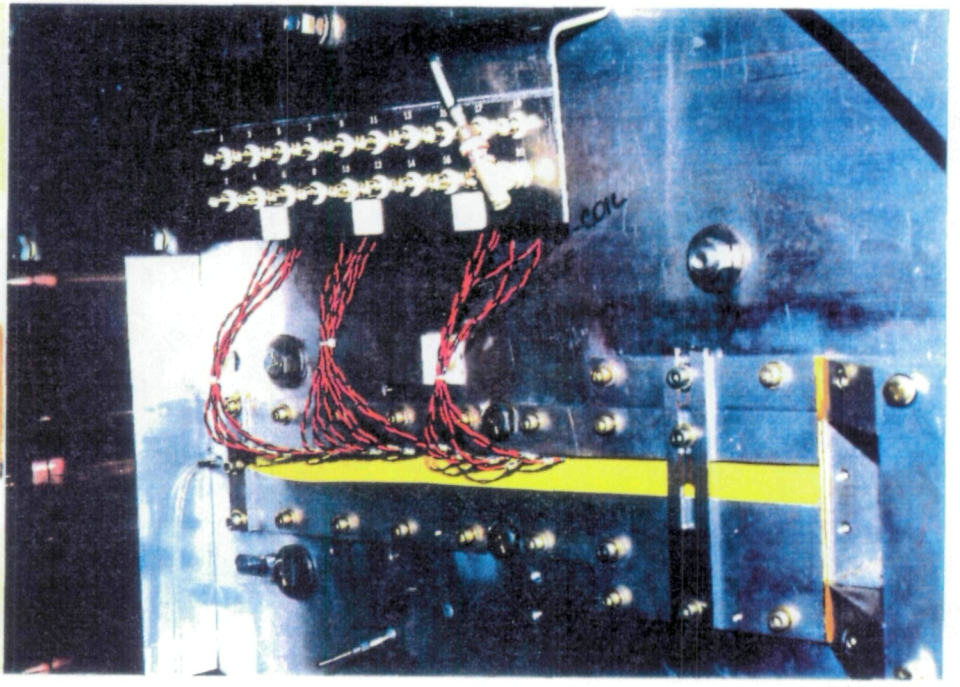

Electrical Connections to the Hot-Films
Through the Two-Piece Window Blank

Fig. 15b - PoC hot film array installed in the nozzle and test section.

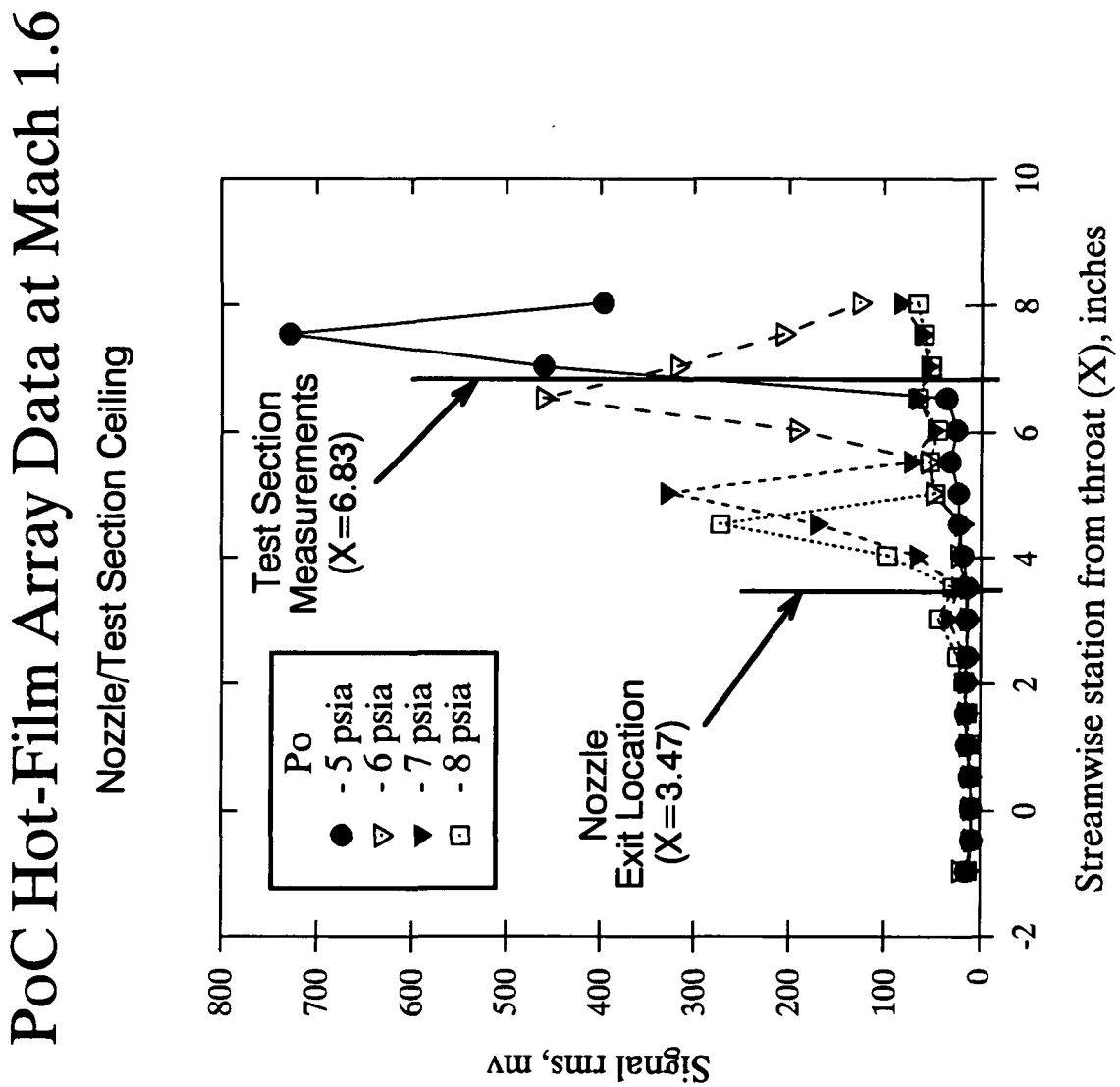

Fig. 16 - Summary of PoC hot film array data variation with Po, at Mach 1.6.

PoC Test Section Pitot Data

Nozzle Exit Centerline (X=3.47); 0.1 inch Probe dia.; Mach 1.6 Operation

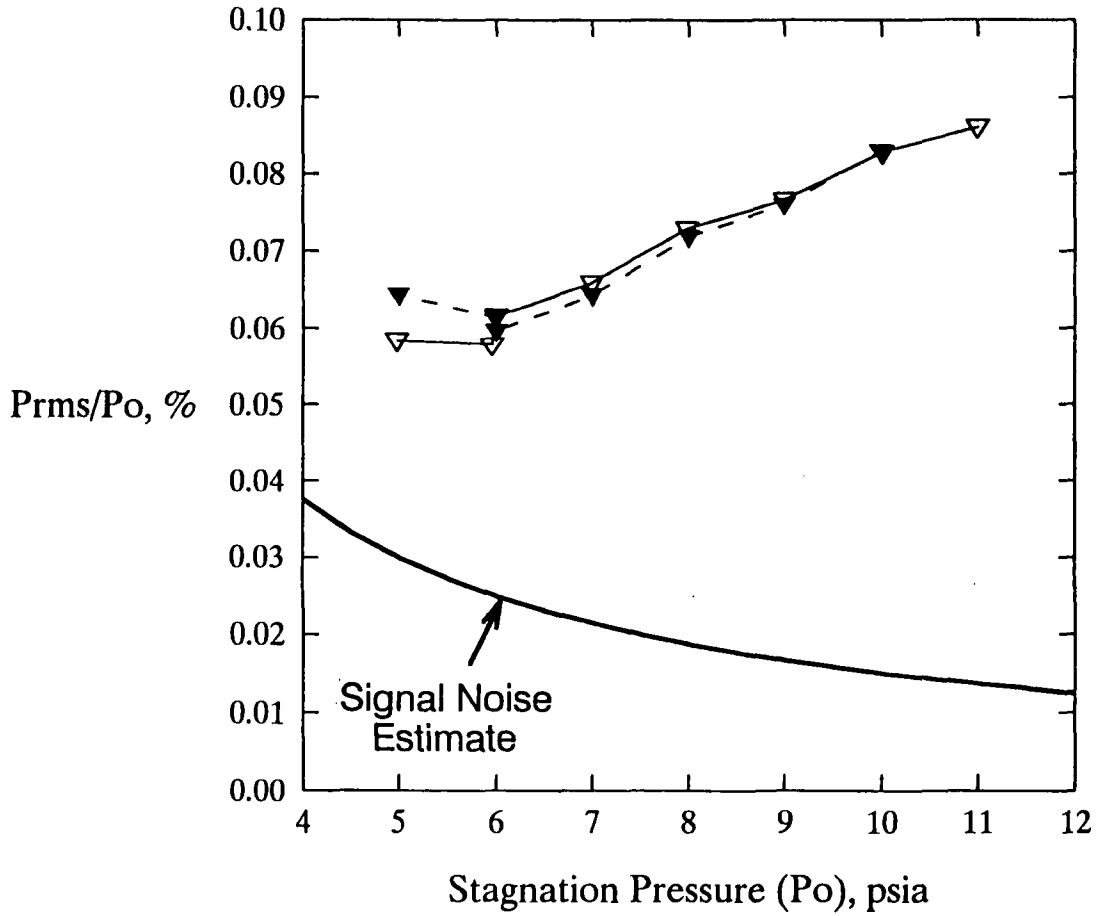

Fig. 17 - Pressure fluctuations measured in the PoC test section entrance (X = 3.47).

PoC Test Section Pitot Data

Nozzle Exit Plane (X= 3.47); 0.5 inch Above Floor; 0.1 inch Probe dia.; Mach 1.6 Operation

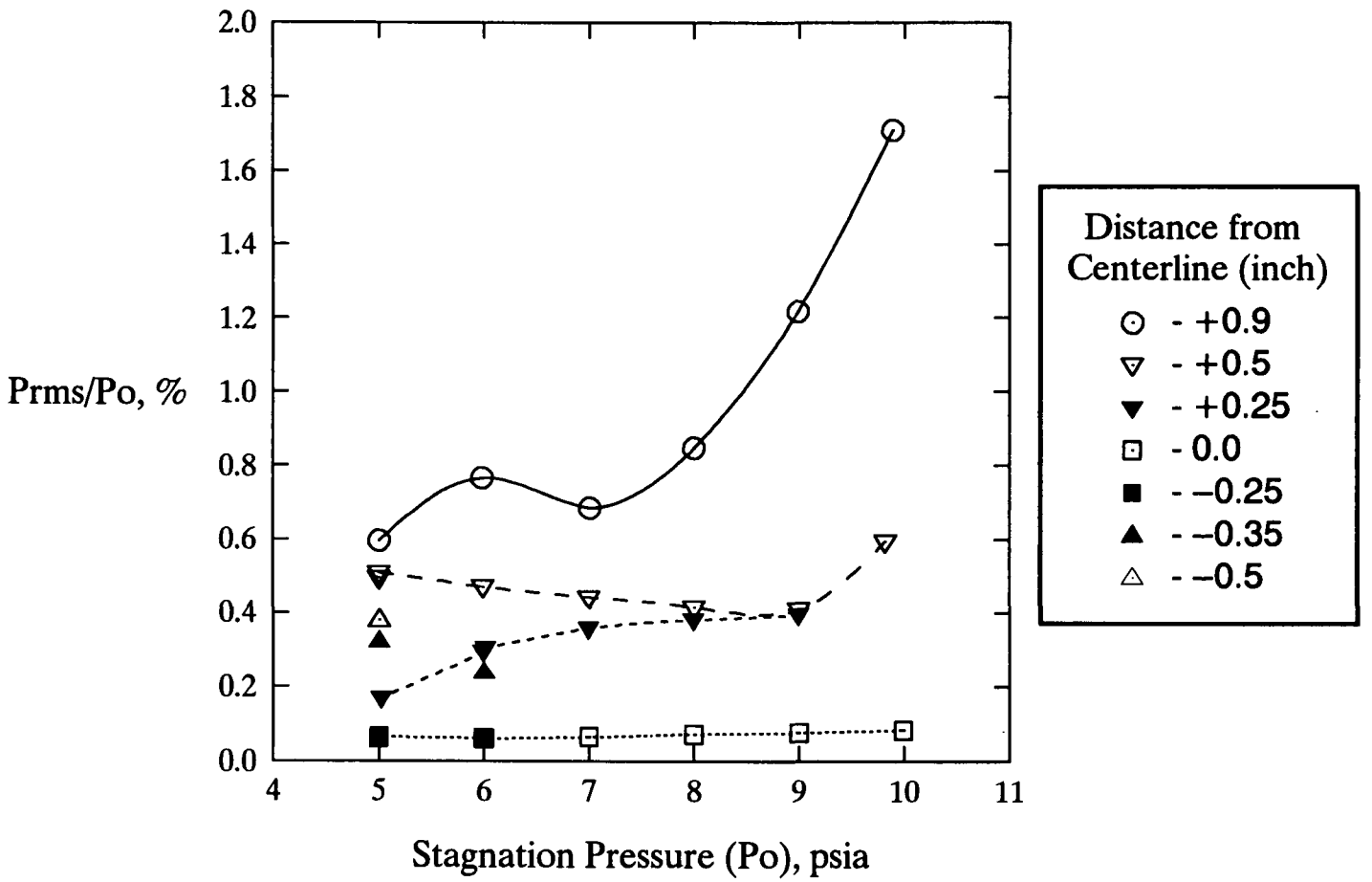

Fig. 18 - Spanwise distribution of pressure fluctuations in the PoC test section entrance.

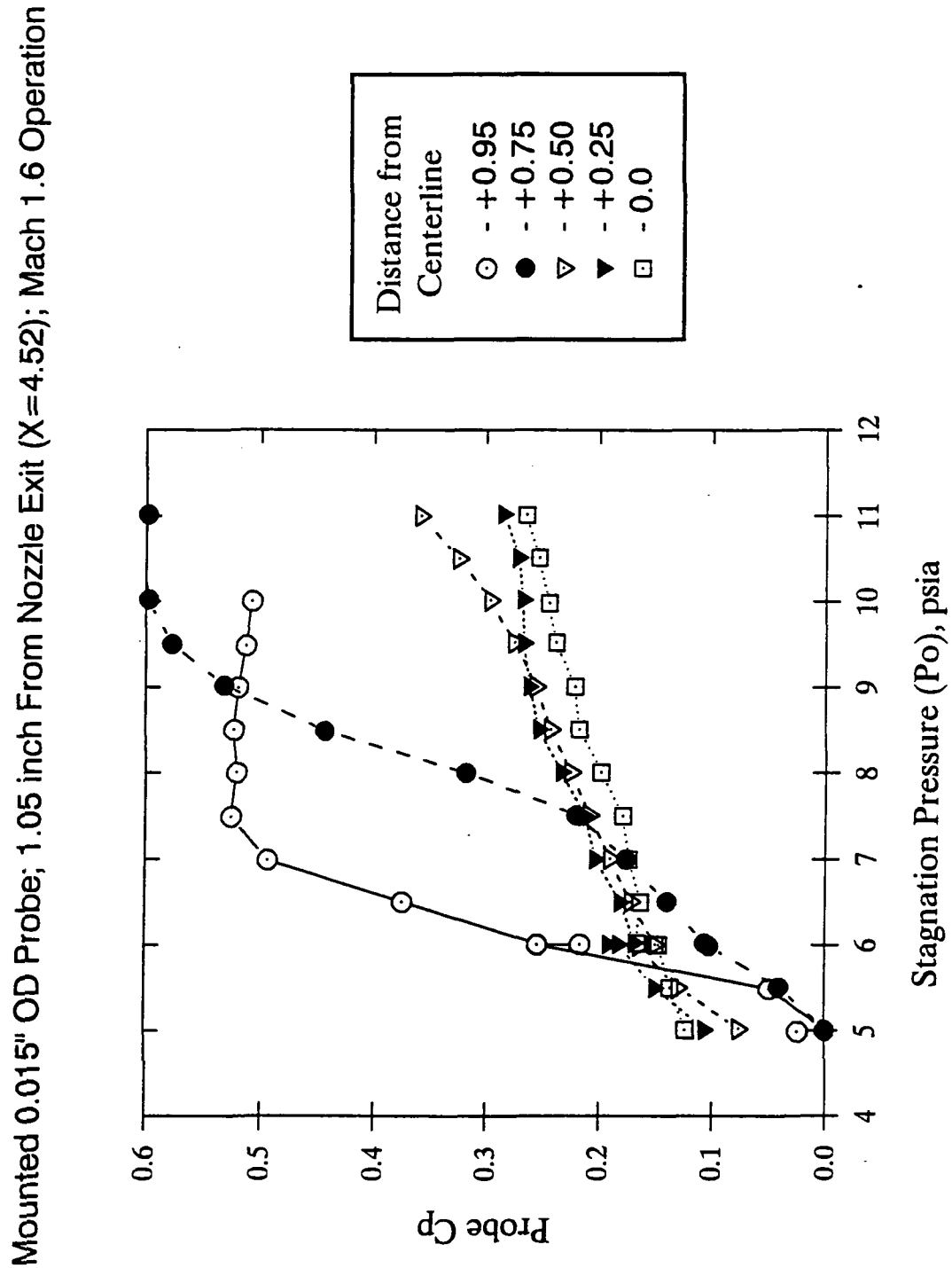

Fig. 19a - PoC floor boundary layer data near the test section entrance (X = 4.52).

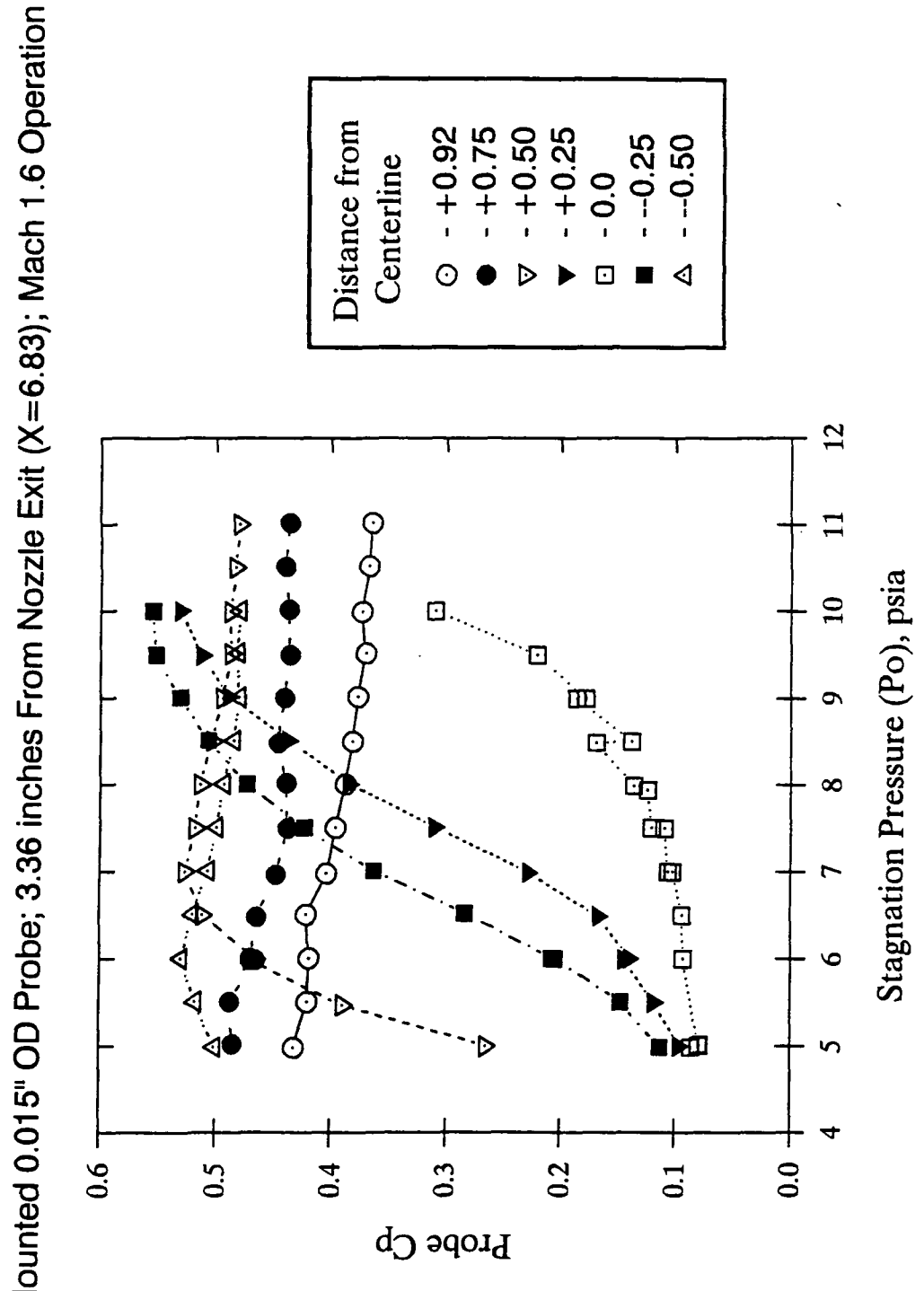

Fig. 19b - PoC floor boundary layer data at near mid-test section (X = 6.83).

PoC Preston Tube Data

Floor Mounted 0.015" OD Probe; 4.91 inches From Nozzle Exit (X=8.38); Mach 1.6 Operation

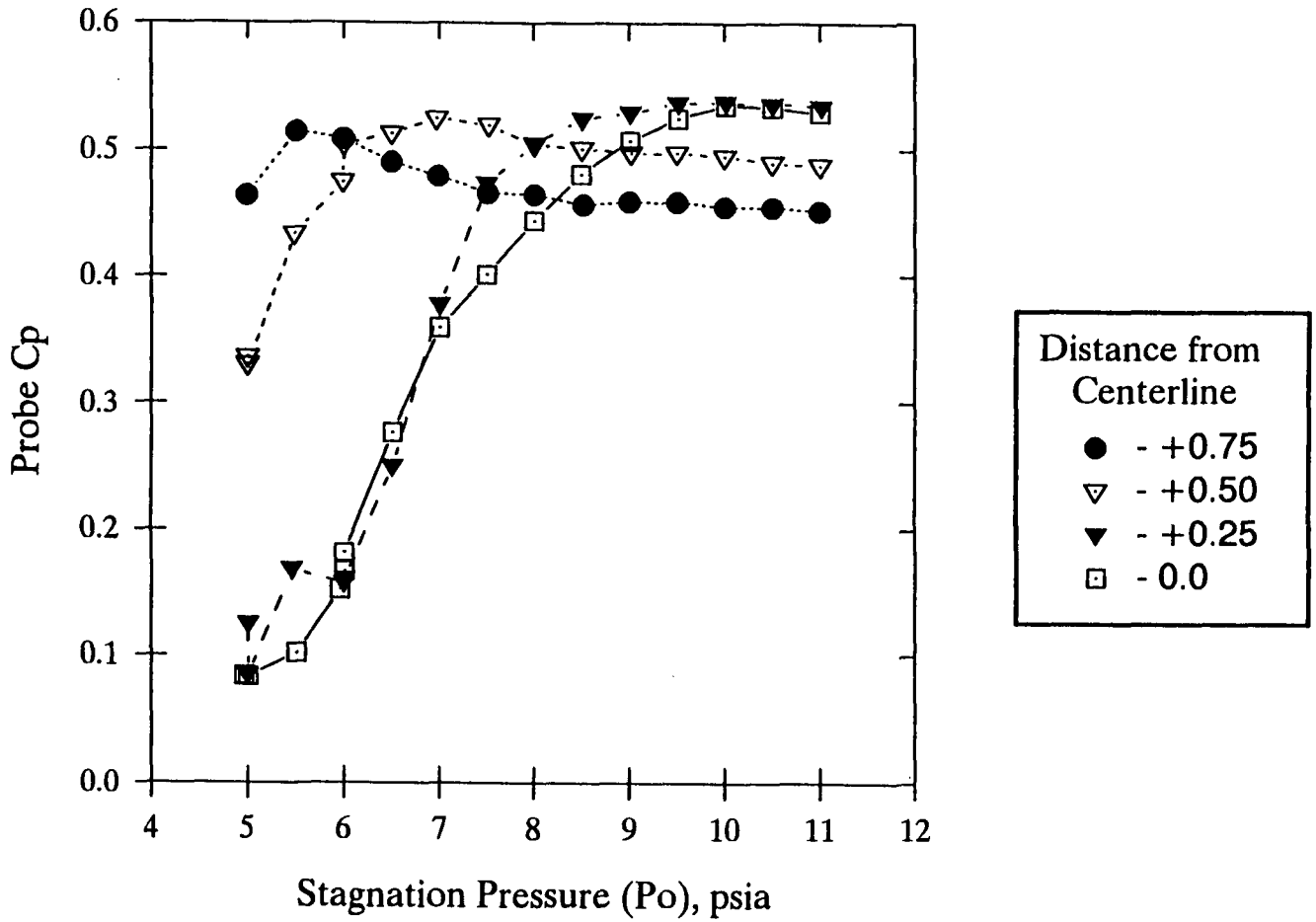

Fig. 19c - PoC floor boundary layer data near the test section exit (X = 8.38).

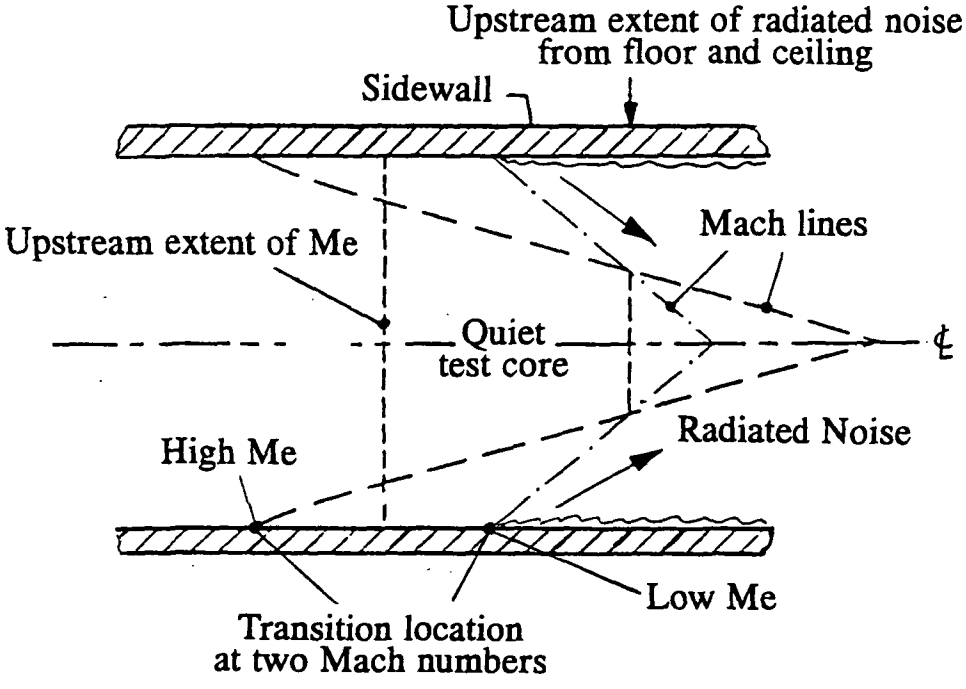

Fig. 20 - Envisaged boundaries of a quiet test core at two supersonic Mach numbers.

LFSWT Settling Chamber and Nozzle Details

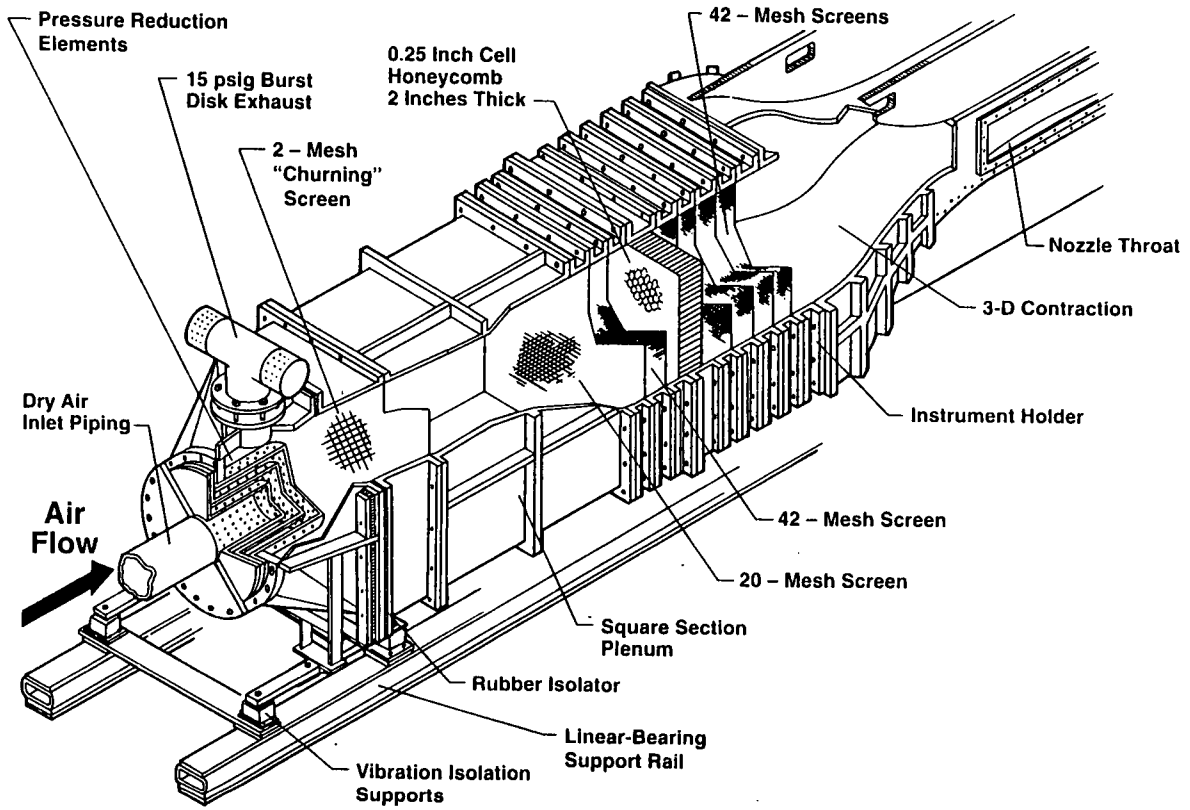

Fig. 21 - Schematic of the LFSWT low-disturbance settling chamber.

View of the LFSWT Nozzle Throat

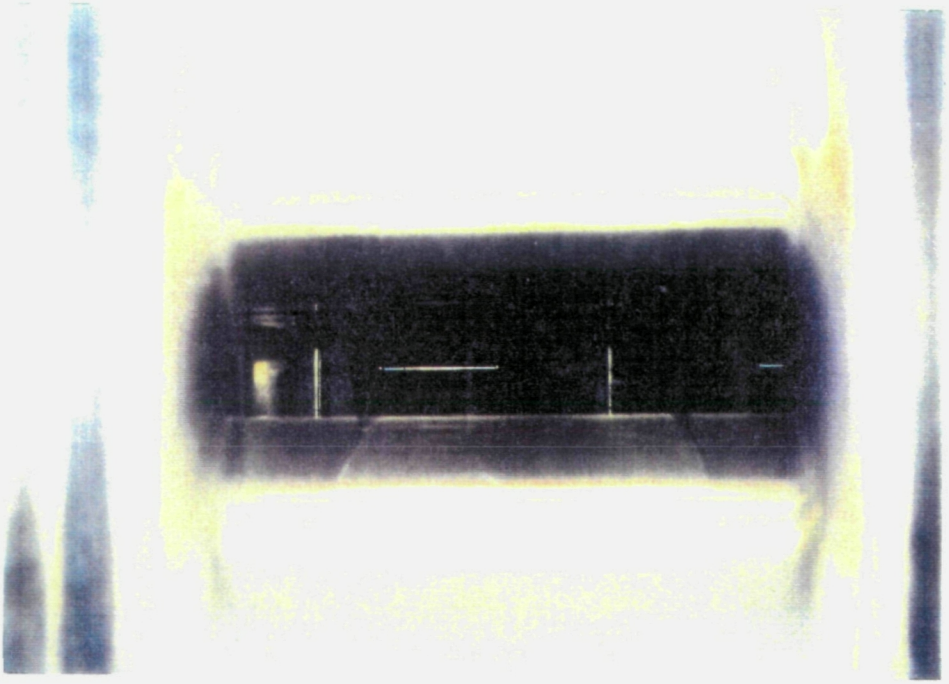

(Shown downstream of the nozzle is the pitot probe mounted in test section)

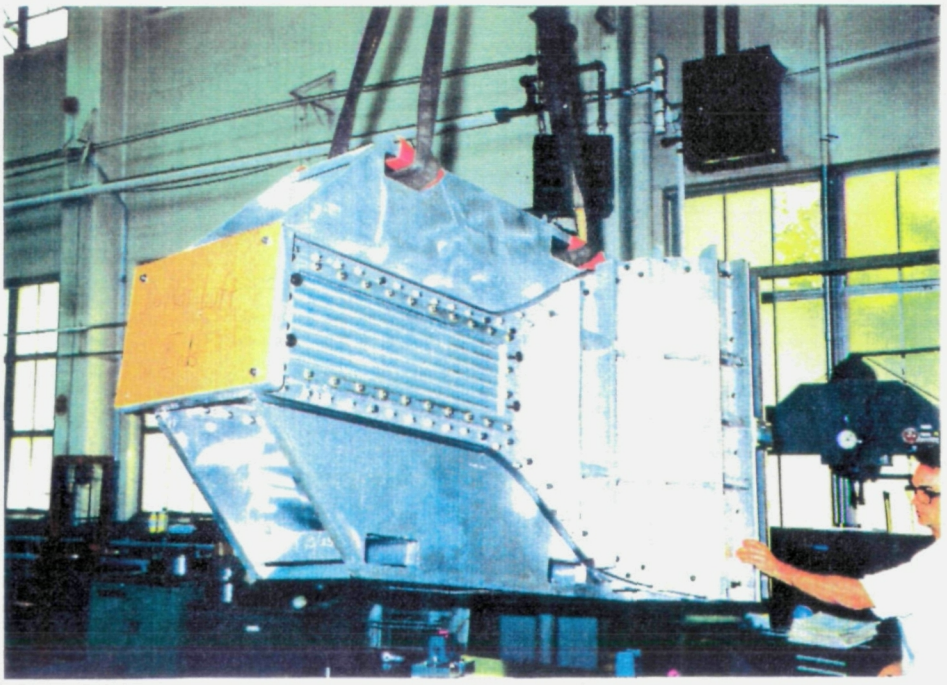

Fig. 22 - LFSWT contraction and nozzle are one component, with a highly polished flow surface (as shown in the lower picture looking through the nozzle throat).

NASA-Ames Laminar Flow Supersonic Wind Tunnel

Test Section and Nozzle

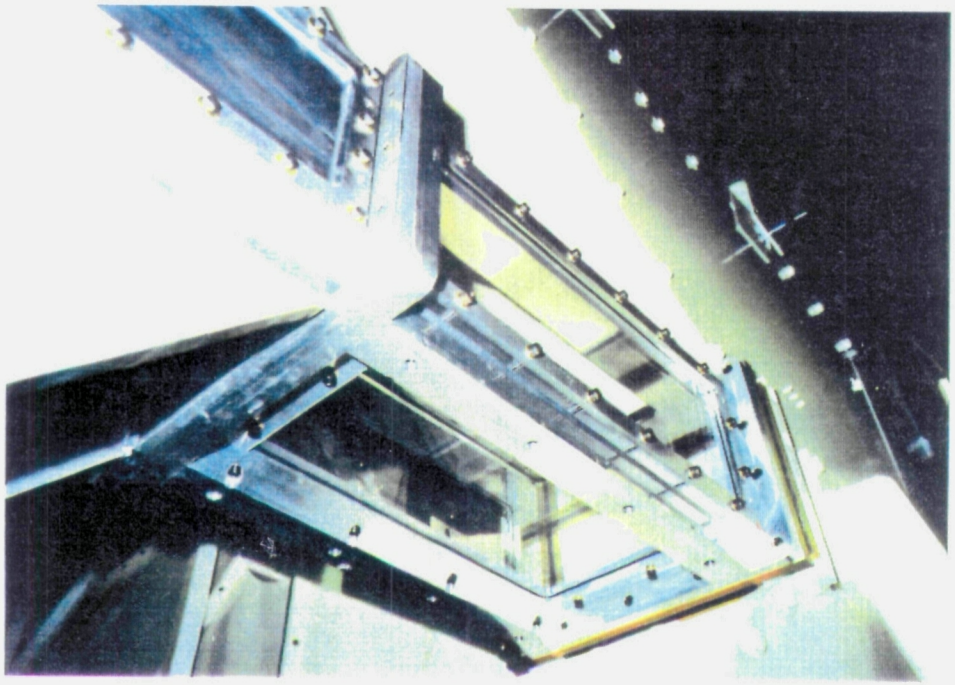

Fig. 23 - Views of the LFSWT test section and nozzle showing the good optical access.

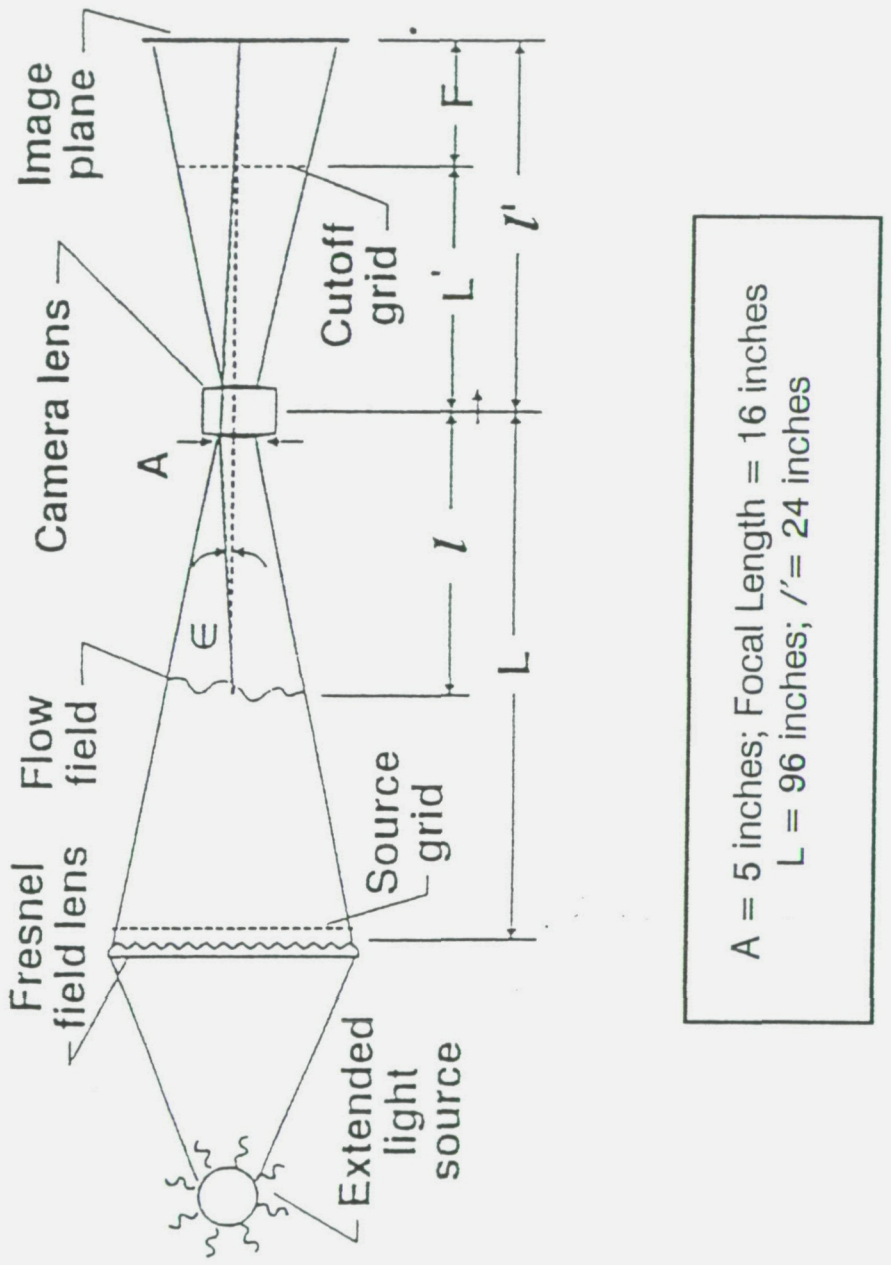

Fig. 24 - Layout of the focusing schlieren system developed with the PoC.

Manifold Kulite Pressures

K-Test 48 - 11/10/93

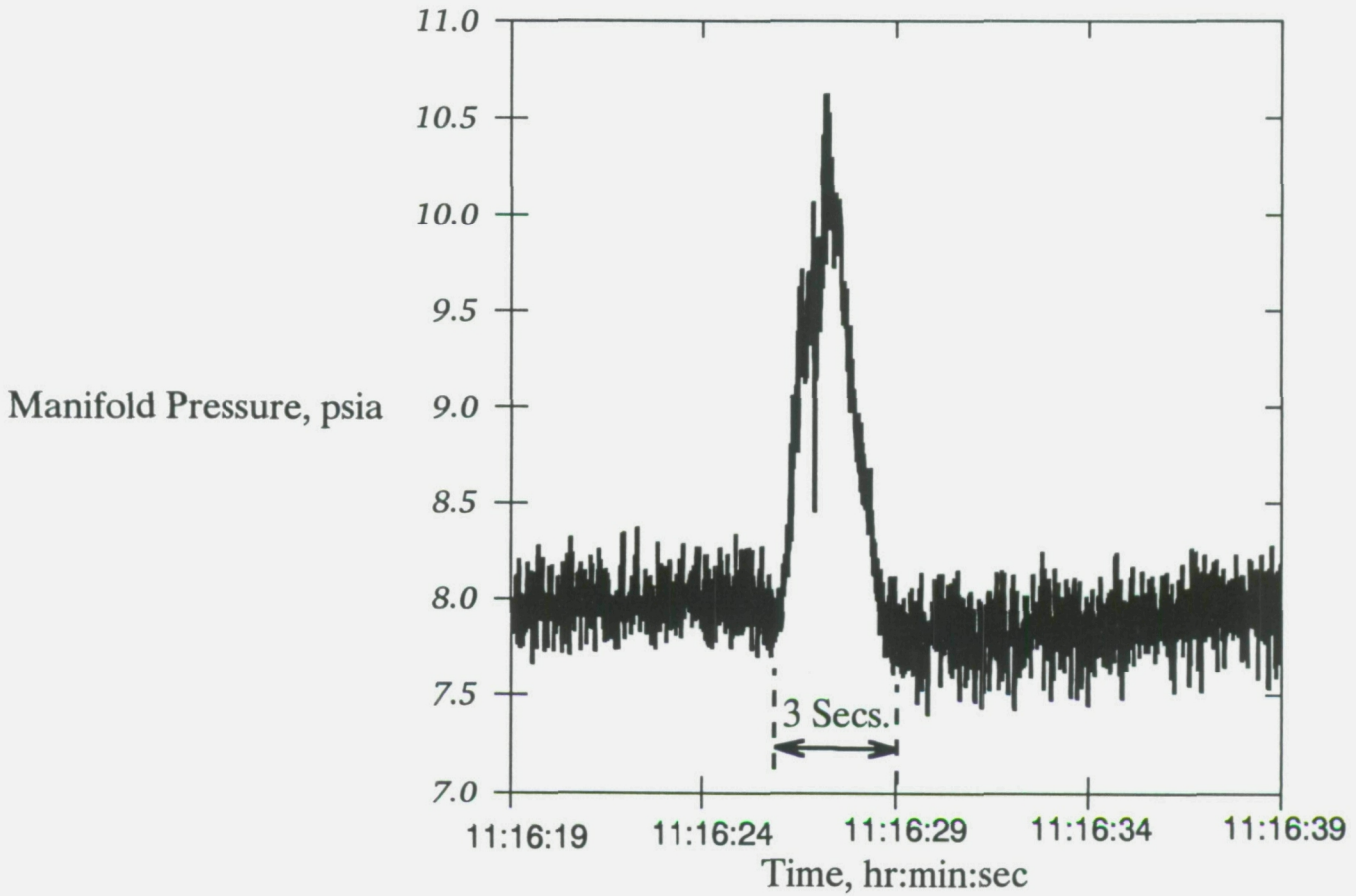

SW 11/11/93

Fig. 25 - Manifold pressure spike during a typical LFSWT startup.

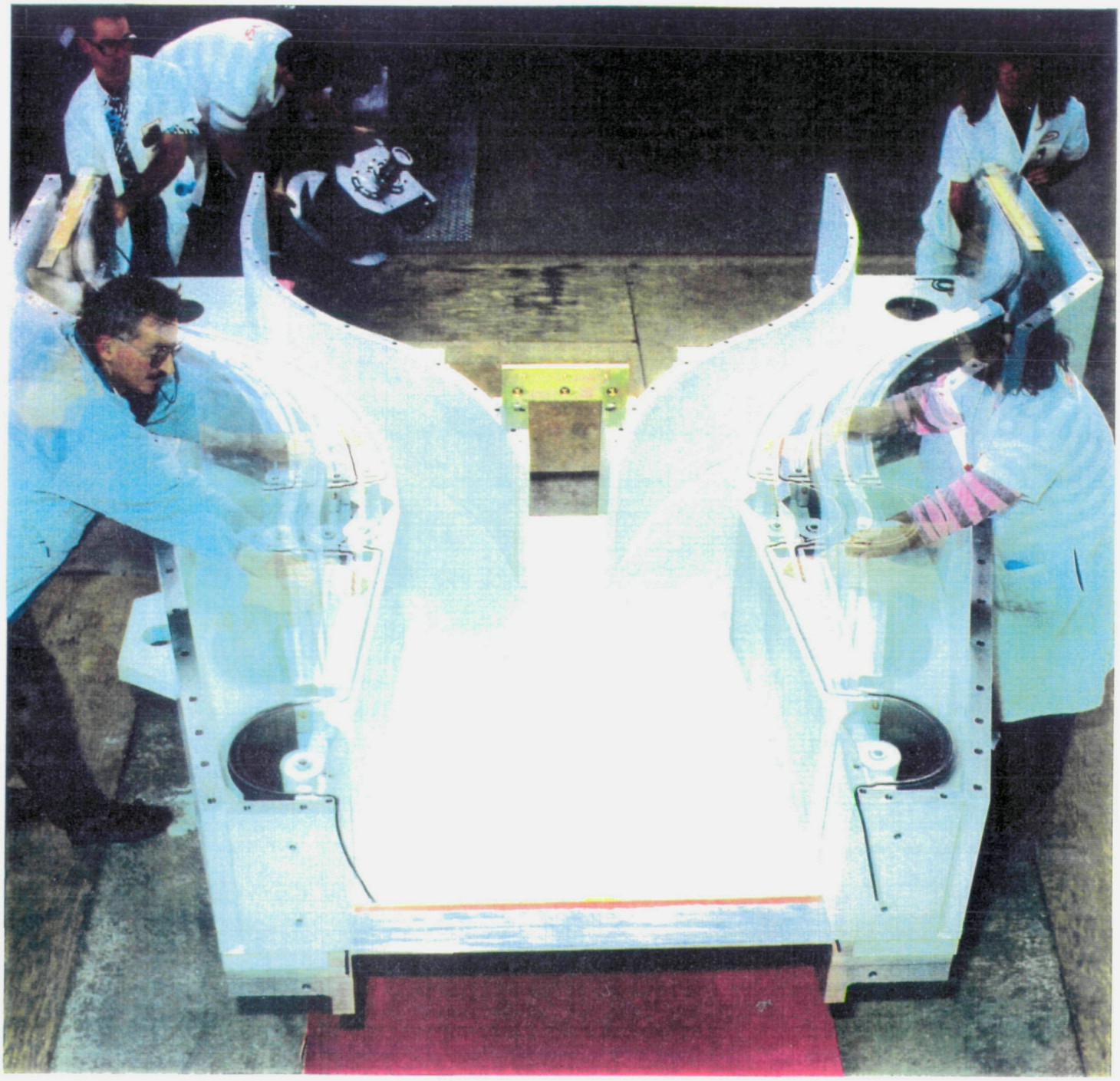

Fig. 26 - Multiple exposure photograph illustrates the adjustability available in the LFSWT primary injectors.

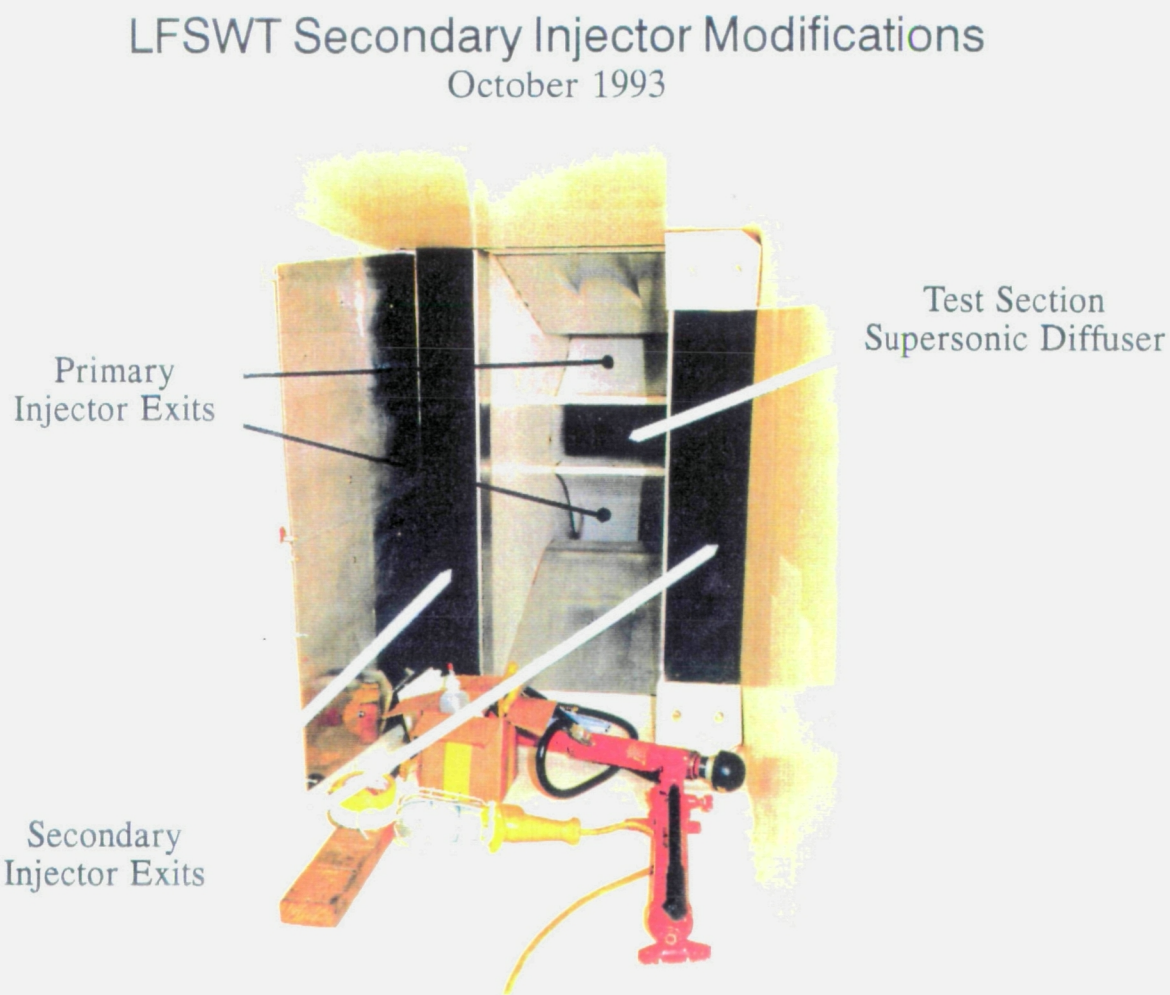

Fig. 27 - Two stages of tuning modifications to the LFSWT secondary injector exits.

NASA-Ames FML Compressor Data

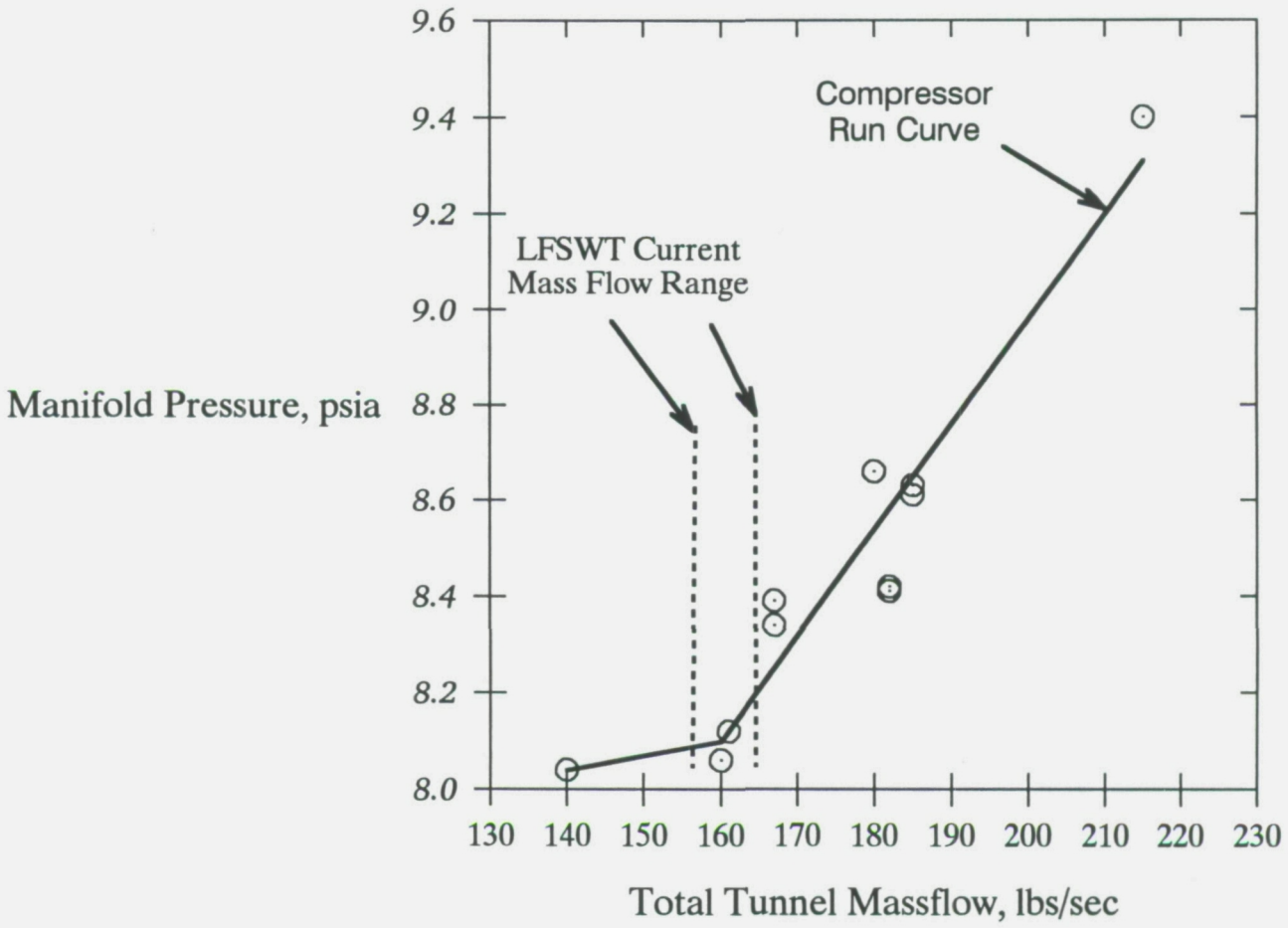

Fig. 28 - Comparison of LFSWT tuning data with the FML compressor run curve.

SW 11/11/93

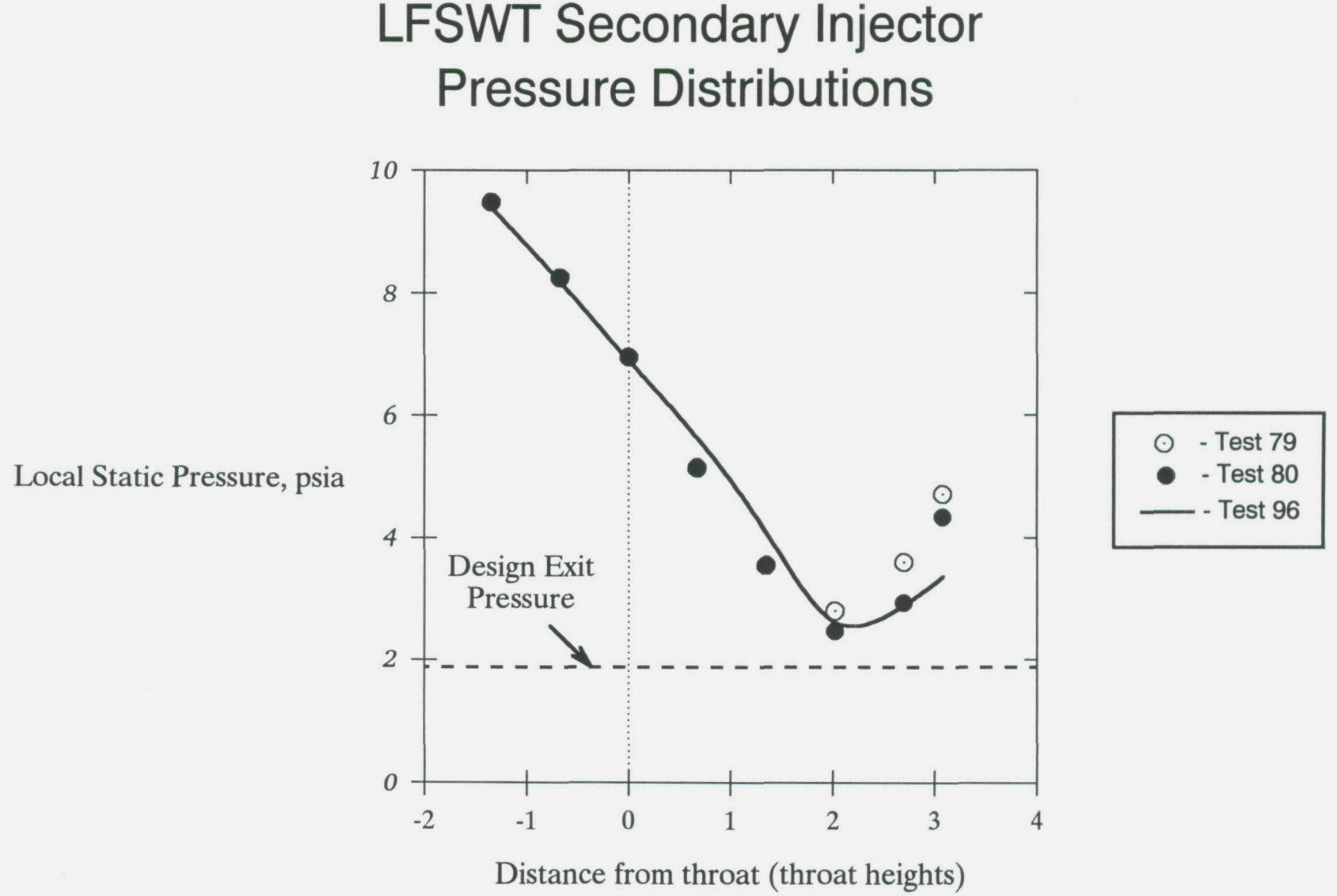

Fig. 29 - Comparison of LFSWT secondary injector pressure distributions at different Po.

Secondary Injector Nozzle Geometry

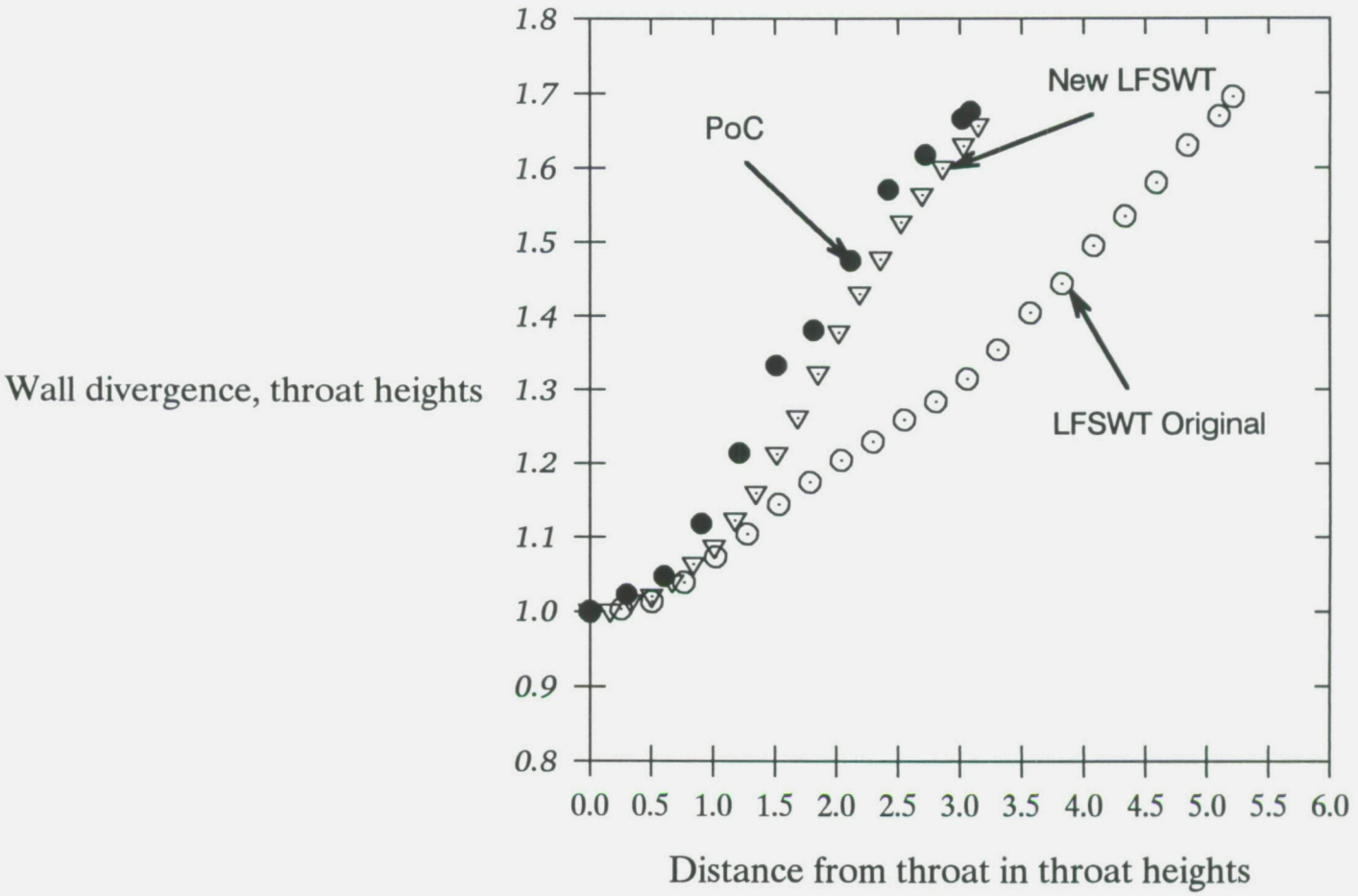

Fig. 30 - Comparison of the improved and original LFSWT secondary injector nozzles.

SW 8/18/93

LFSWT Final Diffuser Configuration Looking Upstream

May 1994

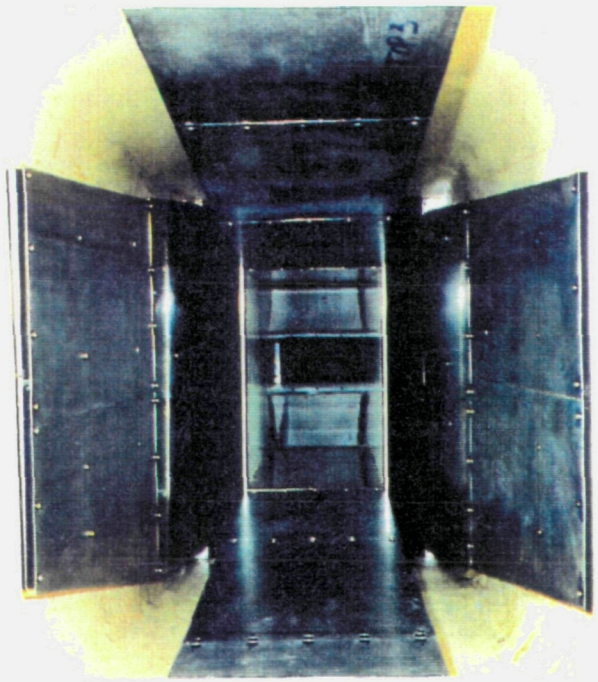

Fig. 31 - Final LFSWT diffuser ramp and injector exit configuration for best performance.

LFSWT Settling Chamber Temperatures
Warm-up Histogram

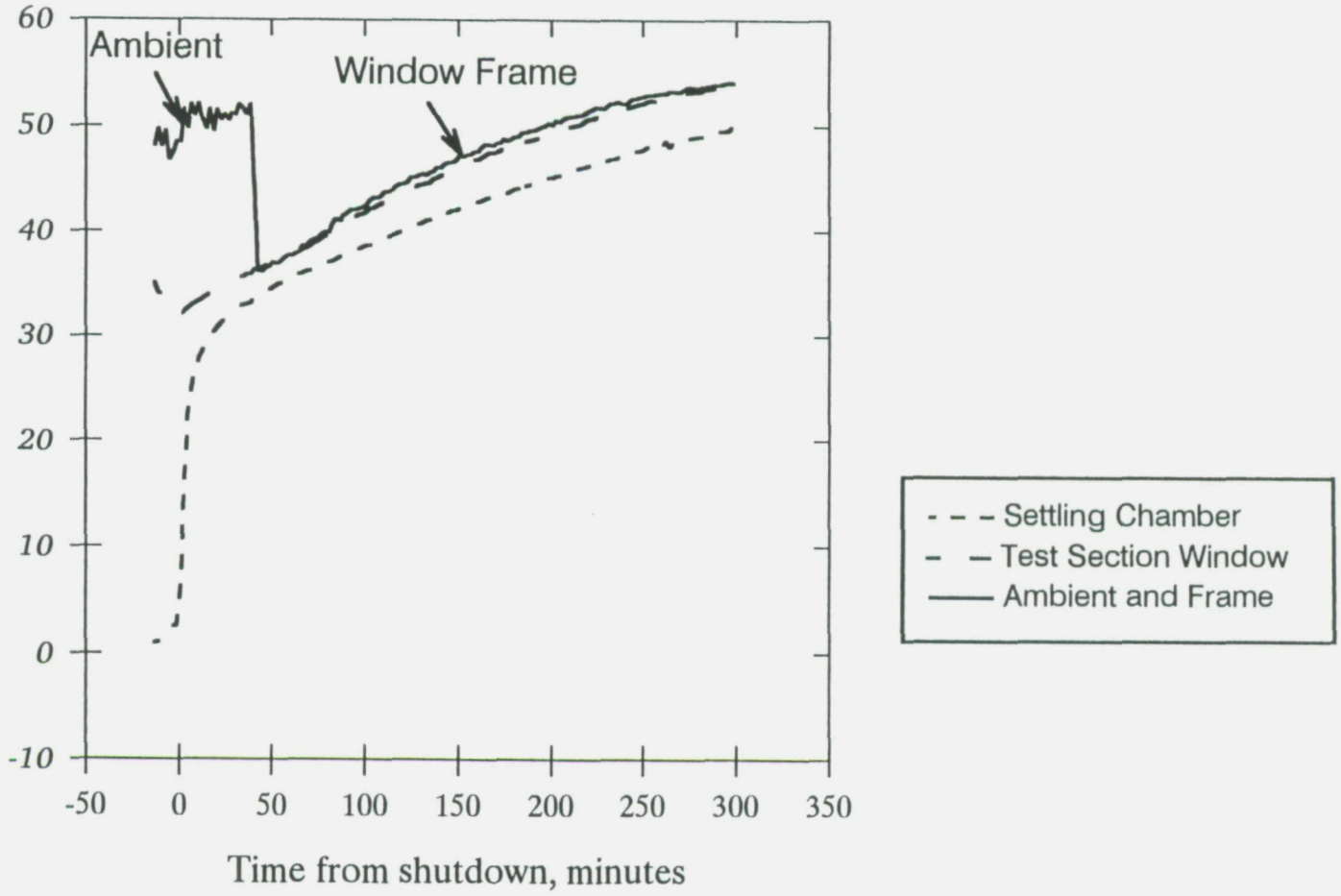

Fig. 32 - Warm-up histogram of LFSWT temperatures after tunnel shutdown.

SW 11/19/93

LFSWT Test Section Temperatures
Cool-down Histogram

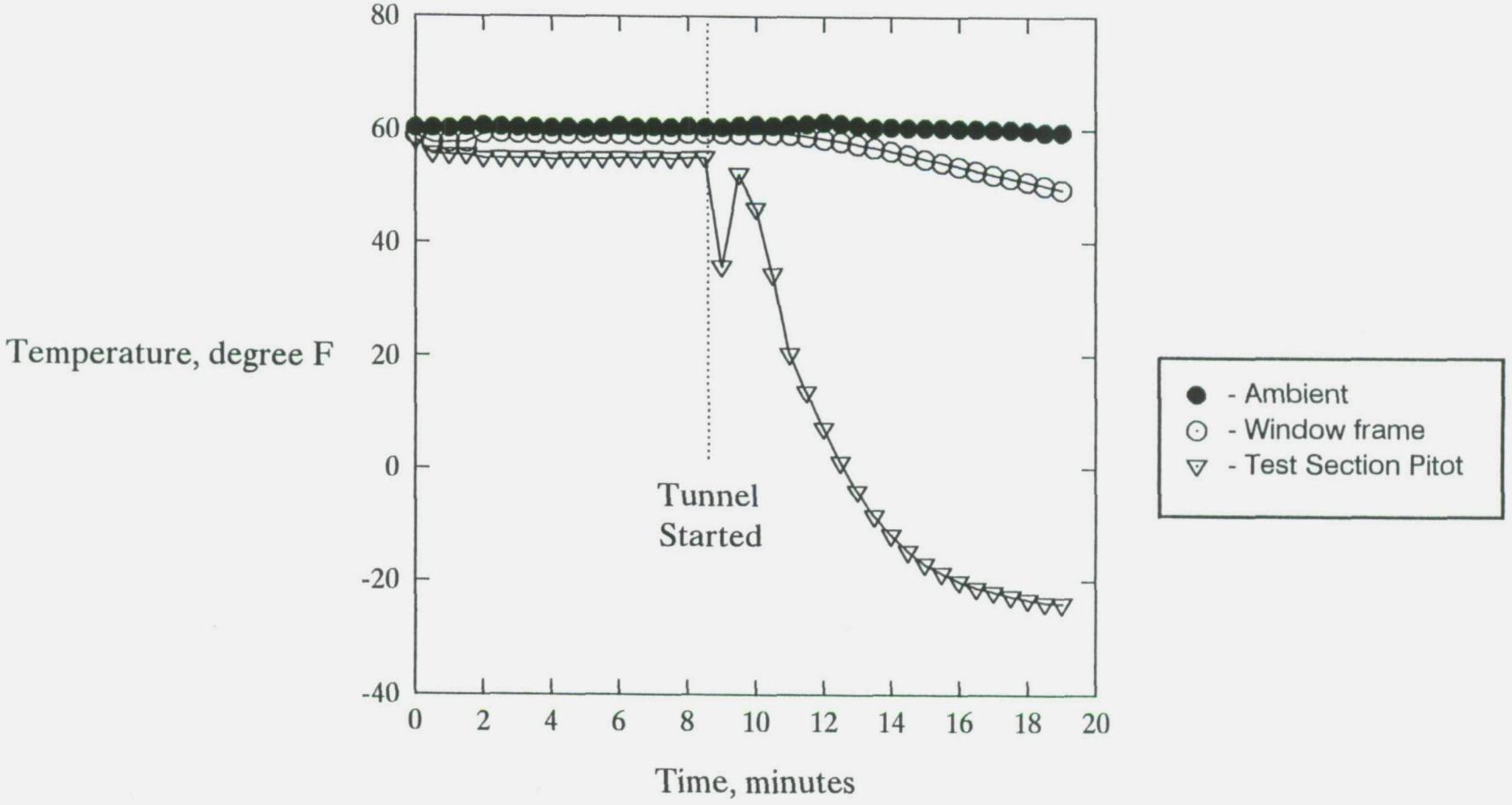

SW 2/25/94

Fig. 33 - Cool-down histogram of the LFSWT temperatures after tunnel start-up.

LFSWT Settling Chamber Disturbance Data

Contraction Entrance Centerline; 250 - 50k Hz range; Traverse Probe

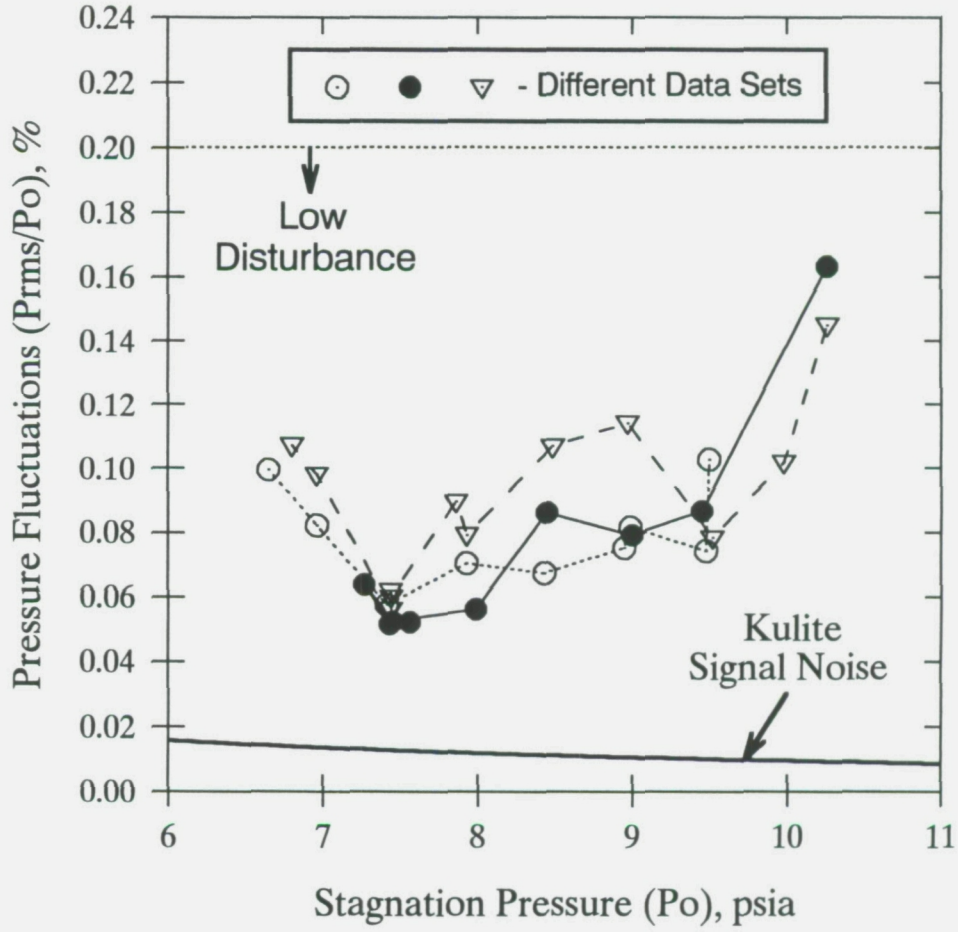

Fig. 34 - Variation of centerline pressure disturbances in the LFSWT settling chamber exit (X = -51.5) over the full range of test conditions.

SW 5/11/94

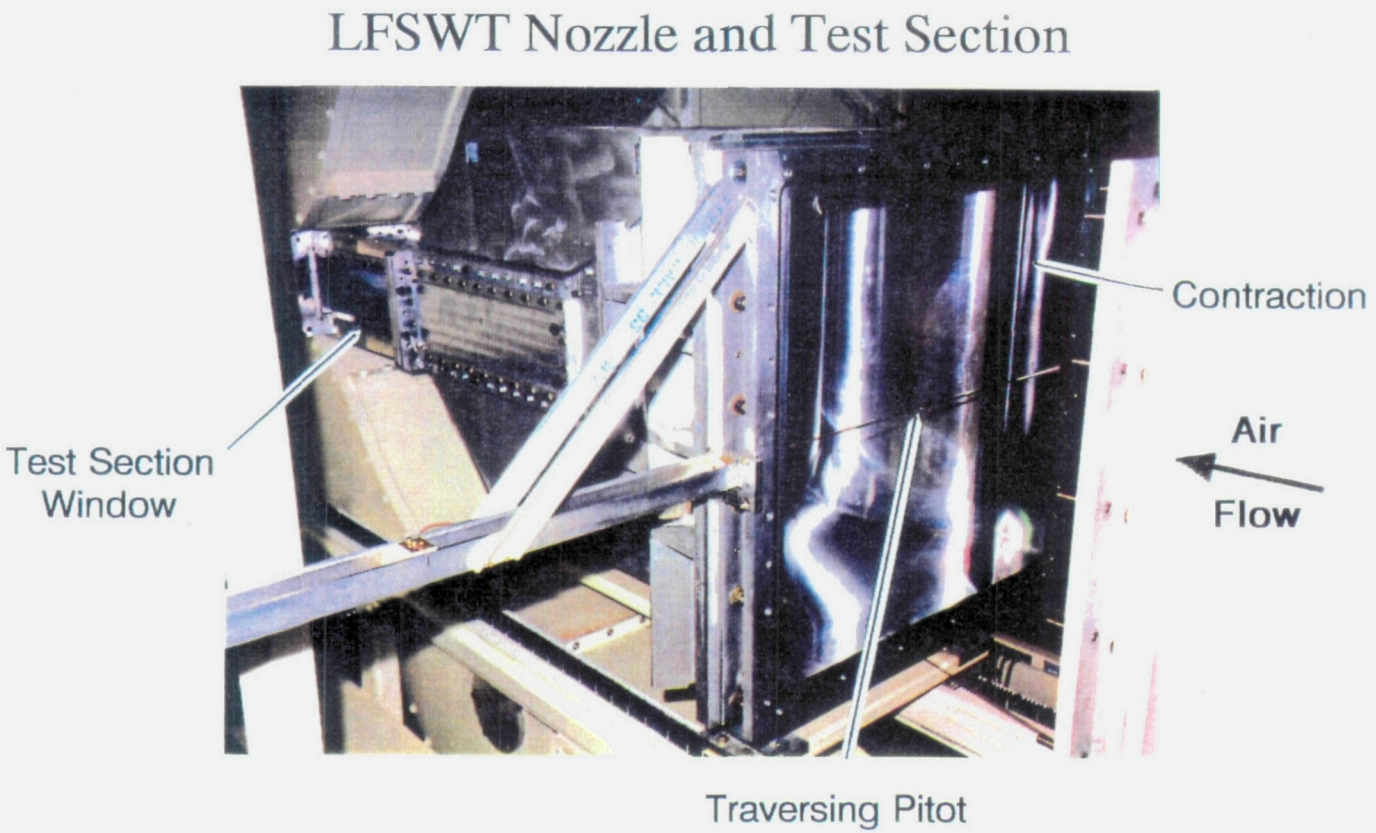

Fig. 35 - Settling chamber traverse mechanism installed in the LFSWT contraction entrance.

LFSWT Pressure Fluctuation Data

Contraction Entrance (X=-51.5): Tunnel Centerline

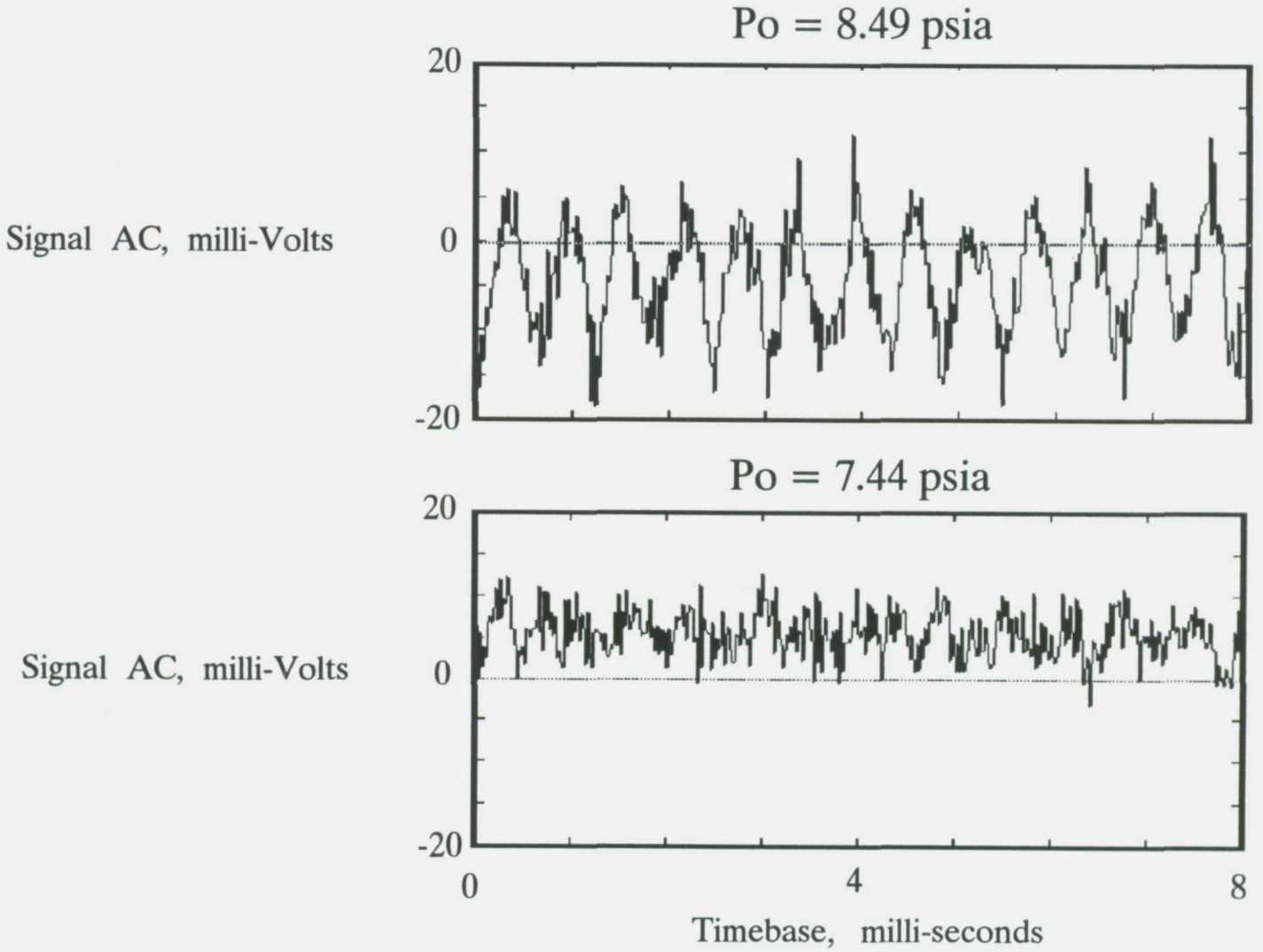

Fig. 36 - Kulite pressure fluctuation signals compared at two values of Po.

LFSWT Settling Chamber Pressure Data

250-50k Hz Range; Contraction Entrance (X=-51.5); Tunnel Vertical Centerline

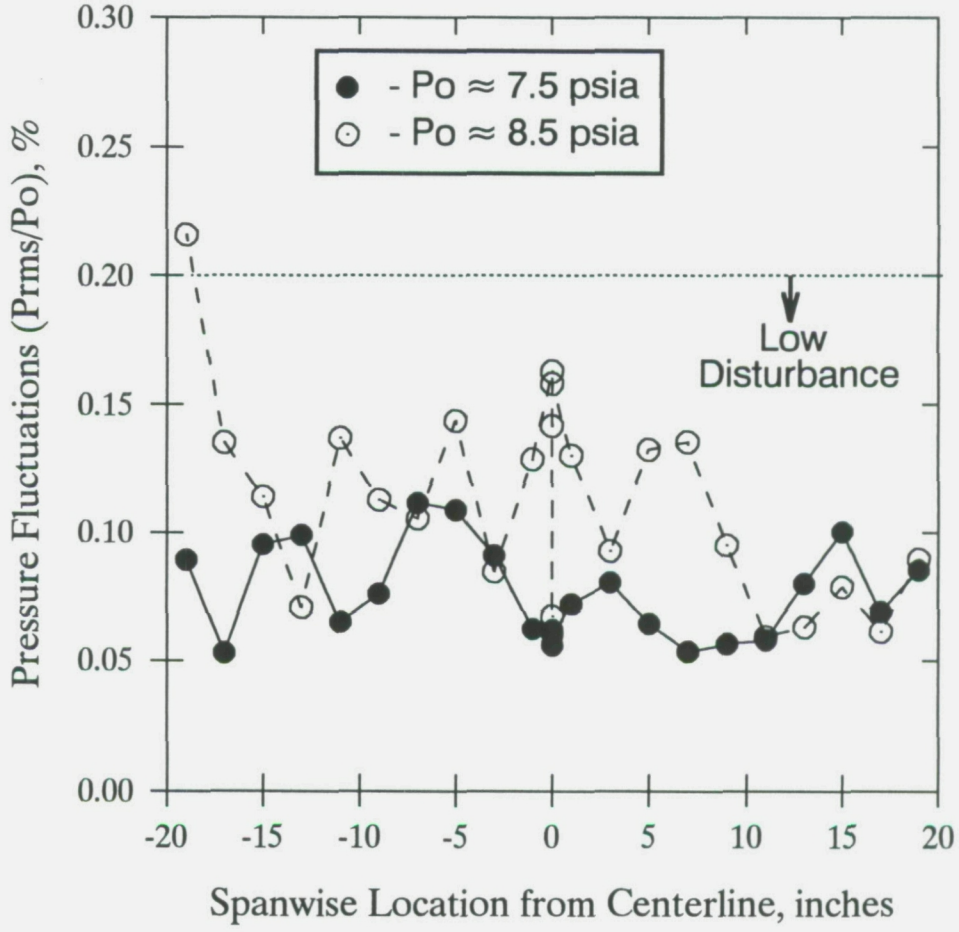

SW 5/11/94

Fig. 37 - Spanwise distribution of pressure fluctuations at the contraction entrance.

LFSWT Settling Chamber Hot-Wire Measurements

Contraction Entrance; Probe 10 inches from South Sidewall

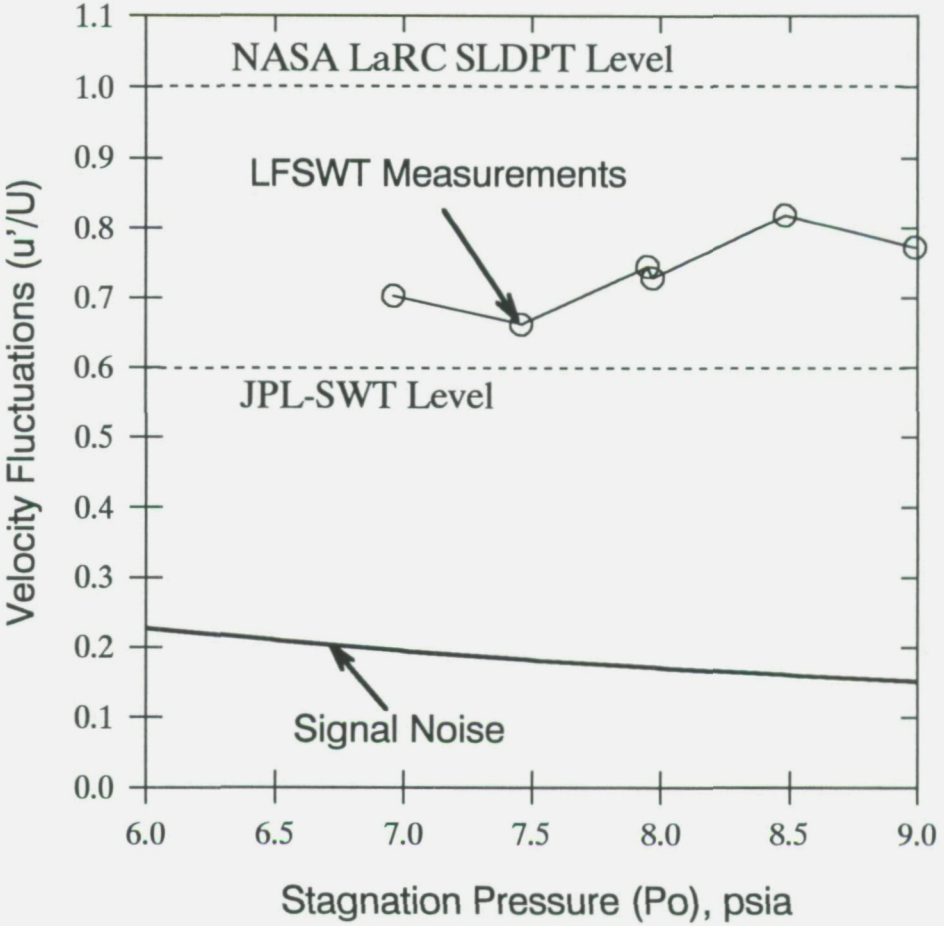

SW 2/22/94

Fig. 38 - Variation of LFSWT settling chamber velocity fluctuations with Po, compared with other quiet supersonic wind tunnels.

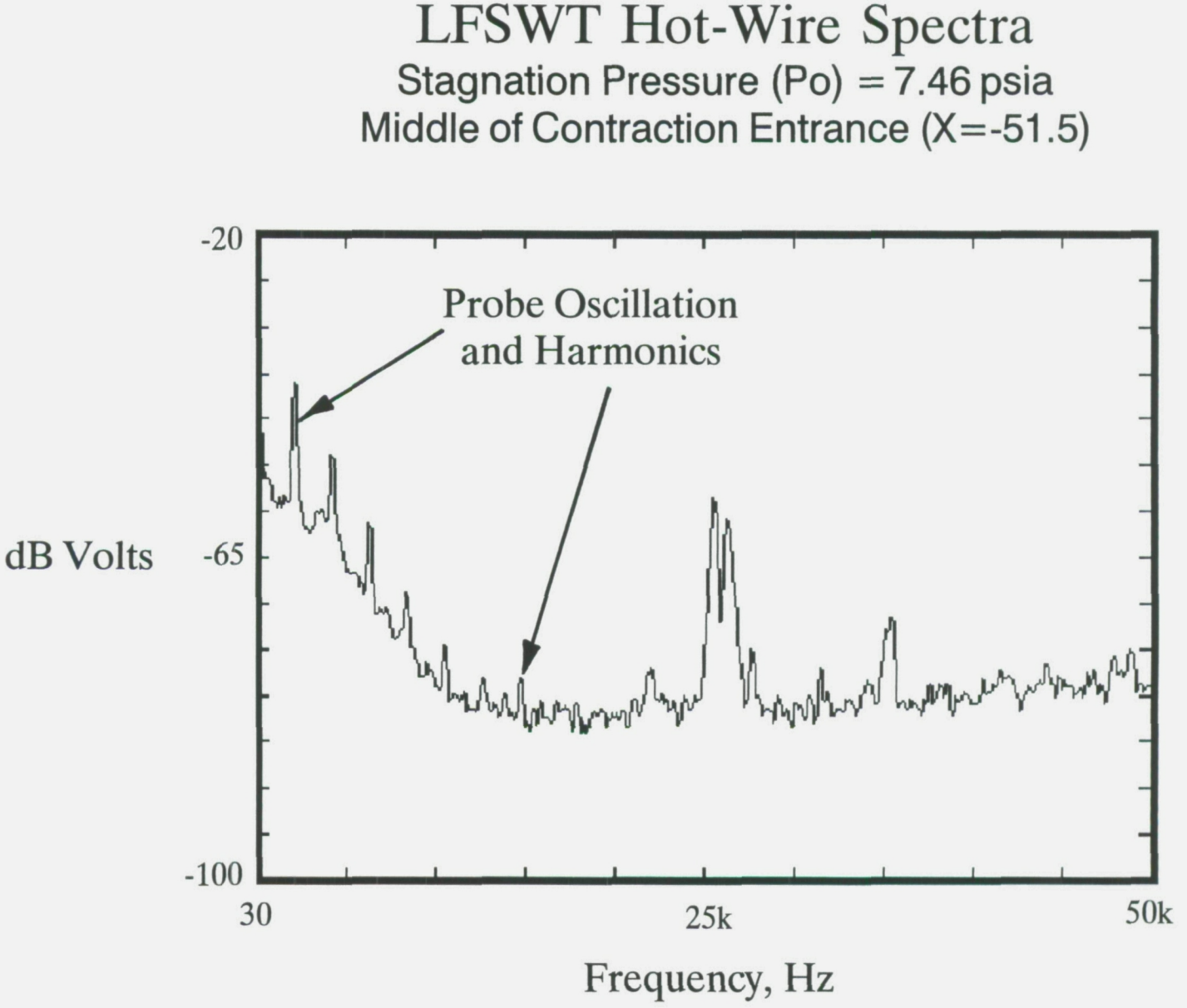

Fig. 39 - Spectra of a hot-wire signal measured in the LFSWT contraction entrance.

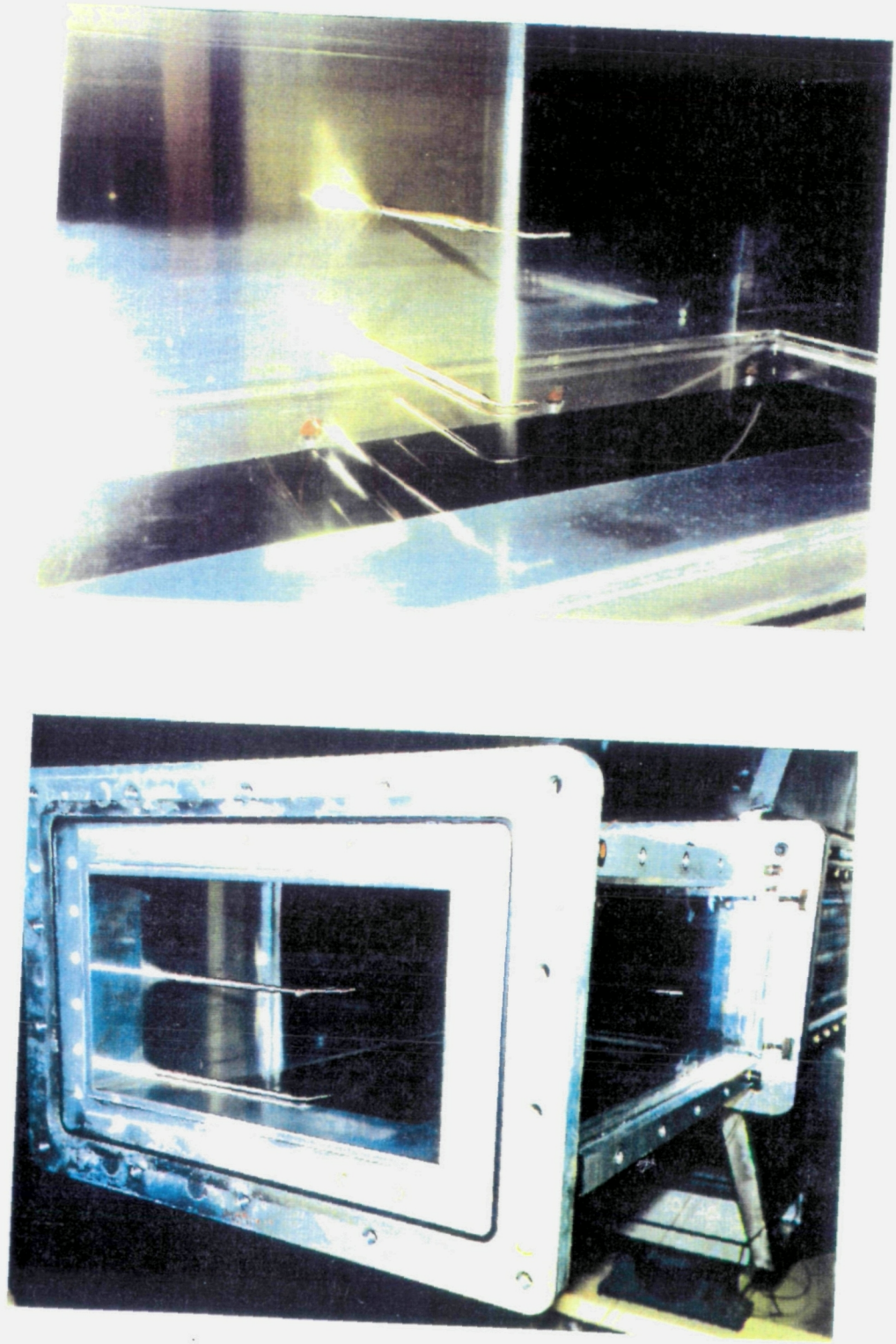

Fig. 40 - View of the pitot and hot-wire probes mounted from the LFSWT test section sidewall (the hot-wire is the lower probe just above the floor window).

LFSWT Test Section Pressure Fluctuation Data

250-50k Hz Range; On Tunnel Centerline

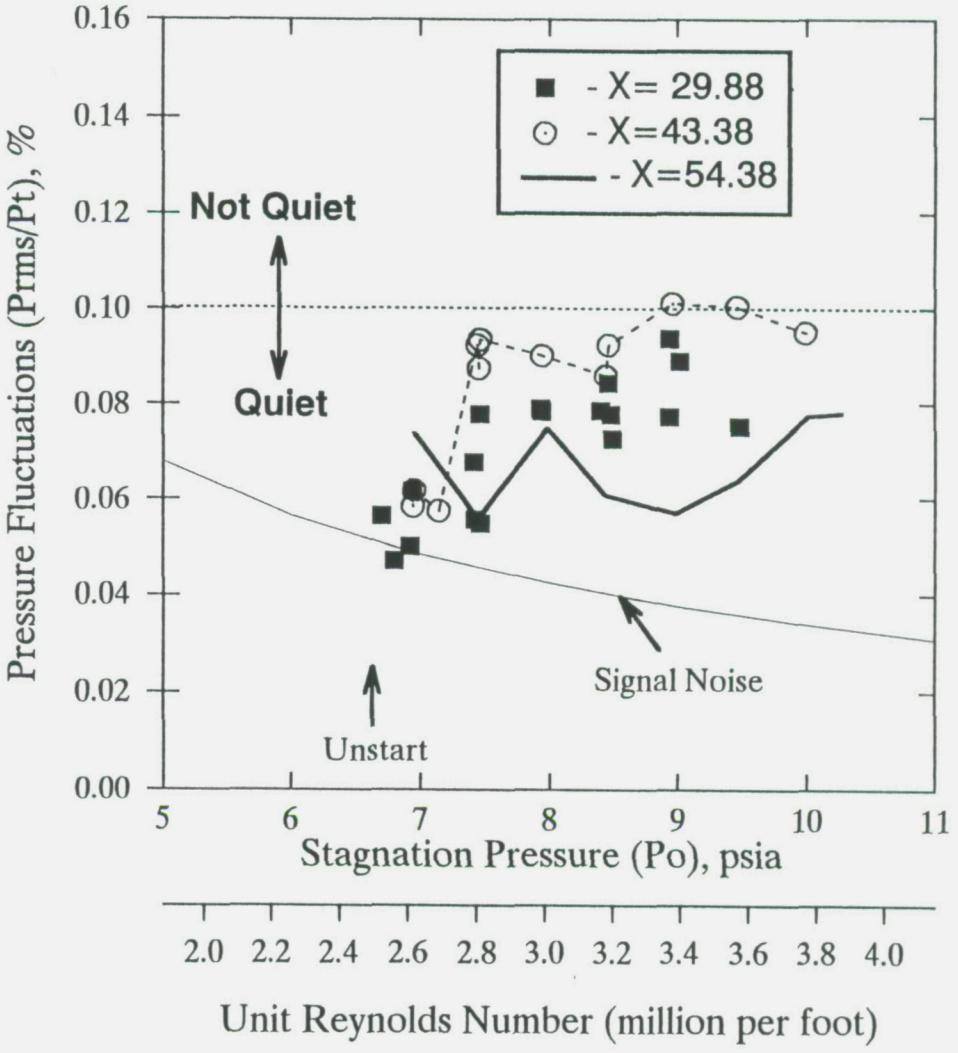

SW 6/11/94

Fig. 41 - Variation of centerline pressure fluctuations with Po, at three streamwise locations along the LFSWT test section.

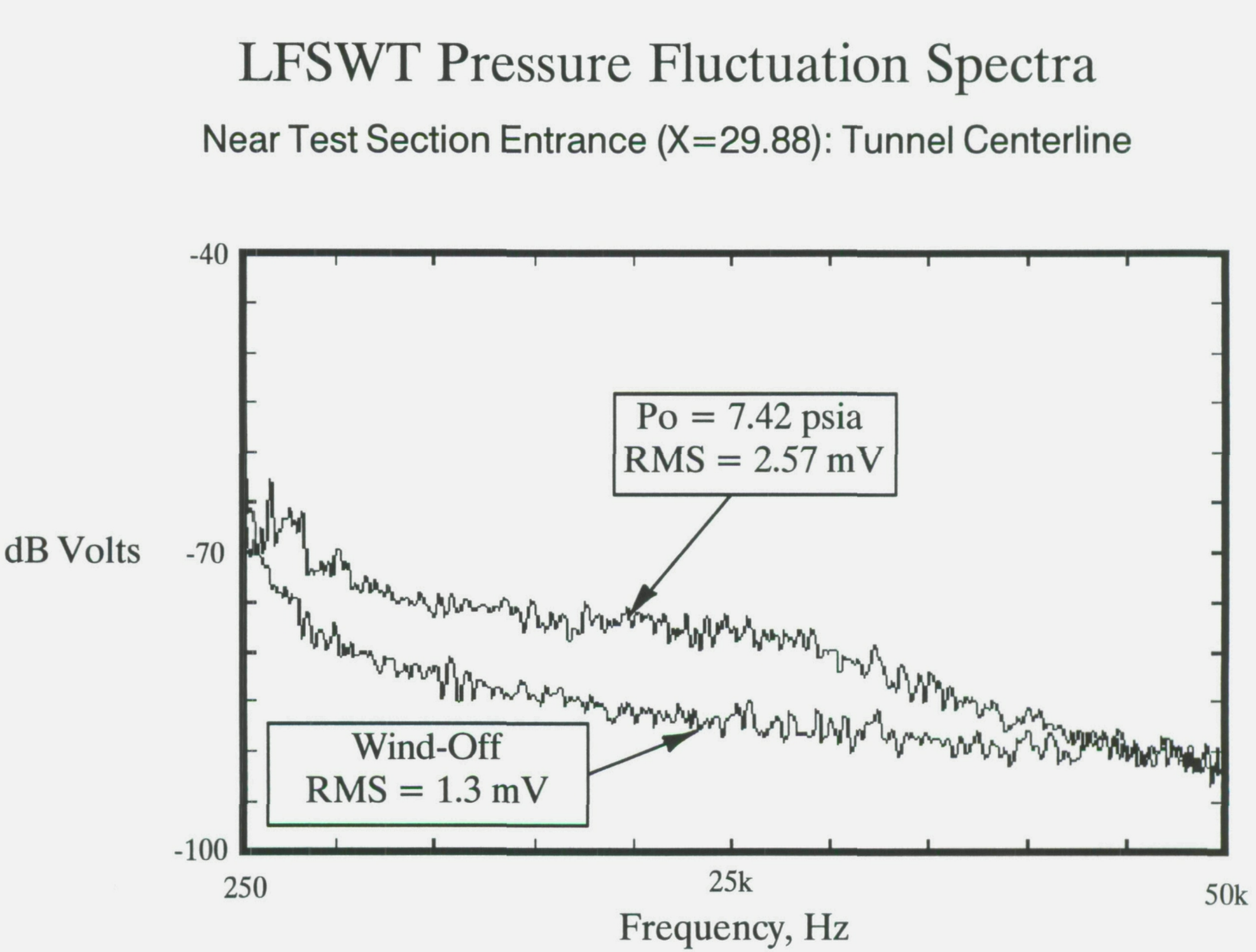

Fig. 42 - Kulite signal spectra measured on the tunnel centerline, near the test section entrance, compared with the wind-off signal spectra.

LFSWT Test Section Kulite Data

2.5 inches Downstream of Nozzle Exit; 250 - 50k Hz Range; Tunnel Vertical Centerline

Test Section 16 inches Wide

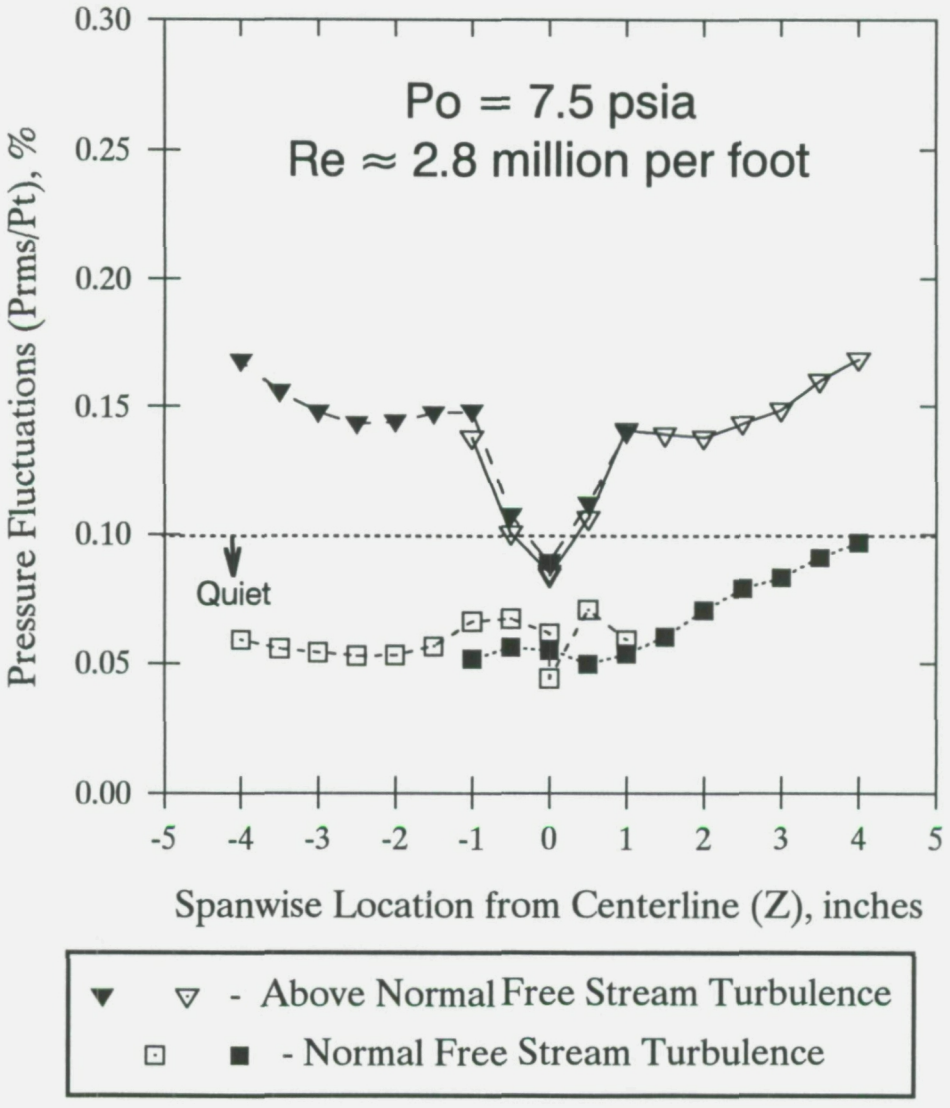

SW 5/18/94

Fig. 43 - Spanwise distribution of pressure fluctuations near the LFSWT test section entrance (X = 29.88), with and without an upstream disturbance.

LFSWT Test Section Pressure Fluctuation Data

250 - 50k Hz Range; Tunnel Vertical Centerline; Test Section 16 inches Wide

Re ≈ 2.8 million per foot Po = 7.5 psia

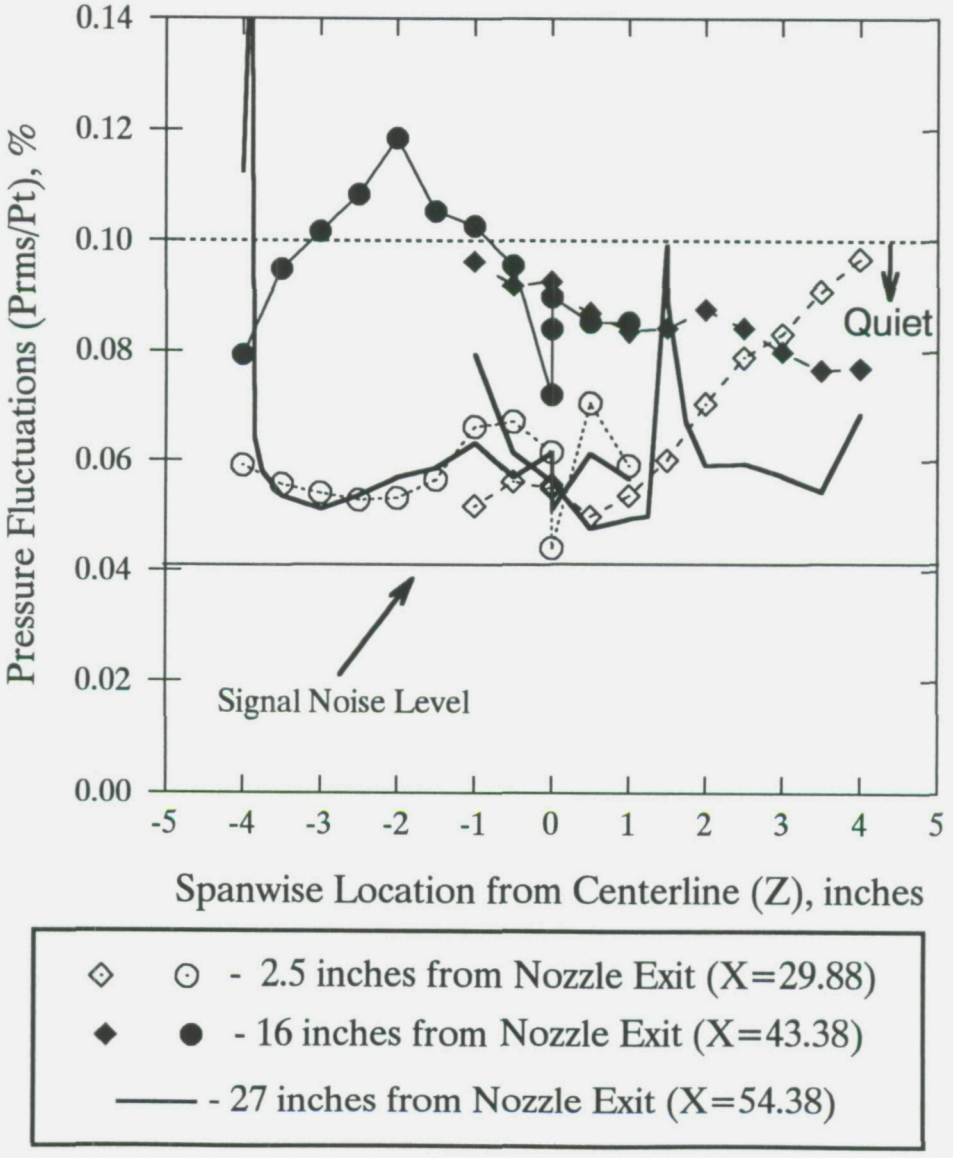

Fig. 44 - Spanwise distribution of pressure fluctuations measured at three streamwise locations in the LFSWT test section (Po = 7.5 psia).

SW 6/11/94

LFSWT Test Section Pressure Fluctuation Data

250 - 50k Hz Range; Tunnel Vertical Centerline; Test Section 16 inches Wide

Re ≈ 3.2 million per foot Po = 8.5 psia

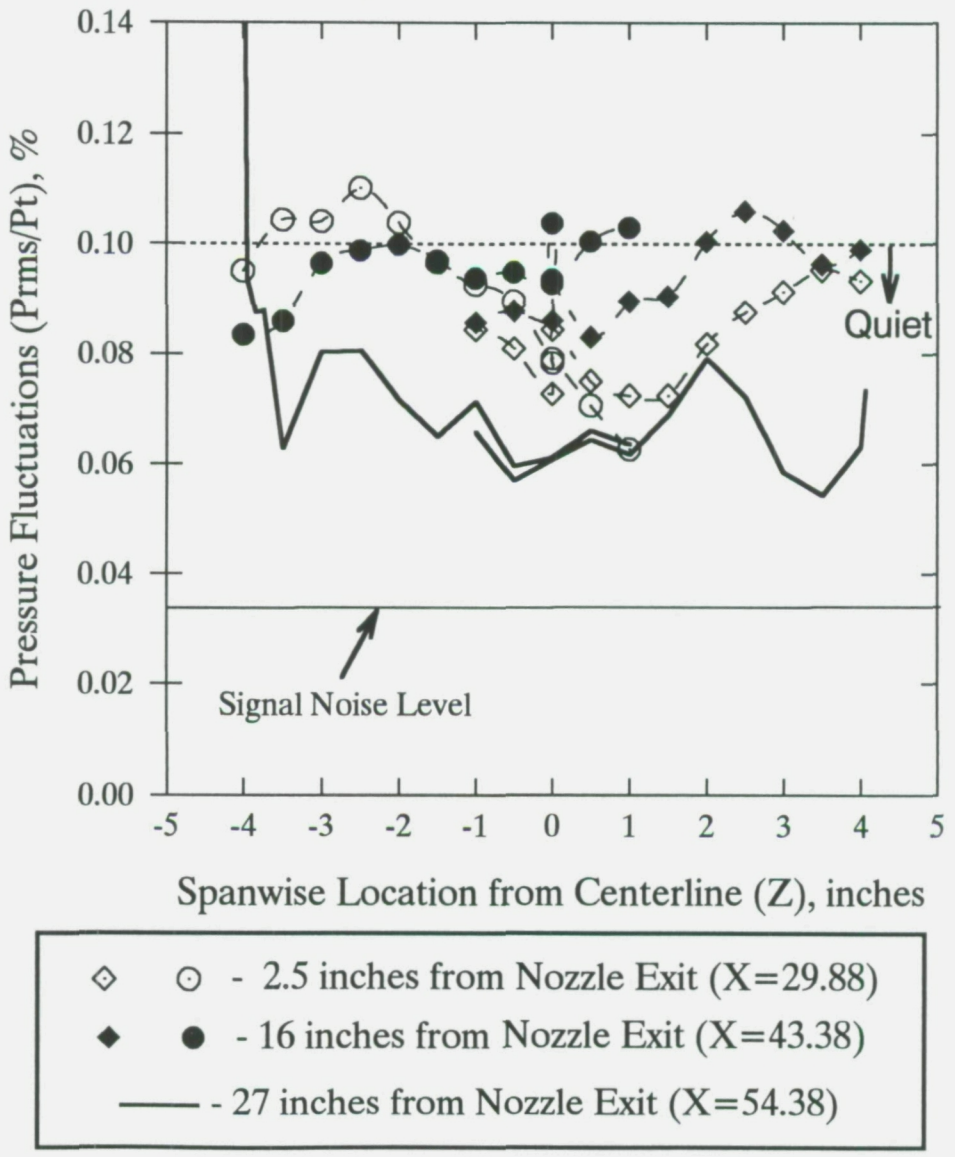

Fig. 45 - Spanwise distribution of pressure fluctuations measured at three streamwise locations in the LFSWT test section (Po = 8.5 psia).

SW 6/11/94

LFSWT Test Section Pressure Fluctuation Data

16 inches From Nozzle Exit (X=43.38) on Tunnel Centerline

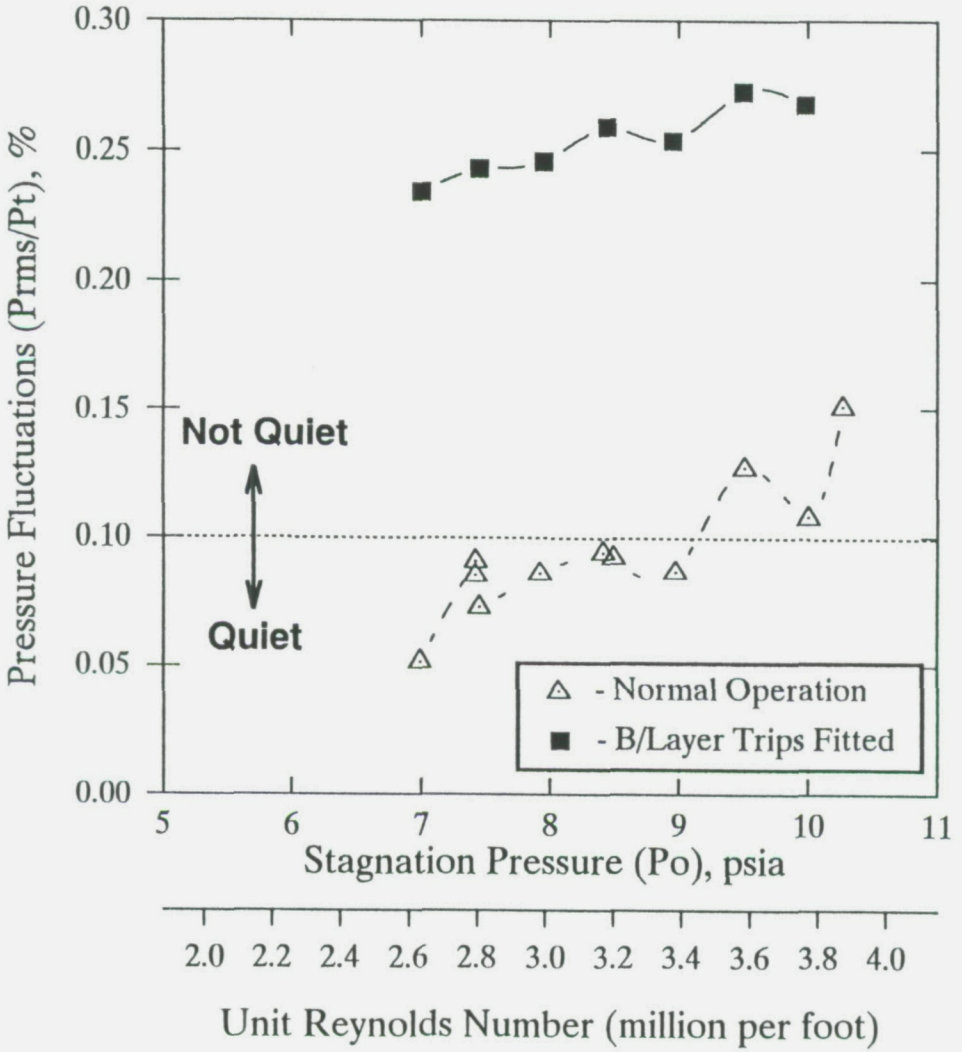

Fig. 46 - Effect of boundary layer trips on pressure fluctuations measured on the tunnel centerline in the middle of the LFSWT test section (X=43.38).

SW 6/1/94

LFSWT Pressure Fluctuation Data

Stagnation Pressure (Po) ≈ 7.5 psia
Middle of Test Section (X=43.38): Tunnel Centerline

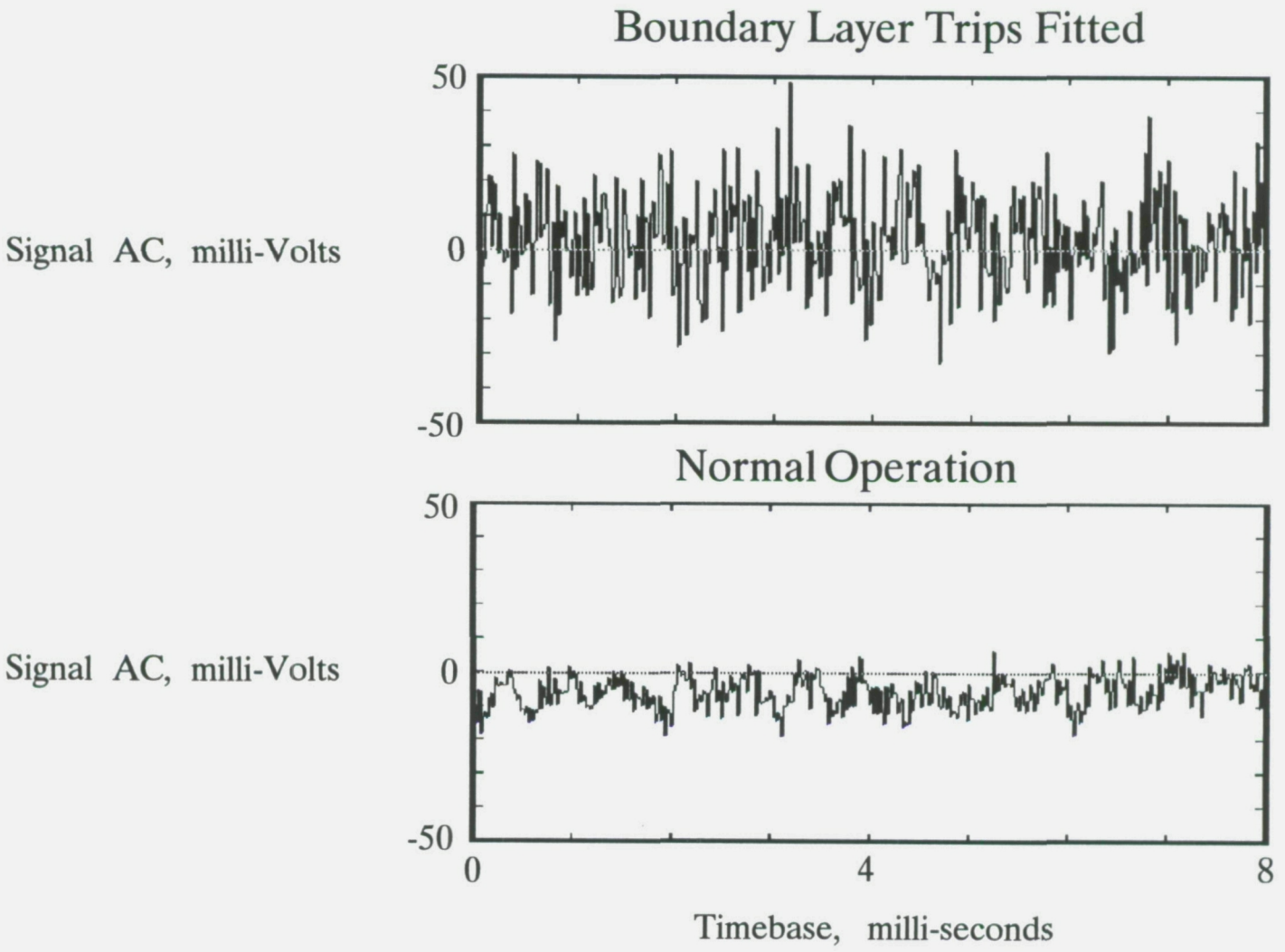

Fig. 47 - Comparison of Kulite signals with and without boundary layer trips fitted, measured in the middle of the LFSWT test section (Po ≈ 7.5 psia).

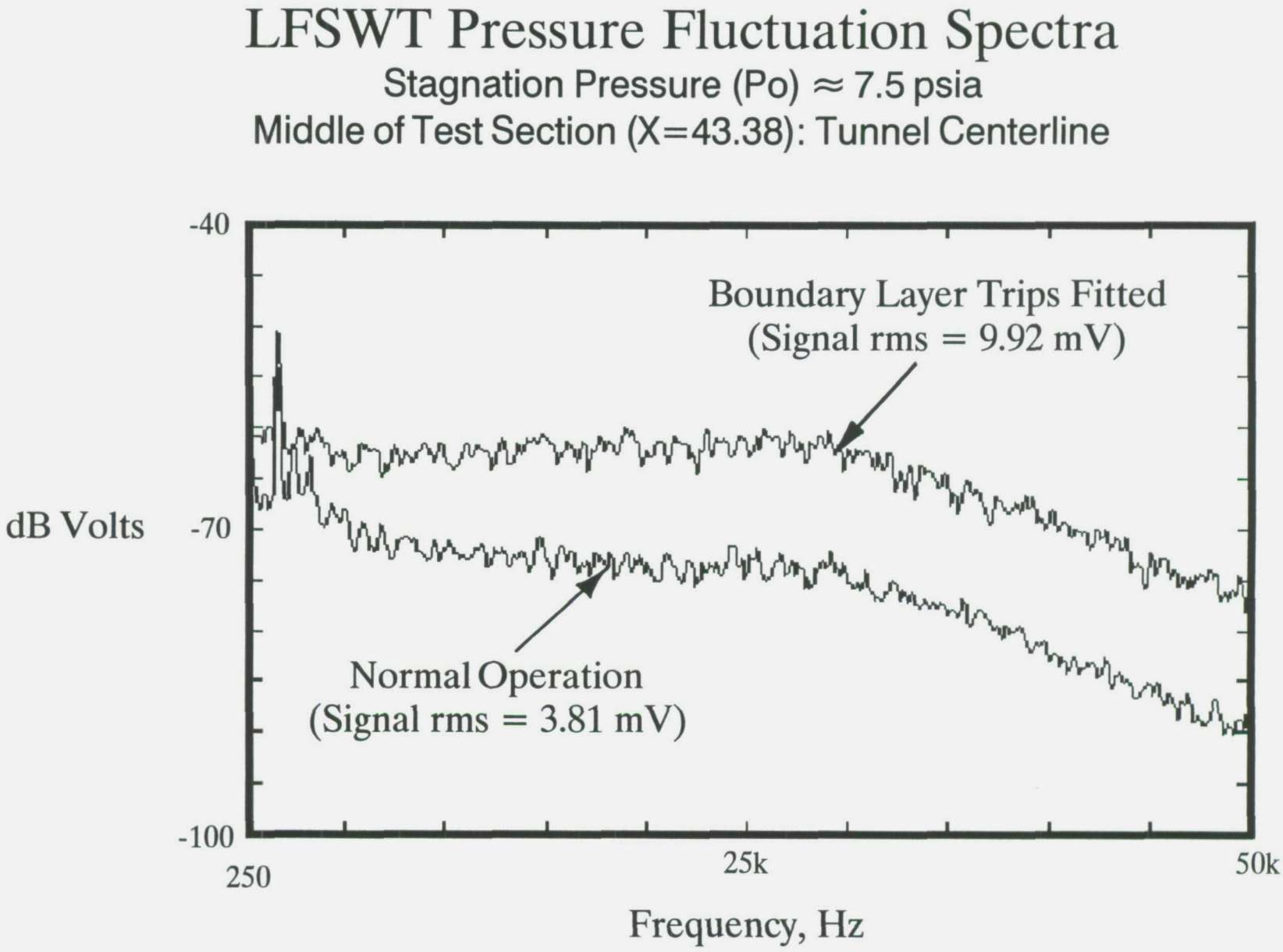

Fig. 48 - Comparison of Kulite signal spectra with and without boundary layer trips fitted, measured in the middle of the LFSWT test section (Po ≈ 7.5 psia).

LFSWT Test Section Hot-Wire Data at Mach 1.6

0.025 inch Above Floor Centerline; 16 inches From Nozzle Exit (X=43.38); 5 micron Tungsten Wire

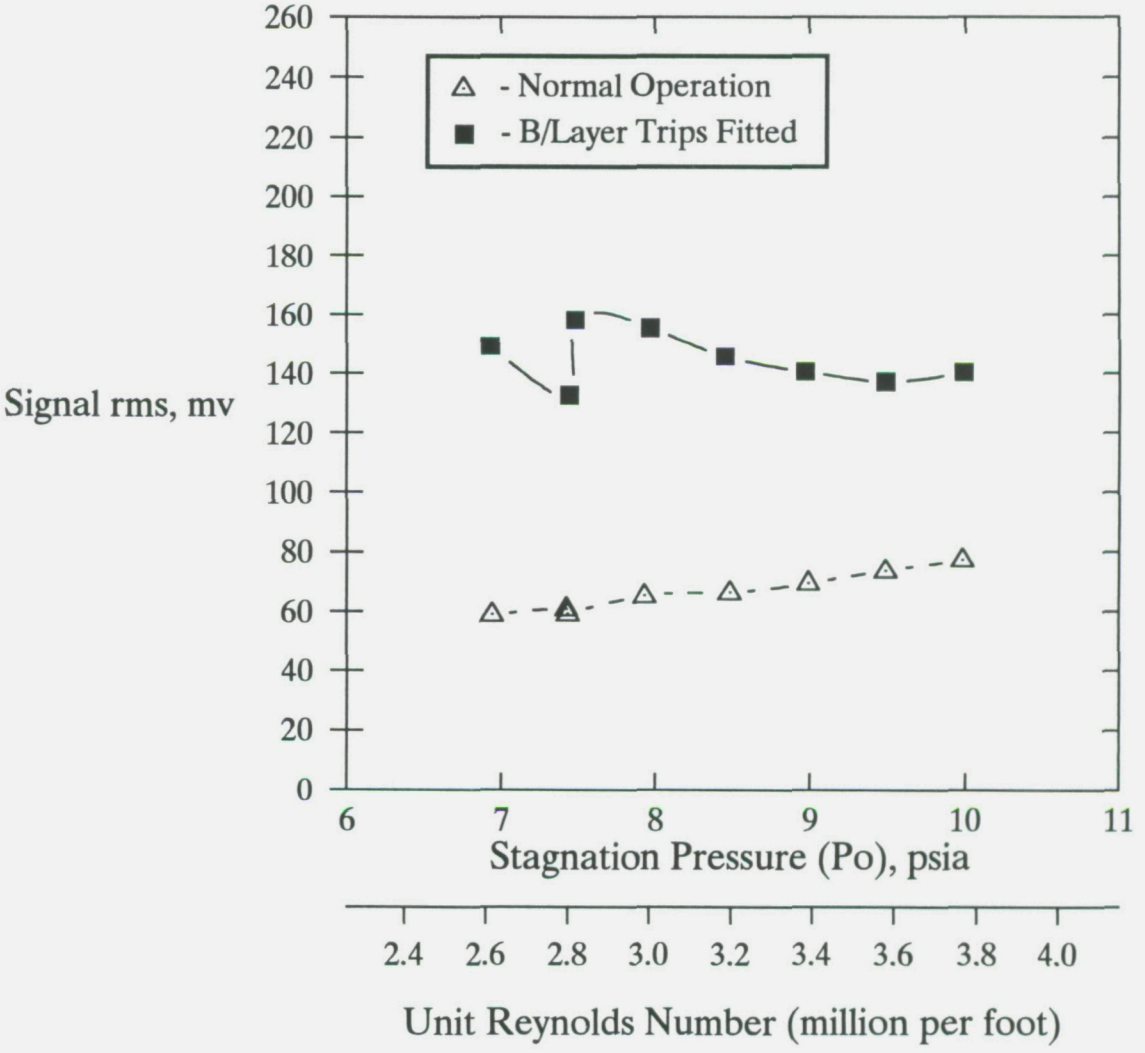

SW 6/3/94

Fig. 49 - Hot-wire data measured in the LFSWT floor boundary layer with and without boundary layer trips fitted 16 inches (40.6 cm) upstream.

LFSWT Hot-Wire Boundary Layer Data

Stagnation Pressure (Po) ≈ 7.5 psia

Middle of Test Section (X=43.38): 0.025 inch Above Floor

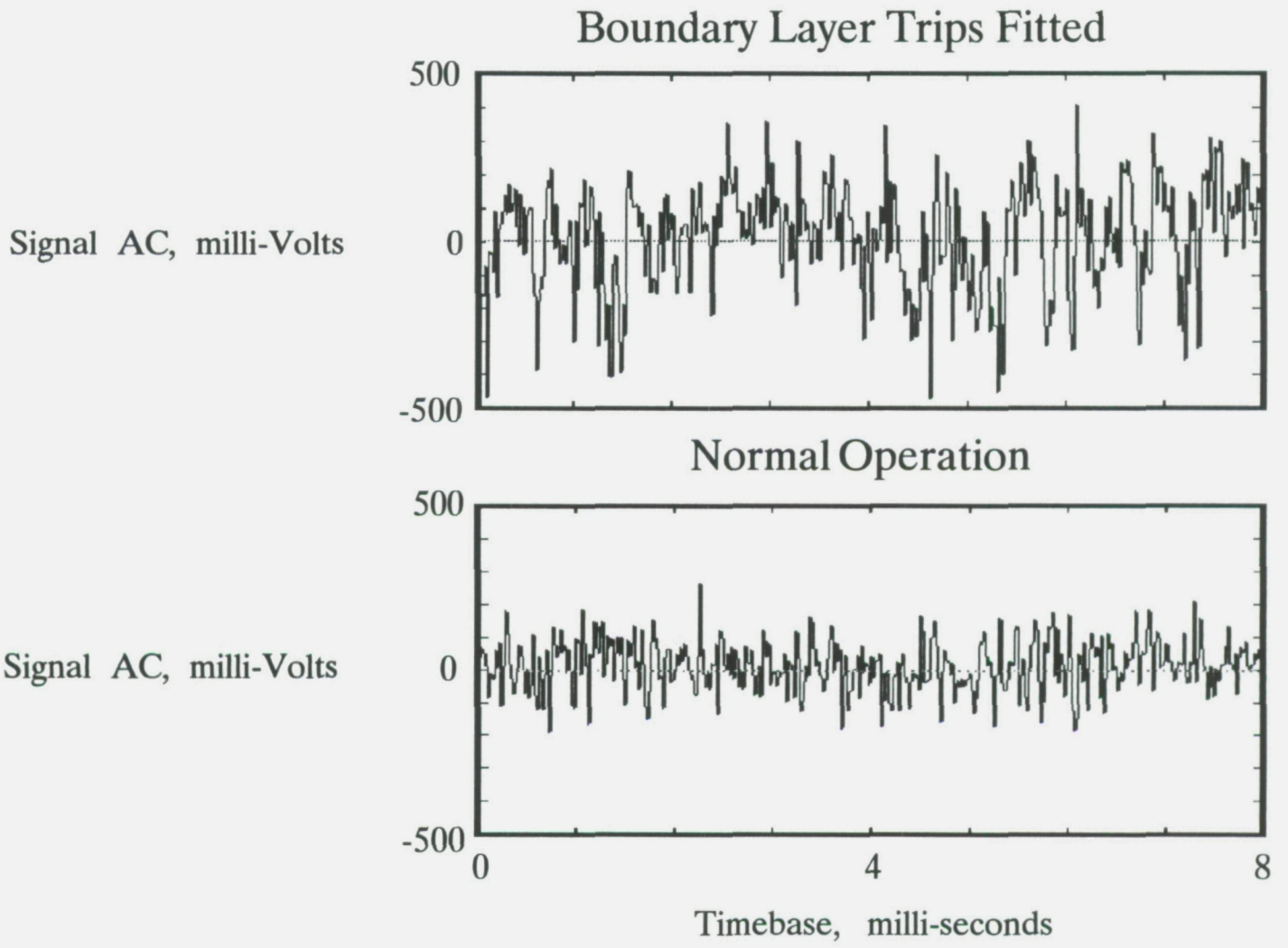

Fig. 50 - Hot-wire signals measured in the LFSWT floor boundary layer with and without boundary layer trips fitted 16 inches (40.6 cm) upstream (Po ≈ 7.5 psia).

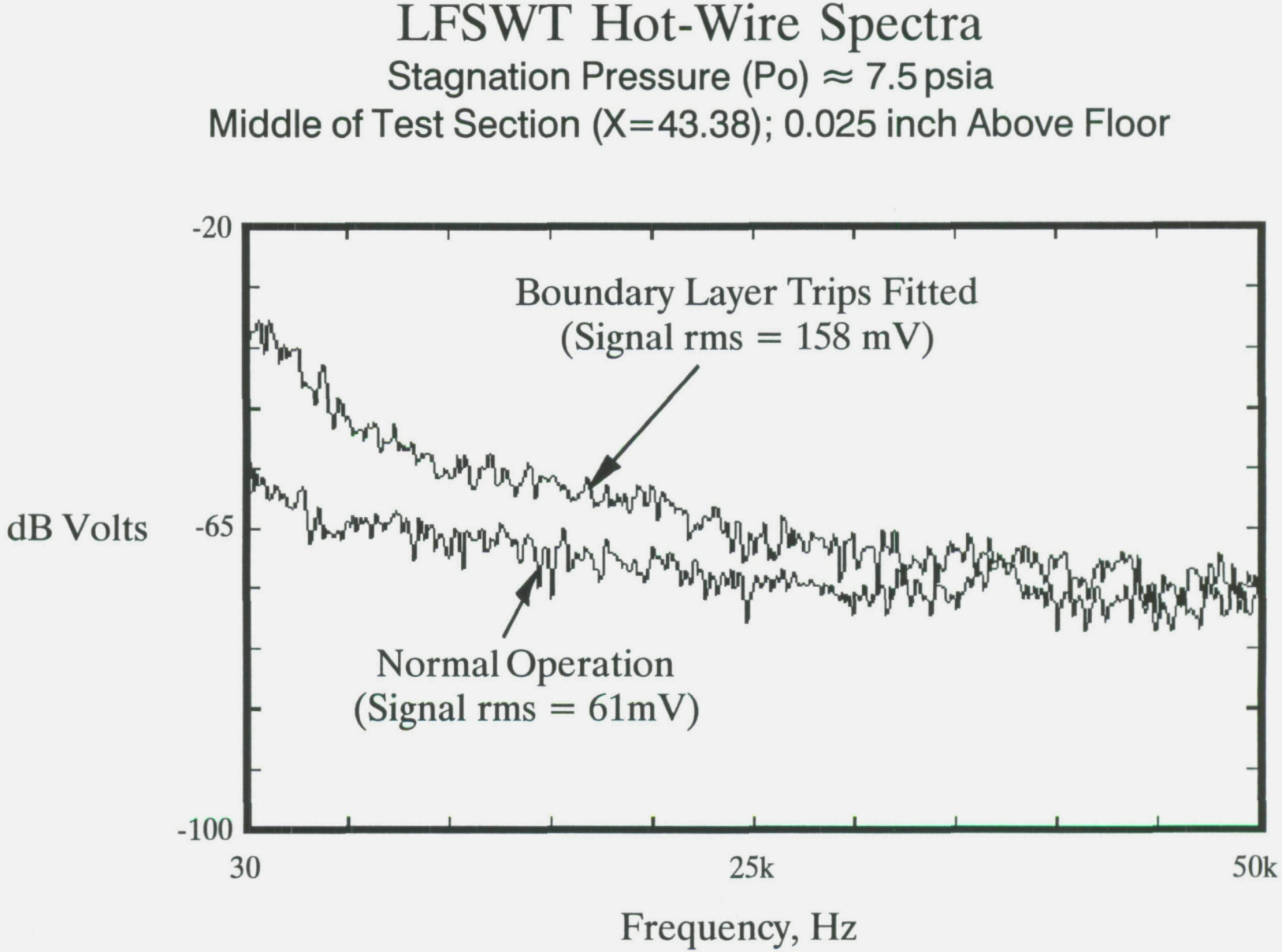

Fig. 51 - Comparison of hot-wire spectra measured in the LFSWT floor boundary layer with and without boundary layer trips fitted 16 inches (40.6 cm) upstream.

Swept-Wing Pressure Model Installed in the LFSWT

NASA-Ames Fluid Mechanics Laboratory - August 1994

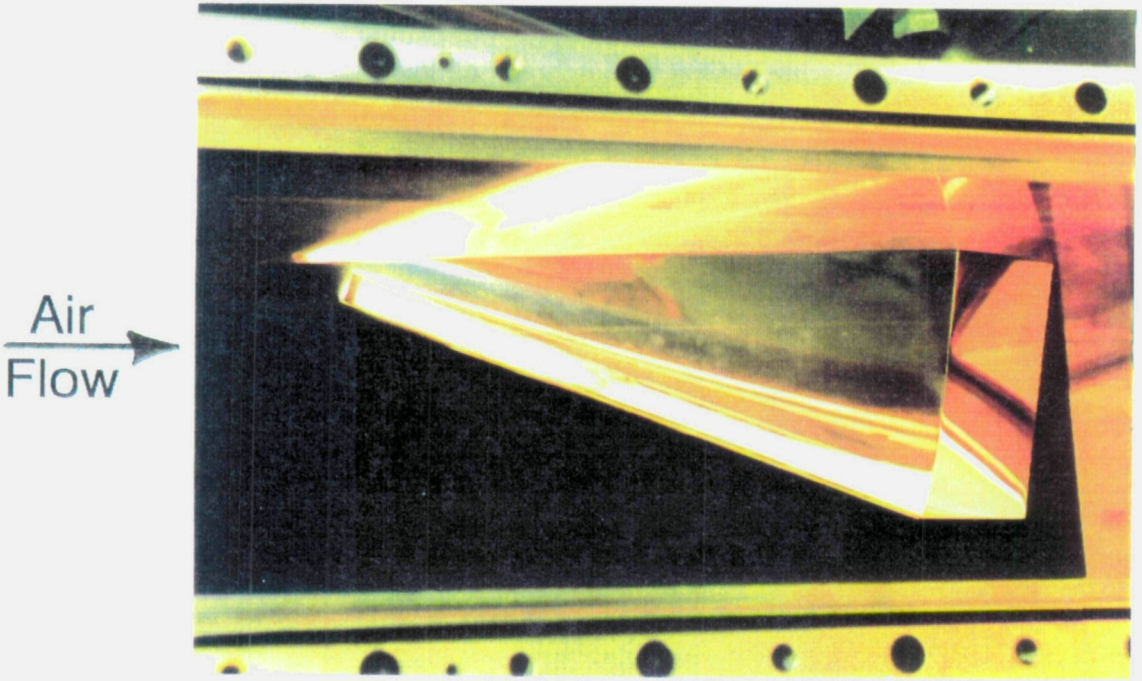

Fig. 52 - Instrumented 70° swept-wing model installed in the LFSWT.

LFSWT Swept-Wing Pressure Model

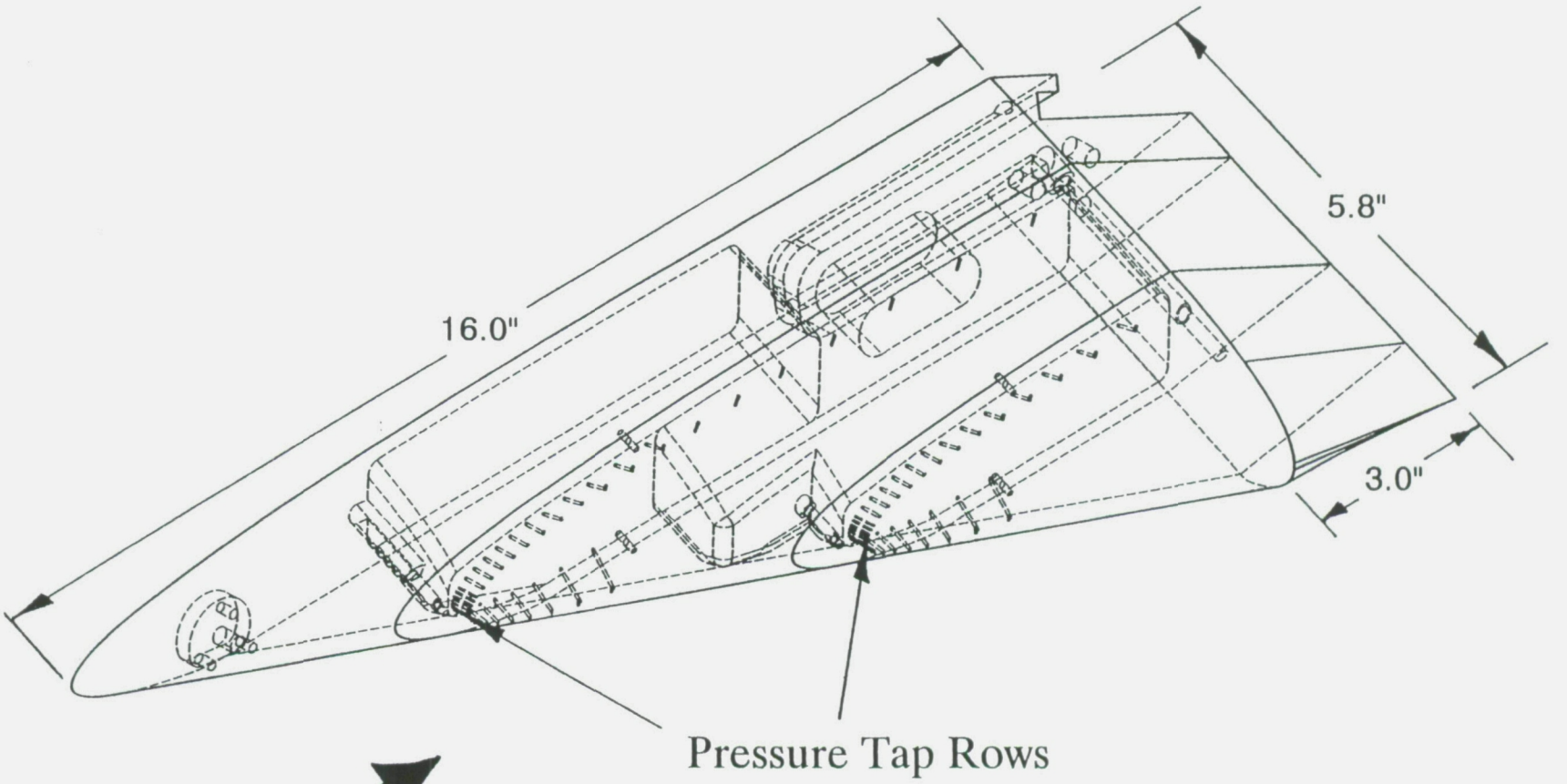

Fig. 53 - Schematic of the instrumented LFSWT 70° swept-wing model.

JL - SW 1/28/94

Swept-Wing Solid Model Installed in the LFSWT

Fluid Mechanics Laboratory - June 1994

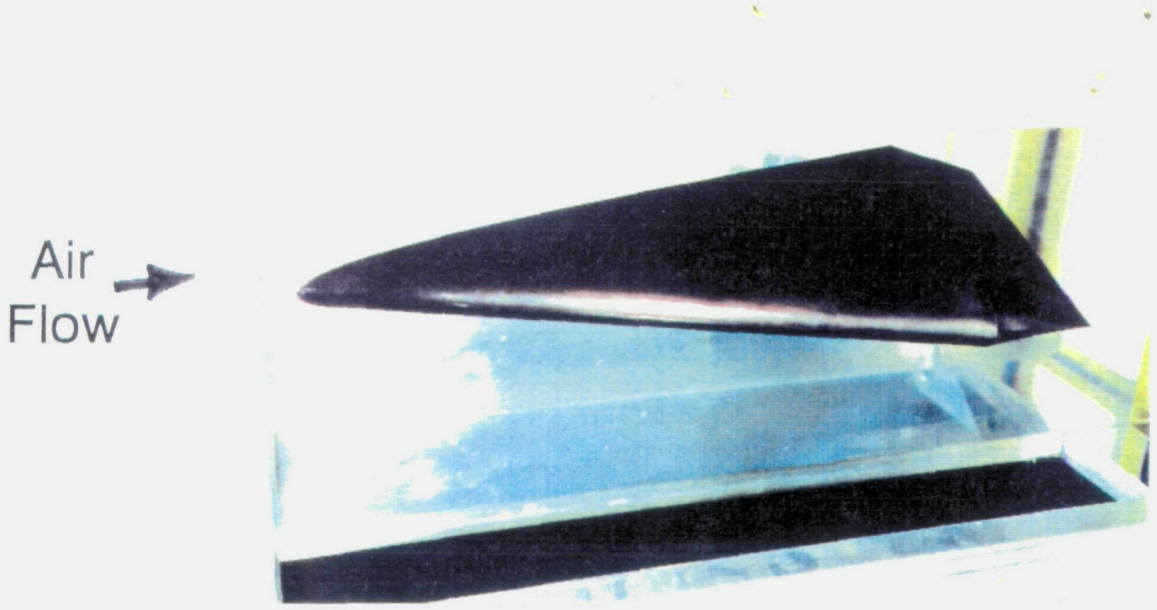

Fig. 54 - LFSWT blockage tests were performed with a solid 70° swept-wing model.

LFSWT Swept-Wing Pressure Instrumentation Location

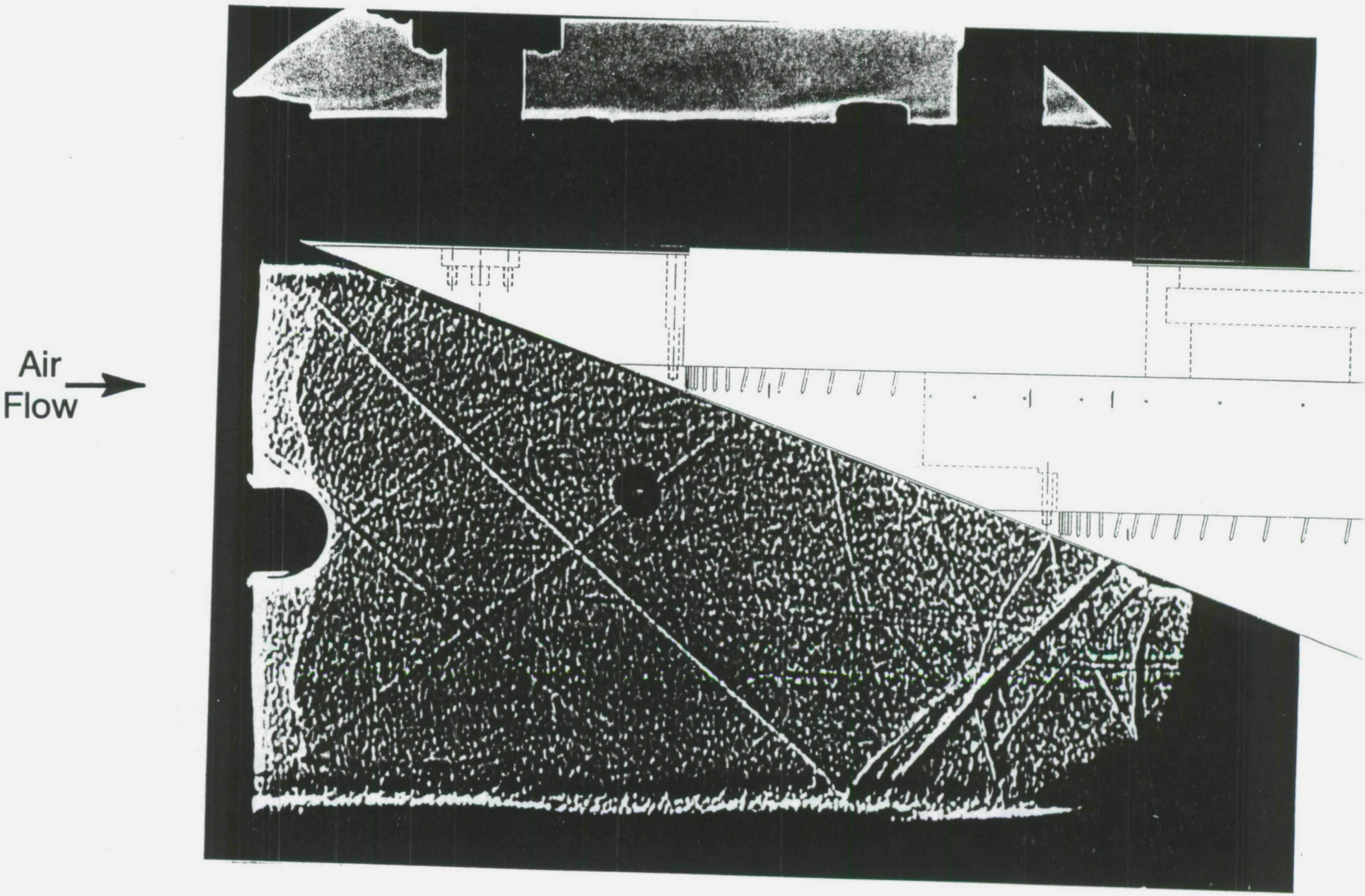

Fig. 55 - Composite shadowgraph photograph shows relative position of the bow shock reflection and the 70° swept-wing pressure tap rows at Mach 1.6.

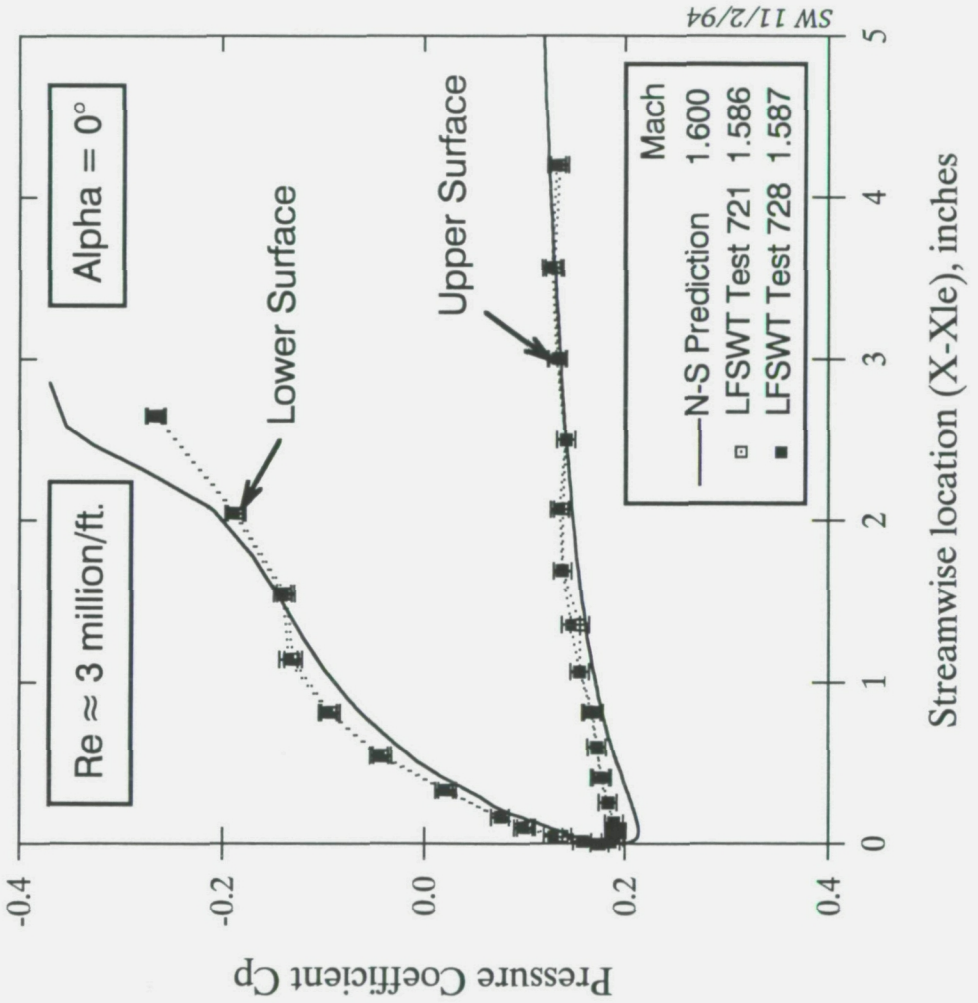

Fig. 56a - Comparisons of pressure distributions from the 70° swept-wing model with Navier-Stokes predictions (inboard row of pressure taps).

NASA-Ames LFSWT Wing Pressures

Row 0 Taps (2/3 Span); Alpha = 0°; Re ≈ 3 million/ft.

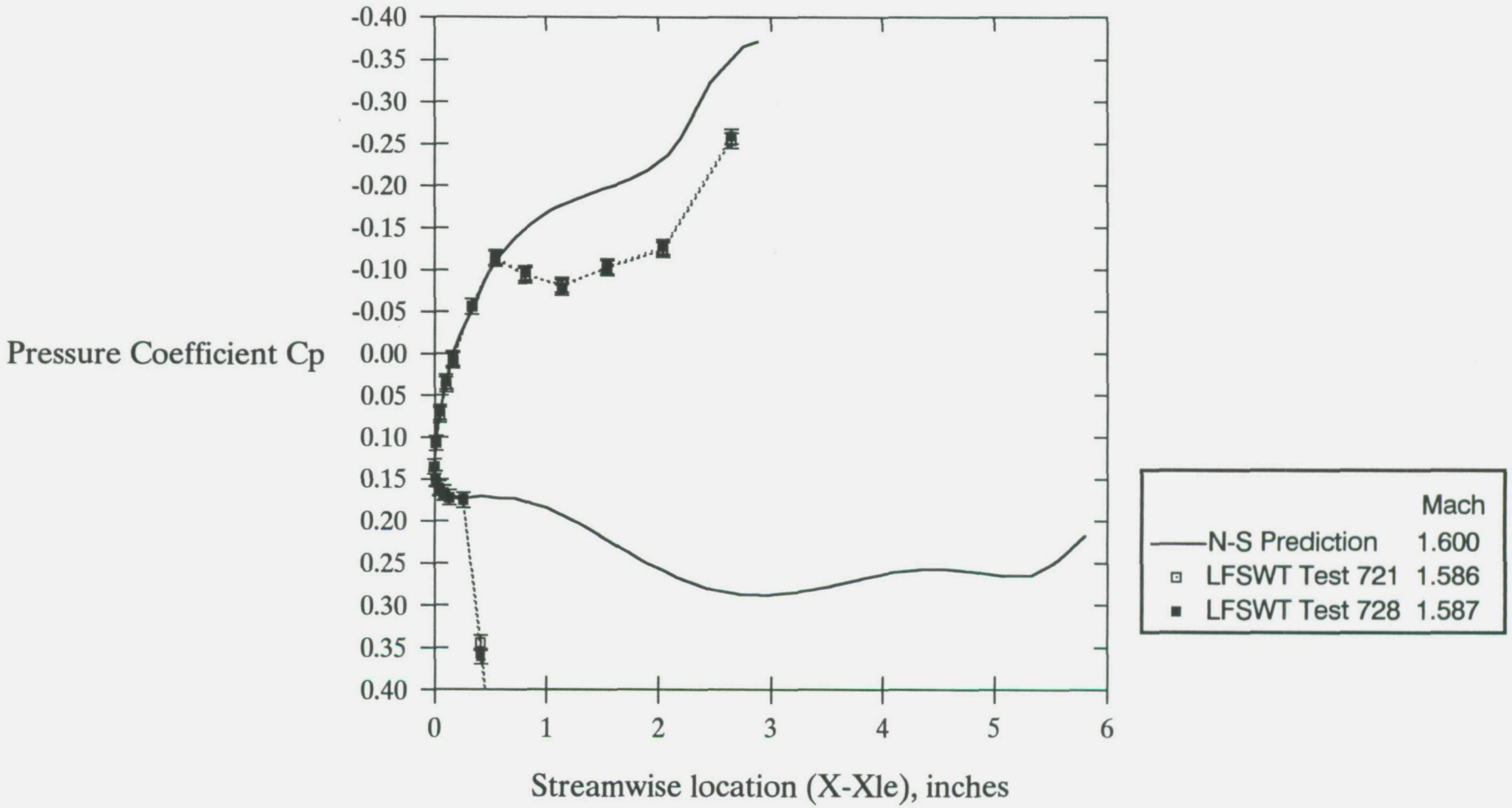

SW 9/12/94

Fig. 56b - Comparisons of pressure distributions from the 70° swept-wing model with Navier-Stokes predictions (outboard row of pressure taps).

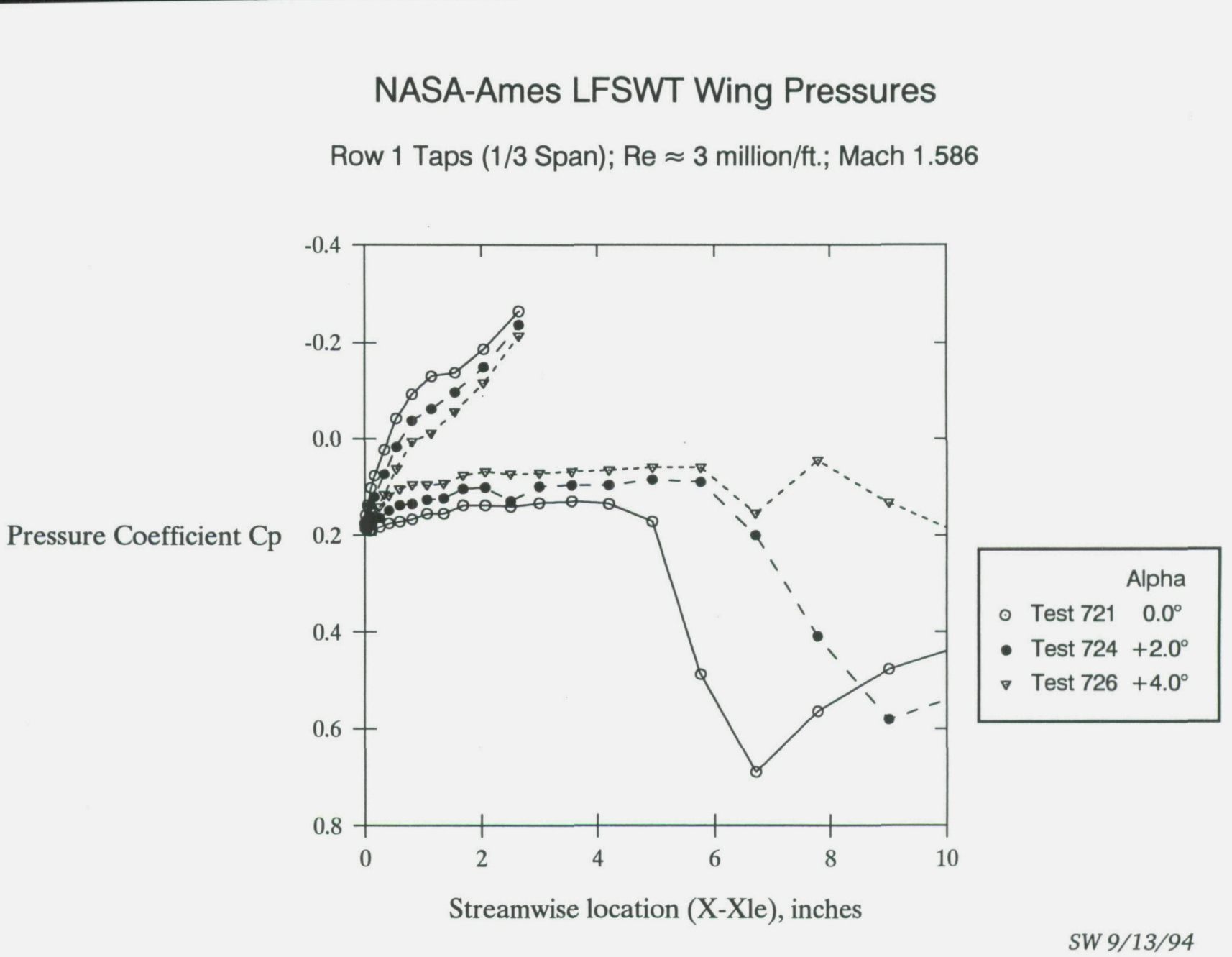

Fig. 57 - Variation of the 70° swept-wing model pressure distributions with angle of attack, at Mach 1.586 (inboard row of pressure taps).

APPENDIX A

LFSWT Design Outline

6th March 1992

Settling Chamber:

Length of *Black Box* pressure reducer . . . . **25** inches

Maximum cross-section - 39.24 inches square

Cone housing length . . . . . **56.69** inches

Honeycomb housing length . . . . . **12** inches

Total length of screen holders. . . . . **48** inches maximum
24 inches minimum

Adjustable length for recirculation chamber etc . . . **48** inches

Settling chamber centerline height - 72 inches above floor

Nozzle/Contraction:

Inlet size - 39.24 inches square

Overall contraction length to nozzle throat . . . . **48** inches

Nozzle width - 16 inches

Nozzle length (Mach 1.6 operation) . . . . . **27.376** inches

Nozzle exit height - 8 inches

Test/Section:

Inlet size - 8 inches high; 16 inches wide

Test section length . . . . . **32** inches

Test section wall divergence - 0.25 degree

Test section centerline height - 72 inches above floor

Exit size - 8.280 inches high; 16 inches wide

Supersonic diffuser:

Supersonic diffuser length . . . . . **41** inches

Minimum throat height - 6.056 inches

Maximum ramp height - 1.112 inches

Ramp length - 8 inches

Floor and ceiling wall divergence - 0.25 degree

Variable exit cross-section - 6.344 - 8.566 inches high; 16 inches wide

Primary Injectors (2 off):

Variable throat area - 90 - 180 square inches

Varaible exit area - 169 - 338 square inches

Variable exit Mach number - 1.8 to 2.2

Variable exit cross-section - 16 inches wide; 10.56 - 21.12 inches high

Throat to exit length - 32 inches

Injection angle (relative to centerline) - 10 degrees

Total mass flow range - 62 - 124 lbs/sec

Mixing Region:

Mixing region length . . . . . **51.68** inches

Exit cross-section - 41.246 inches high; 16 inches wide

Secondary Injectors (2 off):

Throat area (Mass flow = 34.65 lbs/sec) - 106 square inches

Exit area (Mach 1.8) - 152.53 square inches

Exit cross-section - 41.246 inches high; 3.698 inches wide

Throat to exit length - 20 inches

Injection angle (relative to centerline) - 10 degrees

Total mass flow - 69.3 lbs/sec

Length of sidewall flare section . . . . . 12 inches

Subsonic diffuser:

Inlet cross-section - 41.246 inches high; 36.758 inches wide

Outlet cross-section - 60 inch diameter

Length with 7 degree total angle . . . . . **190** inches

Inlet centerline height - 72 inches above floor

Outlet centerline height - 92 inches above ground level

Centerline inclination - 6 degrees

Maximum total length. . . . . **591.754** inches (49.312 feet)

Test Cell #1 length - 38 feet; Distance between FML manifold and test cell wall - 10 feet
Maximum Length of LFSWT in High Bay - (49.312-10-38) = 1.312 feet

Stephen Wolf 3/6/92